

**UNIVERSITE DU QUEBEC**

THESE  
PRÉSENTÉ A  
L'UNIVERSITÉ DU QUÉBEC À CHICOUTIMI  
COMME EXIGENCE PARTIELLE  
DU DOCTORAT EN INGÉNIERIE

PAR  
YADOLLAH SABRI

STATIC MODELLING OF AC FLASHOVER ON CONTAMINATED  
INSULATORS COVERED WITH ICE USING INTELLIGENT  
IDENTIFICATION METHODS

MODELISATION STATIQUE DE CONTOURNEMENT ÉLECTRIQUE  
SUR LES ISOLATEURS CONTAMINÉS COUVERTS AVEC LA GLACE  
EN COURANT ALTERNATIF EN UTILISANT DES MÉTHODES  
D'IDENTIFICATION INTELLIGENTES

**NOVEMBER 2009**



### Mise en garde/Advice

Afin de rendre accessible au plus grand nombre le résultat des travaux de recherche menés par ses étudiants gradués et dans l'esprit des règles qui régissent le dépôt et la diffusion des mémoires et thèses produits dans cette Institution, **l'Université du Québec à Chicoutimi (UQAC)** est fière de rendre accessible une version complète et gratuite de cette œuvre.

Motivated by a desire to make the results of its graduate students' research accessible to all, and in accordance with the rules governing the acceptance and diffusion of dissertations and theses in this Institution, the **Université du Québec à Chicoutimi (UQAC)** is proud to make a complete version of this work available at no cost to the reader.

L'auteur conserve néanmoins la propriété du droit d'auteur qui protège ce mémoire ou cette thèse. Ni le mémoire ou la thèse ni des extraits substantiels de ceux-ci ne peuvent être imprimés ou autrement reproduits sans son autorisation.

The author retains ownership of the copyright of this dissertation or thesis. Neither the dissertation or thesis, nor substantial extracts from it, may be printed or otherwise reproduced without the author's permission.

## **ABSTRACT**

The exposure of the overhead electrical power transmission and distribution lines to the severe icing conditions of the cold regions can cause repetitive flashovers of insulators, sometimes leading to long term power outages. In addition to the icing condition, the surface pollution of insulators is another factor causing the electrical flashover. Natural sources of contamination of insulators are mostly chemical contaminants produced in urban areas. Alongside the chemical pollutions, the high voltage overhead lines in coastal areas or in vicinity of highways are subject to sea type contamination. During the strong and long term windy weather, salt being carried from sea coasts or highways forms a deposition of pollution layer on high voltage insulators surface. The above mentioned sources of pollution lead to the formation of composite ion layers on insulators in overhead high voltage lines. The joint effect of contamination and atmospheric icing has been recognized as a major cause of flashovers of insulators in cold regions of the world. Therefore, the extensive studies are required to understand the nature of the composite ion pollution in modeling the flashover phenomenon of high voltage insulators. Such a model is supposed to take into account the joint effect of pollution and icing for predicting the flashover voltage of insulators subjected to joint effect of icing and pollution.

A static AC model for predicting the flashover voltage of pre-contaminated insulators covered with ice was developed as part of this thesis. Conceptually, the model is based on Obenaus model which simulates an arc in series with a polluted and wet surface. Furthermore, the Ayrton's arc model was used to account for the variation of arc voltage versus leakage current. The arc constants and re-ignition parameters were determined using the physical cylindrical ice models.

The developed model in this study uses intelligent identification methods to determine the relevant variables associated with the mathematical expression of the flashover phenomenon. New approaches based on Least Square Estimator (LSE) and Adaptive Network-Based Fuzzy Inference System (ANFIS) were utilized for extracting the mathematical formula for calculating the voltage of un-bridged part of insulator (residual voltage). The formula thus

proposed, incorporates the major variables influencing the electrical characteristic of residual part of contaminated ice covered insulators during the time period of arc propagation. Moreover, the mathematical expression of residual voltage has also made it possible to develop a formula representing the position-dependent (Differential) resistance of residual part of insulator. The formula incorporates the variables such as applied freezing water conductivity, salt deposit density, leakage current and the length of residual part of insulator.

The model was successfully applied to the artificially contaminated and ice covered industrial insulators, and the calculated flashover voltage based on this model was in good agreement with those obtained from experimental flashover tests.

## RÉSUMÉ

L'exposition des lignes de transmission aériennes à la rigueur des conditions atmosphériques des régions froides, peut causer des contournements électriques répétitifs des isolateurs, entraînant des pannes de courant. À côté de l'impact du froid, les conditions atmosphériques affectant la contamination des isolateurs a été également reconnu comme un autre facteur pouvant affecter considérablement la performance diélectrique des isolateurs. Cette dégradation des performances peut conduire parfois au contournement de l'isolateur. Les sources naturelles de contamination d'isolateurs sont principalement les contaminants chimiques gazeux produits dans les régions urbaines. Les régions côtières exposées aux embruns ou aux vents très forts et polluants venant de la mer constituent une source importante de pollution des isolateurs. Cette situation conduit à la formation d'une pollution d'ions composite sur les isolateurs à haute tension pendant les périodes hivernales. L'effet combinée de la contamination et la glace accumulée a été reconnue comme l'une des causes majeures de contournement d'isolateurs. Par conséquent, des méthodes particulières d'étude sont nécessaires pour comprendre la nature de la pollution d'ions composite dans le cadre de la modélisation du phénomène de contournement des isolateurs en prenant en compte l'effet conjugué de la pollution et de givrage.

Un modèle Statique en courant alternatif permettant de prédire la tension de contournement des isolateurs recouverts de glace contaminée a été développé dans cette étude. Sur le plan conceptuel, le modèle est basé sur le modèle de décharge d'Obenaus qui considère un arc en série avec une résistance. Le modèle d'arc d'Ayrton a été utilisé pour rendre compte de la variation de la tension d'arc en fonction du courant de fuite. Les constantes à l'arc, ainsi que les paramètres de réallumage ont été déterminées en utilisant une modèle physique cylindriques de laboratoire.

Le modèle utilise des méthodes d'identification intelligente pour déterminer les variables pertinentes associées à l'expression mathématique du phénomène de contournement. De nouvelles approches fondées sur un estimateur des moindres carrés (*Least Squares*

*Estimator* : LSE), ainsi que des algorithmes d'apprentissages pour système d'interférence floue (Adaptive Network-Based Fuzzy Inference System : ANFIS) ont été appliquées afin d'en extraire la formule mathématique de la chute de tension aux bornes de l'intervalle non franchi de l'isolateur. La formule ainsi proposée, intègre les principales variables influençant le comportement électrique de la partie résiduelle de l'isolateur recouvert de glace contaminée durant la phase de propagation de l'arc. En outre, l'expression mathématique proposée pour la tension résiduelle aux bornes de l'intervalle non franchi de l'isolateur a permis d'extraire la formule de calcul de la variation spatiale de la résistance résiduelle de l'intervalle non franchi. La formule dépend des principales variables telles que la conductivité de l'eau de congélation, la densité de sel déposé, le courant de fuite et la longueur de l'intervalle non franchi. Le modèle a été appliqué aux isolateurs industriels et les tensions de contournements calculés ont été en bon accord avec ceux obtenus à partir d'essais de contournement en laboratoire.

## Acknowledgment

This work was carried out within the framework of the NSERC/Hydro- Quebec/UQAC Industrial Chair on Atmospheric Icing of Power Network Equipment (CIGELE) and the Canada Research Chair, tier 1, on Engineering of Power Network Atmospheric Icing (INGIVRE) at the University of Quebec in Chicoutimi.

I would like to express my deepest gratitude toward my director of studies, Professor Masoud Farzaneh, for his supervision and supports during the entire project; and my codirector, Dr. Jianhui Zhang for his helpful remarks and his devotion. I would like give recognition to all of my professors during all stages of my academic education for their precious discussions and invaluable advices. I would thank all members of jury of examiners Dr Rizk and Dr Chisholm for their contributions to the evaluation of my thesis. I would specially express my gratitude to Dr Issouf Fofana, president of jury, for conducting my defense session.

I would like to thank M Pierre Camirand, M Marc Andre Perron and M Xavier Bouchard whose assistances and technical supports made it possible to perform all required experiments for this study. I would also like to thank Mme Marion Lougheed whose editorial help was invaluable in making this text legible. I would also appreciate all supports and encouragements I received from all my friends, particularly Mm Linda Guillmette, Mr. Hossein Hemmatjou, Mr. Ping Fu and Mr. Vinay Kumar Jaiswal during the course of my study.

**This work is particularly dedicated to my lovely Parent who gave me the life and brought me up. Their personality, behavior, attitude and lifestyle taught me to love and respect people and consider the ethics and moral values as the highest priorities in my life.**

**This work is also dedicated to all lovely people who have somehow had contributions to the beautiful bunch of unforgettable memories of my entire life.**

## TABLE OF CONTENTS

### CHAPTER I

1.1 INTRODUCTION.....	1
1.2 Description of the problem .....	2
1.3 Objectives of the thesis.....	4
1.4 Methodology.....	5
1.5 Statement of the originality of the thesis.....	6
1.6 Outline of dissertation.....	8

### CHAPTER II

#### REVIEW OF LITERATURE ON THEORETICAL BASIS OF FLASHOVER PHENOMENON ON POLLUTED SURFACES

2.1 INTRODUCTION.....	10
2.2 Basic definitions .....	12
2.2.1 Corona and arcing phenomenon.....	12
2.2.2 Arc modeling on conductive surface.....	15
2.2.2.1 Empirical arc models.....	16
2.2.2.1.1 Ayrton's Equation.....	16
2.2.2.2 Analytical arc models.....	18
2.3 The mechanism of dry bands formation and initiation of discharge process.....	20
2.3.1 Identification of types of pollution.....	22
2.3.1.1 Pollution Severity measurement methods.....	23
2.4 Resistance models on polluted surfaces.....	25
2.4.1 Mc Elroy and Woodson model.....	25
2.4.2 Wilkins resistance model .....	26
2.4.3 Form factor criterion.....	27
2.4.4 Zhicheng and Renyu model.....	28
2.4.5 Mekhaldi Model.....	29
2.5 Static models of pollution flashover.....	30
2.5.1 Direct current models.....	31
2.5.1.1 Obenaus model.....	31
2.5.1.2 Model of Neumarker.....	33
2.5.1.3 Model of L. L. Alston & S. Zoledziowski.....	33
2.5.1.4 Model of R Wilkins .....	35
2.5.2 Alternating current models.....	36
2.5.2.1 Energy re-ignition model.....	36
2.5.2.2 Dielectric re-ignition model.....	37

2.5.2.3 Model of P. Claverie .....	39
2.5.2.4 Model of B. F. Hampton.....	42
2.5.2.5 Model of G. Zhicheng & Zhang Renyu.....	42
2.5.2.6 P. S. Ghosh and N. Chatterje model.....	43
2.5.2.7 Model of H. H. Woodson & A. 8. McElroy.....	43
2.6 Dynamic modeling of flashover.....	44
2.6.1 The Model of F. A. Rizk.....	44
2.6.2 Model of R. Sundararajan & R S. Gonir.....	45
2.7 Physical interpretation of flashover phenomenon.....	45
2.8 Conclusion .....	47

### **CHAPTER III**

#### **LITERATURE REVIEW OF FLASHOVER ON ICE COVERED INSULATORS**

3.1 INTRODUCTION.....	50
3.2 Mechanism of ice accretion on high voltage insulators .....	51
3.3 Flashover of ice covered insulators.....	53
3.3.1 The influence of atmospheric parameters on electrical performance of high voltage insulators under icing condition.....	56
3.3.1.1 Air gaps and partial arcs.....	58
3.3.1.2 Freezing water conductivity.....	60
3.3.1.3 Dry arcing distance.....	61
3.3.1.4 Applied voltage type.....	61
3.3.1.5 Air pressure .....	62
3.4 Modeling of electrical arc on ice surface.....	63
3.4.1 Ice surface conductivity .....	63
3.4.2 Arc constants and re-ignition parameters on ice covered surface.....	63
3.4.3 Supplementary studies on arc behavior on ice surfaces.....	65
3.5 Modeling of flashover on ice covered surfaces.....	67
3.5.1 Static models.....	67
3.5.1.1 DC flashover model.....	67
3.5.1.2 AC flashover model.....	68
3.5.2 Dynamic modeling of flashover on ice covered insulators.....	70
3.6 Conclusion .....	72

### **CHAPTER IV**

#### **THEORETICAL DEVELOPMENT AND MODELLING OF FLASHOVER PHENOMENON ON CONTAMINATED INSULATORS COVERED WITH ICE**

4.1 INTRODUCTION.....	75
-----------------------	----

4.2 Static AC modeling of flashover on contaminated insulators covered with ice.....	76
4.2.1 Complicated nature of residual resistance under condition of joint effect of contamination and icing .....	78
4.2.1.1 Non-uniform pollution layer on insulator surface.....	78
4.2.1.2 Local melting phenomenon.....	79
4.2.1.3 Non linearity of potential and electric field distribution along insulator.....	80
4.3 New approach for determining V-I characteristic of residual part of insulator.....	85
4.3.1 Identification procedure.....	86
4.3.1.1 Structure identification.....	86
4.3.1.2 Parameters identification.....	87
4.3.2 Determination of the parameterized model of residual voltage.....	89
4.3.2.1 Least-squares estimator.....	90
4.3.2.2 Adaptive Neuro-Fuzzy Inference System (ANFIS).....	94
4.3.2.2.1 ANFIS architecture.....	95
4.3.2.2.2 Learning algorithm.....	98
4.4 Mathematical model developed for flashover on contaminated insulators covered with ice .....	98
4.5 Dynamic or differential resistance of contaminated insulators covered with ice.....	99
4.6 Conclusion.....	101

## CHAPTER V

### EXPERIMENTAL FACILITIES, TEST PRECODURES AND RESULTS

5.1 INTRODUCTION.....	103
5.2 Facilities of high voltage laboratory.....	104
5.2.1 High voltage equipments.....	104
5.2.2 Climate room.....	104
5.2.3 Data acquisition system.....	106
5.2.4 High speed camera.....	106
5.3 Test procedures.....	107
5.3.1 Test procedure for determining the arc constants and re-ignition parameters.....	107
5.3.1.1 Arc constants $A_p$ and $n_p$ .....	112
5.3.1.2 Arc re-ignition parameters $K_p$ and $b_p$ .....	115
5.3.2 Test procedure for determining the residual voltage $V_{Res}$ .....	117
5.3.2.1 Determination of V-I characteristic of residual voltage using LSE method.....	121
5.3.2.2 Determination of V-I characteristic of residual voltage using ANFIS.....	127
5.4 Dynamic or differential resistance of contaminated insulator covered with ice.....	132
5.4.1 Calculation of dynamic resistance using LSE.....	132

5.4.1.1 Quantitative comparison between dynamic and residual resistance .....	136
5.4.2 Calculation of dynamic or differential resistance using ANFIS.....	138
5.4.2.1 First approach.....	138
5.4.2.2 Second approach.....	141
5.5 validation tests.....	143
5.6 Application of the model to the industrial insulators and discussions.....	148
5.6.1 Discussion of the results . .....	152
5.6.1.1 Flashover voltage prediction for lower levels of SDD and $\sigma$ .....	156
5.6.1.2 The effect of arcing distance on flashover voltage.....	158
5.7 Conclusion.....	159

## **CHAPTER VI**

### **CONCLUSIONS AND RECOMMENDATIONS**

7.1 Concluding remarks.....	162
7.2 Recommendations for future works.....	167

<b>REFERENCES</b> .....	169
-------------------------	-----

Appendix A.....	179
Appendix B.....	182

## LIST OF FIGURES

Figure	Title	Page
2.1	Type A site pollution severity Relation between ESDD/NSDD and SPS for the reference cap and pin insulator	24
2.2	McElroy and Woodson circular disc model	25
2.3	Wilkins model for resistance of pollution layer	26
2.4	Cap and pin insulator and its equivalent plane model	28
2.5	Plane model for pollution layer. a) Near HV electrode, b) Near ground electrode	30
2.6	Equivalent circuit for Obenous model	31
2.7	Alston cylindrical model	34
2.8	Dependence of $V_{cr}$ on arc length x	34
2.9	Claverie's model	40
3.1	Air gaps formed on IEEE suspension and post-type insulators covered with artificial ice	59
3.2	Typical waveform used for determining arc constants	64
3.3	Calculated and experimental results of flashover voltages for wet-grown ice sample of 0.3 m length	69
3.4	Calculated and experiment results of flashover voltage with 5 units of IEEE insulator	70
3.5	Equivalent circuit used for modeling arc propagation on iced surface	71
4.1	Circuit representation of static model	77
4.2	Ice covered insulator at three steps of arc propagation.	78
4.3	Electric potential distribution along tiny porcelain surface in parallel with salt and ice strips.	80
4.4	Electric field distribution.	82
4.5	Electric field distribution along ice surface.	83
4.6	Block diagram of parameter identification procedure	97
4.7	Flowchart representation of structure and parameter determination process.	93
4.8	ANFIS based system identification	94
4.9	a) A two-input first-order Sugeno fuzzy model with rules; b) Equivalent ANFIS architecture	96
5.1	Climate room	105
5.2	Cylindrical sample	108
5.3	Laboratory sample used for investigating arc characteristic	109
5.4	Arc propagation along the cylindrical model.	110
5.5	Arc voltage and leakage current waveform at the moment when the arc passes the measuring electrode.	110
5.6	$E/I_m$ curve obtained for arc length: $X=8.5$ cm	113

5.7	$E/I_m$ curve obtained for arc length $X=10.5$ cm	113
5.8	$E/I_m$ curve obtained for arc length $X=12.5$ cm	114
5.9	The measured results for the re-ignition condition	116
5.10	Five-unit IEEE standard insulator string used for determination of $V_{Res}$	118
5.11	Laboratory setup used for determining $V_{Res}$	119
5.12	Arc length observation using high speed camera.	121
5.13	Estimated and recorded residual voltage ( $V_{Res}$ )	124
5.14	V-I characteristic of residual part of insulator	126
5.15	MATLAB graphic user interface (GUI) for ANFIS	128
5.16	ANFIS structure	129
5.17	Membership functions used for input variable SDD	130
5.18	ANFIS training	131
5.19	Comparison between calculated $V_{Res}$ using LSE and ANFIS	132
5.20	Dynamic or differential resistance as a function of ESDD and $\sigma$	134
5.21	Comparison of individual effect of SDD and $\sigma$ on dynamic residual resistance. a) $R(x)$ versus SDD, $\sigma = 30 \mu S / cm$ b) $R(x)$ versus $\sigma$ , $SDD = 0.03 mg / cm^2$	135
5.22	Comparison between calculated resistance using LSE and the formula of R. Wilkins	136
5.23	A sample waveform used for establishing $(U_i, (\frac{dV}{dt})_i)$ data set.	139
5.24	Magnified waveform corresponding to the time interval $p_1$ shown in	140
5.25	Magnified waveform corresponding to the time interval $p_2$ shown in	140
5.26	Estimated resistance using LSE and ANFIS (First method)	141
5.27	V-I characteristic of $V_{Res}$ used for calculating the resistance	142
5.28	Estimated resistance using ANFIS and LSE. (Second method)	143
5.29	Validation test resulted with withstand	144
5.30	Validation test resulted with flashover	145
5.31	Five-unit IEEE standard insulator string used for validation test and the moment just after flashover.	146
5.32	Flashover test results on five-unit IEEE standard insulator string	147
5.33	$V_m$ versus x. SDD=0.03 ( $mg/cm^2$ ) and $\sigma=30(\mu S)$	150
5.34	$V_m$ versus x. SDD=0.05 ( $mg/cm^2$ ) and $\sigma=30(\mu S)$	150
5.35	$V_m$ versus x. SDD=0.1 ( $mg/cm^2$ ) and $\sigma=30(\mu S)$	151
5.36	Calculated and experimental results of flashover voltage with 5 units of IEEE standard insulators	152
5.37	Flashover voltage & Critical current versus ESDD	154
5.38	Recorded Voltage and Current waveforms during last minute of flashover test	155
5.39	Calculated flashover voltage for SDD=0.01 ( $mg/cm^2$ ), $\sigma = 10(\mu S)$ and $L=809$ (mm)	156

5.40	Flashover voltage versus freezing water conductivity	157
5.41	Calculated flashover voltage versus relative insulator length. L=870 (mm), SDD=0.1 (mg/cm <sup>2</sup> ) and $\sigma = 30(\mu S)$	158

## LIST OF TABLES

Table	Title	Page
1.1	Salt deposited on highway lanes	3
2.1	Arc constants used by different investigators	17
3.1	Ice types' characteristics	52
3.2	Ice accumulation regimes and ambient conditions	53
3.3	Maximum withstand stress of short string of IEEE standard 62 insulators under wet-grown ice	62
4.1	Electrical properties of materials	83
4.2	Two passes hybrid learning procedure of ANFIS	98
5.1	Ice type and ambient conditions	105
5.2	The range of parameters characterizing test conditions	111
5.3	Input variables of train and test dataset	120
5.4	Validation test conditions	146

## LIST OF ABBREVIATIONS AND SYMBOLS

<b>AC</b>	Alternating current
<b>ANFIS</b>	Adaptive Neuro-Fuzzy Inference System
<b>CIGELE</b>	NSERC/Hydro-Quebec/UQAC Industrial Chair on Atmospheric Icing of Power Network Equipment
<b>DC</b>	Direct current
<b>DC+</b>	Positive direct current
<b>DC-</b>	Negative direct current
<b>DDGIS</b>	Dust Deposit Gauge-Index Soluble
<b>DDGIN</b>	Dust Deposit Gauge-Index Non-Soluble
<b>ESDD</b>	Equivalent salt deposit density
<b><i>E - I</i></b>	Voltage gradient-current characteristic
<b>HV</b>	High Voltage
<b>IEC</b>	International Electro technical Commission
<b>INGIVRE</b>	Canada Research Chair, tier 1, on Engineering of Power Network Atmospheric Icing
<b>IEEE</b>	Institute of Electrical and Electronics Engineers
<b>LTE</b>	Local Thermodynamic Equilibrium
<b>NaCl</b>	Sodium Chloride
<b>NSDD</b>	Non-Soluble Deposit Density
<b>PID</b>	Proportional Integral Differential
<b>UQAC</b>	University of Quebec in Chicoutimi
<b><i>V-I</i></b>	Voltage – Current characteristic
<b>A</b>	Arc gradient constant
<b><math>A_p</math></b>	Arc gradient constant of contaminated and ice covered surface
<b>b</b>	Arc re-ignition component
<b><math>b_p</math></b>	Arc re-ignition component of contaminated and ice covered surface
<b><math>E_{Arc}, E_a</math></b>	Arc voltage gradient
<b><math>E_{Ws}</math></b>	Maximum withstand stress
<b><math>E_c</math></b>	Critical field strength
<b><math>E_p</math></b>	Voltage gradient across polluted layer
<b>g</b>	Arc conductance
<b><math>g_0</math></b>	Arc conductance at current zero
<b><math>I_m</math></b>	Current (Peak Value)
<b><math>I_{Arc}</math></b>	Arc current
<b>I</b>	Critical arc current
<b>K</b>	Arc re-ignition parameter
<b><math>K_p</math></b>	Arc re-ignition parameter of contaminated and ice covered surface
<b><math>k_s</math></b>	Conductivity of the pollution layer
<b>L</b>	Insulator length
<b><math>L_{Arc}</math></b>	Arc length
<b>n</b>	Arc constant
<b><math>n_p</math></b>	Arc constant of contaminated and ice covered surface

$P$	Air pressure
$P_0$	Air pressure at sea level
$P_{in}$	Power injected to the arc column
$P_{out}$	Power dissipated by the arc column
$\hat{P}$	Parameter vector
$r, r_0$	Arc radius
$R_p$	Resistance of the polluted layer
$r_p$	Resistance of the polluted layer per unit length
$S$	Thermal flux of arc column
$T$	Arc column temperature
$U_d$	Dielectric strength of the residual gap
$U_i$	Input vector of identification method
$V_{app}$	Applied voltage
$V_b$	Breakdown voltage of air gap
$V_c$	Critical flashover voltage
$V_{Res}$	Residual voltage
$y$	Target system's output
$\hat{y}$	Model's output
$\rho$	Relative air density
$\tau$	Arc time constant
$\sigma_s$	Surface conductivity of the pollution layer
$\sigma_e$	Conductivity of the pollution layer at the flashover moment
$\gamma_e$	Equivalent surface conductivity
$\delta$	Ice thickness

# CHAPTER I

## 1.1 INTRODUCTION

A reliable and continuous power delivery has always been the highest priority for maintaining an effective and high quality performance of a power network from both technical and economic viewpoints. Therefore, maintaining the effective performance of the power system requires minimizing the number of factors that are major threats to the reliability of the network.

Generally, in developed countries with power networks supervised by sophisticated control systems, the most deteriorating factor on network reliability is the power outages caused by severe atmospheric conditions which are out of human control. In Canada and North America and many cold climate areas, these atmospheric conditions mainly appear as heavy ice or snow accumulation on overhead transmission line structures accompanied by wind effect causing mechanical damage. [45, 71, 115].

Alongside the power failures originating from mechanical damage on power system equipment, the majority of power outages occur in adverse winter weather as the result of deterioration of electrical performance of high voltage insulators used in overhead transmission lines under icing conditions [6, 9, 76, and 77]. The presence of ice on the surface of insulators causes a drastic decrease in the electrical insulation level, which may lead to electrical flashover and a consequent power outage. This phenomenon has been reported in several cold climate countries, particularly Canada [6,18], China [100], Japan [9], Norway [41], the United States [62], and former Yugoslavia [113]. Therefore, the importance of this phenomenon has motivated many studies on understanding the nature of electrical

discharge and the resulting flashover phenomenon on ice covered insulators. These studies mainly include field observations [18], laboratory investigations of the ice accretion process and prediction of critical flashover voltage on ice-covered insulators [19,20,21,22,23,24]. The most recent and comprehensive studies in this field were conducted in the high voltage laboratory at NSERC / Hydro-Quebec / UQAC Industrial Chair on Atmospheric Icing of Power Network Equipment (CIGELE) and Canada Research Chair, tier 1, on Engineering of Power Network Atmospheric Icing (INGIVRE) at Université du Québec à Chicoutimi, including the investigations and development of mathematical models on arc development on an ice surface [25,26,27,28,29,30,31]. The results of these studies do not only supply key knowledge to further academic research, and also are of very high importance from a technical viewpoint on power network coordination, so that the results of this research have contributed to modeling and manufacturing a proper shape and surface of suitable insulators used in cold climate regions [32,33].

## **1.2 Description of the problem**

In addition to the above mentioned problem caused by flashover of insulators under icing conditions, pollution is another factor that decreases the insulating strength of insulators under wet conditions. The condition of contamination accompanied by icing is substantially worse than that of a single pollution type. The ice layer supplies the wet conditions to the pollution layer and in return the conductive materials in the pollution layer could increase the conductivity of the water film on the ice surface.

The deterioration in electrical performance of insulators due to the joint effect of ice and pollution in power lines in China and England has been reported to cause insulator flashover

[100,42]. Moreover, the destructive effect of cold precipitation and insulator contamination was reported on Norwegian and North American power lines, caused by sea salt and man-made ions containing sulphur and nitrogen in the vicinity of highways or urban regions especially with heavy industries. [41, 38]

Salt usage for de-icing of highways, especially in North America during long wintertime, is one of the major natural sources for insulator contamination [88]. Table 1.1 summarizes the amount of salt used in urban regions for de-icing purposes. In the areas with such an amount of salt usage, the insulators of transmission lines are subjected to a pre-contamination process. Salt being deposited on the surface of insulators forms a complicated type of contamination layer on insulators under icing conditions.

**Table 1.1** Salt deposited on highway lanes [39]

<b>Highway type</b>	<b>Winter season density Tons of salt per lane mile</b>
<b>Four-lane divided highway</b>	<b>16-17</b>
<b>Interstate (six lanes)</b>	<b>23-26</b>

These reports confirm that the presence of atmospheric ice together with superimposed contamination sometimes leads to flashover and consequent power outages [22]. So far a large number of studies accompanied by experiments have been carried out on understanding the flashover phenomena on either polluted or ice-covered insulators. Also many efforts have been made on establishing mathematical models with the aim of predicting the flashover voltage of polluted [95] or ice-covered insulators, separately [25,26,27,28,29,30,31]. The analytic basis of the majority of models is the Obenaus concept of discharge phenomenon [88], by which the mechanism of the flashover process was represented by a local arc in series with the residual resistance of pollution or ice layer. It is

also well known that calculation of residual resistance plays an important role in prediction of the flashover voltage of polluted or ice-covered insulators [38].

A review of literature and publications on polluted or ice covered insulator flashover confirms the lack of a comprehensive study on flashover caused by the joint effect of pollution and ice accumulation. This fact has motivated this study to focus on modeling the flashover voltage of H.V. insulators exposed to the atmospheric condition of pollution accompanied by ice.

### **1.3 Objectives of the thesis**

The main goal of this PhD thesis is to study the flashover phenomenon of contaminated insulators covered with ice, mainly concentrating on analyzing the extremely complex nature of residual voltage of the un-bridged part of the insulator, as well as calculating the residual resistance based on new approaches relying on analytic-empirical identification methods, under condition of the joint effect of pollution and ice accumulation. More specifically, this project includes the followings steps:

1.3.1 Investigating the flashover phenomenon on ice covered contaminated insulators by practical experiments in the HV laboratory of CIGELE for understanding the special nature of flashover and determination of arc characteristics including constants  $A$  and  $n$ , as well as the arc re-ignition conditions.

1.3.2 Developing a mathematical expression for the voltage of the residual part based on the

experimental results using intelligent identification methods.

1.3.3 Establishing a mathematical model based on the Obenaus concept of the discharge phenomenon for predicting the flashover voltage of insulators under the condition of pollution and icing.

1.3.4 Extracting a mathematical formula representing the resistance of the un-bridged part of the insulator from V-I characteristic proposed in this study.

1.3.5 Verifying the validity of the model by performing a series of tests on HV insulators.

#### **1.4 Methodology**

This study primarily deals with the analysis of the joint effects of major parameters influencing the arc characteristics on contaminated surfaces covered with ice. The model has accounted for the major parameters to determine the arc characteristics such as ice thickness  $\delta$ ; freezing water conductivity  $\sigma$ ; ambient temperature  $\theta$ ; and the salt deposit density, SDD.

Based on the results obtained from a series of experiments carried out on cylindrical laboratory samples, as well as practical insulators, a mathematical model of flashover on contaminated insulators covered with ice is presented in this study. A static arc model developed on the basis of Obenaus concept of arc discharge in series with a residual

resistance [84]. The arc constants  $A_p$  and  $n_p$ , as well as the arc re-ignition parameters  $K_p$  and  $b_p$ , were determined.

The application of intelligent identification methods such as Least Square Estimator (LSE), as well as Adaptive Network-Based Fuzzy Inference System (ANFIS), made it possible to propose a mathematical expression for the V-I characteristic of the voltage of the residual part of the insulator. The mathematical model thus proposed enabled us to determine the residual resistance of contaminated insulators covered with ice.

### **1.5 Statement of the originality of the thesis**

As previously stated, the importance of decreasing the number of power outages caused by flashover of ice covered or polluted insulators has always been considered a vital factor for maintaining a reliable power delivery at the highest possible level. A brief review of the literature on polluted and ice covered insulators is presented in Chapter II and III, respectively. Although the results of these studies had their own contributions for promoting the accuracy of mathematical models on predicting the flashover voltage, the extent of the publications on investigating the joint effect of pollution and ice accumulation on electrical performance of insulators was limited to a few reports of flashover occurrences in power networks under this condition. [42,77,100,41]. A survey of the literature reveals the lack of studies directly dealing with quantitative calculation of the flashover voltage of high voltage insulators under the condition of contaminated surface covered with ice.

Because of the complicated nature of the residual resistance of contaminated insulators covered with ice, the study of this condition requires particular methods of analysis with the

aim of taking into account the effects of the factors governing the variation of the voltage of the residual part of a real insulator during the arc propagation.

The major factors preventing us from applying all previously proposed classical models in this condition may be described as follow:

- 1) Local melting phenomenon leading to the interaction of pollution and the ice layer.
- 2) Migration of pollutants from polluted layers through the ice thereby providing the ionized particles to the ice surface. This situation causes an instantaneous change in the conductivity of residual resistance during arc propagation.
- 3) Non-linear electrical stress along the insulator's length.
- 4) Non-uniform distribution of the polluted layer.
- 5) Non-uniform ice accumulation and the presence of multiple air gaps.

A new investigation approach based on analytical methods in addition with the results obtained from observations and measurements was followed in this study. The application of this method made it possible to derive a mathematical expression as a function of the major parameters influencing the voltage of the residual part of a real insulator such as freezing water conductivity ( $\sigma$ ), salt deposit density (SDD), leakage current (I), and arc length (x). The mathematical formula derived based on this method was then supplied to the static AC model to complete the required set of mathematical equations for calculating the flashover voltage. Moreover, a mathematical formula representing the resistance of the residual part of the pre-contaminated insulators covered with ice was also proposed.

## 1.6 Outline of dissertation

The PhD thesis presented in this dissertation discusses major topics dealing with analysis and modeling of the flashover phenomenon of contaminated insulators covered with ice through the following chapters:

- **Chapter 1** introduces the problems caused by the insulator flashover phenomenon in power networks, as well as a brief review of the literature and reports on the deterioration of insulators' electrical performance under icing and contamination conditions.
- **Chapter 2** provides literature reviews of basic definitions on the mechanism of discharge and arcing phenomena, including arc modeling and resistance models of contaminated surfaces. A summary of the mathematical models for predicting the flashover voltage of polluted insulators under DC and AC excitation is also given in this chapter.
- **Chapter 3** is a survey of the literature on investigation of arc characteristics on ice covered surfaces. The influence of ice types, as well as atmospheric parameters on the flashover voltage of ice covered insulators is discussed in this chapter followed by a brief review of modeling of flashover on ice covered insulators.
- **Chapter 4** presents the theoretical basis of the model developed for calculating flashover voltage under the joint effect of pollution and icing. This chapter proceeds with introducing the mathematical tools used for structure and parameter identification of the mathematical formula proposed in this study. The Least Square

Estimation (LSE) and Adaptive Network Based Fuzzy Inference System (ANFIS) were used for identification purposes. Alongside the calculation of the flashover voltage of contaminated and ice covered insulators, a formula is proposed for calculating the residual resistance  $R(x)$  under this condition.

- **Chapter 5** describes the test facilities, test procedures and methodology followed in this study. A comparison between the calculated results and those obtained from validation tests is also provided in this chapter.
- **Chapter 6** provides the conclusions and the general features of future works that may follow within this framework.

## **CHAPTER II**

### **REVIEW OF LITERATURE ON THEORETICAL BASIS OF FLASHOVER PHENOMENON ON POLLUTED SURFACES**

#### **2.1 INTRODUCTION**

The problem of flashover of polluted insulators has motivated a large number of theoretical studies over many decades to the better understanding of the mechanism of this phenomenon [1,2,14,48,49,89], as well as to develop mathematical models [95] with the aim of devising realistic solutions to overcome this problem. The flashover phenomenon has demonstrated itself to be a limiting constraint since the power transmission was accomplished at higher voltage levels to achieve a more effective power delivery. Problems of power dissipation due to the corona or partial discharges in high voltage transmission lines were related to higher level of electric field stress and were managed with the use of bundle (multiple conductors). The flashover phenomenon initiated by partial discharges has also more recently been recognized as an undesirable manifestation of the discharge phenomenon of high voltage networks operated at higher level of electric field stress.

It is well known that flashover is a phenomenon that takes place as a result of the joint effect of partial discharge accompanied by a conductive layer deposited on an insulator's surface. The origins of the formation of this conductive layer on the insulator's surface may be natural or man-made pollutants such as dust, chemicals and salt in industrial areas or in the vicinity of highways [34]. Until now, many intensive studies and much

laboratory work have been accomplished or are still ongoing with the aim of improving insulator design to promote electrical performance under contaminated conditions [15]. However, owing to the complexity of the problem, the modeling of flashover on polluted insulators is still a challenge since the proposed models should take into account a majority of physical conditions, such as the insulator's geometry and non-uniform pollution layers on the insulator's surface. Moreover, although the basic nature of the formation of a pollution layer under the joint effect of various forces is quite well known, but the interaction between the insulator's surface and the surrounding medium supplying pollutants to the conductive layer exacerbates the situation to be analyzed [70]. Hence, the modeling of the flashover phenomenon under these conditions requires some simplifying assumptions paving the way toward attaining proper models capable of simulating the nature of arc behavior from its early initiation until completion. In spite of several obstacles mentioned above, there are many partially successful attempts at establishing models capable of predicting the insulating performance of polluted insulators.

In this chapter, an overview of the different existing mathematical models for flashover on insulator's surface is provided. Because of their importance as a basis to this study, most of these models are static models predicting the flashover voltage under DC and AC excitation.

High voltage insulators under DC excitation are more likely to be susceptible to flashover, since DC insulators are subjected to the higher degree accumulation of contaminants than that of AC insulators [11]. However, in most electrical energy transmission networks, power delivery is accomplished under AC conditions emphasizing the importance of studies and modeling of the flashover phenomenon under AC conditions. It should be mentioned that the

basis of AC static modeling is the same as DC modeling, with additional re-ignition conditions [14].

Static models have been proven to provide flashover voltage predictions in excellent agreement with experimental results [14,82,118], however they were not able to account for all major factors characterizing the flashover phenomenon, such as the mechanism of arc propagation or arc velocity during the course of arc propagation. These aspects of particular studies of arc propagations have mostly been covered by dynamic models proposed for better explaining the arc propagation process [16, 60,94,101].

Before proceeding to discuss flashover on polluted surfaces, a brief review of electrical discharge and the arcing phenomenon will be presented, as they are the theoretical basis of all mathematical models dealing with flashover of insulators.

## **2.2 Basic definitions**

### **2.2.1 Corona and arcing phenomenon**

Corona is a partial electrical discharge initiated by the ionization of a the air surrounding a conductor or electrode which occurs when the potential gradient exceeds a certain value but conditions are insufficient to cause a complete electrical breakdown leading to the formation of an electric arc. However, when the electric field intensity is high enough at a point in the fluid, the fluid at that point ionizes and becomes a conductive medium forming an electric arc. [12,86].

Corona discharge is one of the major origins of power losses on transmission lines as the discharge current is in the phase with the applied voltage so that it is considered as pure Ohmic losses. However in certain circumstances it was found to be a positive factor in the

situation when a lightning surge loses its energy due to corona dissipation while it is traversing power lines. Corona discharge may also cause audible noise or interference in telecommunication, radio and television systems. Because of its importance in electrical engineering applications, corona has been the main subject of extensive studies. Based on many measurements, an empirical relation of corona inception under AC voltage in air was developed by Peek [86], Kuffel and Zaengl [64, 65] as:

$$\frac{E_c}{\rho} = 31.53 + \frac{9.63}{\sqrt{\rho r}} \quad (2-1)$$

Where  $E_c$  is the critical field strength of corona inception in kV/cm,  $\rho$  is the relative air density and  $r$  is the radius of the inner conductor in cm. Alongside the atmospheric conditions and geometry of the electrode, another factor influencing the visual appearance of corona is the polarity of the applied voltage, so that if the negative field threshold is reached, *trichel* pulses are observed, whereas a *Hermstein* glow zone and pre-breakdown streamers are observed above the positive threshold field. On a transmission conductor and under negative polarity, the corona appears as reddish glowing spots distributed along the conductor. The number of spots increases with the field gradient at the conductor's surface.

When the electric field intensity at the tip of an electrode or on a conductor surface is high enough and the surrounding medium is sufficiently susceptible for ionization, the state of partial discharge can change to an electrical arc [12, 65]. The current of the electrical arc is greater than that of glow discharge since the electrical arc is a completely ionized gas. At

atmospheric pressure, this arc column has a concentration from  $10^4$ - $10^8$  electron/cm<sup>2</sup> in high temperature plasma with good electrical conductivity [12, 86].

It was deduced from physical behavior that an electric arc could be defined in terms of current and voltage drop across it, but many factors, such as atmospheric pressure, type of power sources and electrode forms, have their individual influence on its behavior [12,86]. The most representative expression for electric arc behavior is a non-linear relationship between current and voltage with a decreasing resistance manifestation, so that, once the arc becomes established, any increase in leakage current results in a lower voltage drop between the arc tips. This diminishing impedance property of the arc requires some augmenting form of impedance to be inserted in the circuit, if it is desired to maintain a stable arc or reduce it to the extinction level. This property is the reason that uncontrolled electrical arcs in a high voltage apparatus become so destructive that they are capable of causing a flashover as happens on high voltage insulators.

Owing to the relatively high density of electrons and positive ions in an arc column, the electric arc cannot be initiated only by secondary electron emission. Kuffel and Zaengl have classified electric arcs into three categories according to the mechanism of their ionization process as [65]: 1) Thermionic arc, from a cathode being heated by an external source. When the temperature of the electrode is increased up to 1500-2500°K, the electrons receive sufficient energy to cross the surface barrier and leave the metal; however, the mechanism of this kind of emission also depends on the type and form of the metal from which the electrode was made. 2) Thermionic arc, from a cathode being heated by the arc itself. The mechanism of creation of this kind of arc is almost the same as thermionic arc

except in this case the electrode is being heated by the arc itself instead of an external source.

3) Arc initiated solely by field emission. This kind of emission takes place under a high electrostatic field capable of drawing electrons out of a metal surface. In order to produce an emission current of a few microamperes, the required electrostatic field is in the order of  $10^7$  to  $10^8$  V/cm [65].

### 2.2.2 Arc modeling on conductive surfaces

The investigations carried out by several researchers on the physical behavior of the arc as an electrical circuit element resulted in significant ramifications for the mathematical models proposed for arc simulation. However, as a general classification, the major approaches on dealing with the arcing phenomenon may be classified into two categories.

With the first category, a certain group of investigators were interested in modeling the dynamic arc by expressing the instantaneous arc states in terms of ordinary or partial differential equations to be solved in proper initial and boundary conditions [78,43,72,8]. The results of these methods (referred to as analytical arc models) have provided the theoretical basis for the investigations carried out on designing power system apparatuses such as high voltage breakers [3,68], as well as the dynamic modeling of insulators' flashover under various atmospheric conditions [16,101,60,4,35].

The second group of researchers, however, has dealt with modeling the electric arc by proposing mathematical relations between arc voltage and current, incorporating a number of parameters to be determined by experimental data. It was assumed in this method of arc modeling (referred to as the empirical method) that the electric field is uniform over the arc

length, so the proposed models were expressed as parametric relations between the voltage gradient across the arc  $E_{Arc}$  and the current  $I_{Arc}$  flowing through the arc column.

#### 2.2.2.1 Empirical arc models

##### 2.2.2.1.1 Ayrton's Equation

As an attempt to derive a mathematical expression for analyzing the arc behavior, Ayrton introduced a non linear formula relating the arc voltage to the arc current as given below: [10]:

$$V_{Arc} = (a + b.l) + \frac{c + d.l}{I_{Arc}} \quad (2-2)$$

Where  $V_{Arc}$ ,  $I_{Arc}$  and  $l$  are the voltage across the arc, arc current and arc length, respectively. The constants  $a$ ,  $b$ ,  $c$  and  $d$  should be determined by experimental data. The arc voltage gradient and current ( $E_{Arc} - I_{Arc}$ ) characteristic has been, however, expressed in the following form was utilized in static modeling the flashover of the polluted insulators by many researchers.

$$E_{Arc} = A.I_{Arc}^{-n} \quad (2-3)$$

Where,  $A$  and  $n$  are the arc constants to be determined based on experiments carried out under certain ambient conditions. The equation (2-3) implies that the arc voltage gradient is constant across arc length so that the arc voltage is calculated by multiplying the  $E_{arc}$  with the arc length  $x$ .

Table 2.1 Arc constants used by different investigators

	Investigator	Current (A)	$A$	$n$	Excitation	Medium
1	Suits and Hocker (1939)	1-10	65 220 81	0.6 0.6 0.6	NS NS NS	air stem nitrogen
2	Obenaus <i>et al.</i> (1958)	0.1-2	100	0.7	ac	air
3	L. Alston <i>et al.</i> (1963)	0.1-15	63	0.76	ac	air
4	E. Nasser <i>et al.</i> (1963)	0.1-1.0	63	0.76	dc	air
5	Hampton (1964)	0.1-0.5	65 52	0.8 0.1	NS NS	air steam
6	E. Los <i>et al.</i> (1971)	1-3	52	0.43	dc	air
7	Nottingham (1973)	NS	44 310 39.2 203	0.67 0.985 0.67 1.38	dc	air
8	Claverie <i>et al.</i> (1973)	1-2	113 98.99	0.5 0.5	ac	air
9	Jolly <i>et al.</i> (1974)	1-3	296	0.397	ac	air
10	El-Arbaty <i>et al.</i> (1979)	NS	40	0.8	ac	air
11	F. A. M. Rizk (1981)	0.05-2.0	130 210.6	0.45 to 1	dc	air
12	Gers <i>et al.</i> (1981)	0.1-5	46.05 44.77 43.80 59.64	0.91 0.822 0.822 0.773	dc impulse dc dc	air
13	M. P. Verma (1983)	NS	53.45	0.5	ac	air
14	Mayr <i>et al.</i> (1986)	NS	40.6 50.20 114	0.724 0.708 0.714	dc	air helium nitrogen
15	D. A. Swift (1989)	1-3	80 60	0.5	dc	air
16	G. Zhicheng <i>et al.</i> (1990)	0.1-1.0	138 140	0.69 0.67	dc ac	air
17	F. L. Topalis (1992)	NS	131.5	0.374	NS	air
18	R. Sundararajan <i>et al.</i> (1993)	NS	60 63	0.8 0.5	dc	air
19	R. P. Singh <i>et al.</i> (1994)	NS	31 to 100	0.43 to 0.98	ac	air
20	N. Chatterjee <i>et al.</i> (1995)	NS	NS	0.7	ac	air
21	H. G. Gopal <i>et al.</i> (1995)	NS	60 100	0.25 1.20	NS	air
22	D. C. Chaurasia <i>et al.</i> (1996)	0.01-1.2	50 100	0.25 to 1.1	ac	air
23	A. S. Farag <i>et al.</i> (1997)	NS	530	0.24	ac	air
25	M. Farzaneh <i>et al.</i> (2000)	NS	84 209 205	0.77 0.45 0.56	dc- dc+ ac	air, on the ice
24	J. P. Holtzhausen (2001)	NS	59	0.53	ac	air

Table 2.1 summarizes the values for  $A$  and  $n$  used by several investigators [95,84,2,34,15,60,101,46, 17, 47, 52, 83, 102,103,109, 111 and 119].

The arc constants  $A$  and  $n$  were determined by several researchers in the ranges of [31-310] and [0.1- 1.3], respectively. Obenaus *et al* have determined unique values of  $A=100$  and

$n=0.7$  for the AC arc, whereas these constants were recorded for the DC arc in the range of [130-210.6] and [0.45-1.0], by F. A. M Rizk [99]. The wide range of variation in arc constants is due to their dependency on several factors such as the medium in which the arc propagates, the ambient conditions, the electrolytic surface where the arc burns, as well as the voltage type [49 and 89].

It may be mentioned that the arc model presented by Ayrton is not the only empirical expression that has ever been proposed for arc modeling. Gopal and Rao have also proposed a slightly more elaborated expression than that of Ayrton with satisfactory results on analyzing the arc characteristics [46], but from the viewpoint of modeling purposes, the latter is of great importance as the theoretical basis for a majority of investigators on developing static models for predicting the flashover voltage of insulators under pollution or icing conditions.

#### 2.2.2.2 Analytical arc models

As previously stated, analytical arc models are mostly based on the equations of fluid dynamics governed by the laws of thermodynamics in combination with Maxwell's equations of electromagnetism theory. The arc is considered as plasma sustained by chemical reactions in addition to conservation of mass equations describing the rate equations of different chemical reactions [110].

When the arc is considered to be in local thermodynamic equilibrium under certain simplified conditions as a monatomic gas, the rate equations become the equilibrium of mass action laws known as Saha's equation describing the degree of ionization in the gas [53,90,91]. Because of the electrically conductive nature of the arc, the terms describing the

interaction of magnetic fields are taken into account in dynamic arc modeling. Moreover, the resistive heat dissipation of the electric energy calculated using Ohm's law is also a part of the energy equations. Based on the arc characteristics as mentioned above, the general differential equation describing the arc conductance was given as:

$$\frac{d[\ln(g)]}{dt} = \frac{F'(Q)}{F(Q)} (P_{in} - P_{out}) \quad (2-4)$$

Where  $g$  is the momentary arc conductance,  $Q$  is the energy content,  $F$  is a function of  $Q$  to be determined,  $P_{in}$  and  $P_{out}$  is the power injected to and dissipated by the arc column, respectively.

The solution of equation (2-4) requires appropriate assumptions relying upon a realistic hypothesis by which the appropriate mathematical model for function  $F$  is to be determined.

A.M. Cassie proposed a solution to the arc general equation under certain assumptions stating that the arc is a highly ionized gas with a variable channel in diameter because of being cooled down by gas flow, while the arc temperature  $T$  and the conductance per unit of arc volume of the remaining plasma channel are not affected. The Cassie model was applicable to study the behavior of arc conductance in the high current time interval where the temperature of the plasma is above  $8000^{\circ}K$  [8], therefore the model was appropriate to study the circuit breaker arc behavior in the high current regime.

Another solution was proposed by Mayr describing the arc conductance around current-zero conditions. In this model, arc channel is assumed to be cylindrical with a constant diameter where the arc channel loses its energy by radial heat transfer, which can be expressed as an approximation of Saha's solution for the general arc equation given by (2-4). By considering this assumption accompanied with the substitution of a constant power loss of the arc per

unit length channel into its general equation (2-4), the following equation for analyzing the arc conductance was attained:

$$\frac{d[\ln(g)]}{dt} = \frac{(u_{arc} i_{arc} - P_0)}{Q_0} \quad (2-5)$$

By recalling the fact that at the instant of current zero condition the input power  $u_{arc} i_{arc}$  to the arc channel is zero, the homogenous solution for (2-5) then reads as:

$$g = g_0 e^{-P_0 / Q_0 t} \quad (2-6)$$

Where  $Q_0 / P_0$  is the time constant  $\tau$  of the arc cooling without thermal input to the arc channel. The Mayr model as described above is quite suitable for analyzing the arc conductance behavior in the vicinity of current zero when the arc temperature is below  $8000^\circ K$  [78].

Following Cassie and Mayr, T.E. Browne proposed a combinational model utilizing the Cassie equation for a high current time interval and the Mayr equation for the current zero period [7].

The foregoing section was a brief review of the electrical arc models which were utilized in either static or dynamic modeling of flashover phenomenon. Following section deals with describing the joint effect of major atmospheric factors leading to initiation and establishment of the electrical arc on polluted insulator surfaces.

### 2.3 The mechanism of dry bands formation and initiation of discharge process

The voltage gradient needed to initiate a spark over in the air is about 30 kV/cm in uniform field, while for an outdoor high voltage insulator the required voltage gradient is about 500V/cm. Therefore, in order to initiate an arc on a polluted insulator surface, the voltage distribution should be highly non uniform. Generally, the formation of a dry band on a polluted insulator surface takes place in the following steps: [49]

A polluted surface subjected to wetting condition is initially dry and the voltage distribution is linear as long as the resistance per length of the conductive layer is uniform. As the layer becomes wet, its resistance decreases so the surface leakage current increases consequently. This condition does not last long due to the presence of slightly higher resistance zones formed by the joint effect of the leakage current and a non uniform voltage gradient. The voltage gradient in these locations may be high enough to result in arc discharges along small portions of the insulator's surface. Owing to the heat generated at the discharge root, the area in the near vicinity of the discharge dries out. The heat dissipation is more intense in these locations and therefore the area dries more rapidly than the remaining surface, resulting in the formation of dry bands. If several dry bands are formed, then after a short time only one dry band remains and due to its high resistance nearly all portions of the source voltage appear across this dry band. The width of the dry band changes until the voltage across it is slightly less than the voltage required to initiate a discharge in the air across it. Any moisture falling on the dry band distorts the electrical field in the band and discharge occurs: and a surge of current is generated. This surge current dissipates the heat energy in the discharge leading to a greater dryness of the band. The frequency of these surges, each of which may last for several cycles, is such that the mean power dissipated in the dry band is just enough to keep it dry. After the formation of the dry band, a sudden

increase in the applied voltage may lead to flashover of the surface, while a gradual increase may cause the dry band to widen. This process can occur every half cycle of AC waveform and the arc extinguishes at current zero and re-ignites in the next half cycle. During the subsequent cycles, the leakage current increases, leading to the formation of a longer arc along the insulator, which causes a greater portion of the applied voltage to appear across the rest of the polluted surface. This mechanism may result in either flashover or arc extinction depending on several factors influencing the discharge process, among which are environmental factors. The type and severity of the pollution play a key role in this process. Following is a brief review of the classification of pollution types, as well as the severity adopted by IEC 60815 Standard.

### 2.3.1 Identification of types of pollution [56]

There are two main basic types of insulator pollution that can lead to flashover:

*Type A:* where solid pollution with a non-soluble component is deposited onto the insulator's surface. This deposit becomes conductive when wetted. This type of pollution can be best characterized by Equivalent Salt Deposit Density / Non-Soluble Deposit Density (ESDD/NSDD) and Dust Deposit Gauge-Index Soluble / Dust Deposit Gauge-Index Non-Soluble (DDGIS/DDGIN) measurements.

Type A pollution is most often associated with inland, desert or industrially polluted areas. This kind of pollution can also arise in coastal areas in cases where a dry salt layer builds up and then rapidly becomes wetted by dew, mist, fog or drizzle.

*Type B*: where liquid electrolytes are deposited on the insulator with very little or no non-soluble components. This type of pollution can be best characterized by conductance or leakage current measurements.

Type B pollution is most often associated with coastal areas where salt water or conductive fog is deposited onto the insulator surface. Other sources of type B pollutions are, for example, crop spraying, chemical mists and acid rain.

#### 2.3.1.1 Pollution Severity measurement methods [56]

Depending on the conditions under which the pollution severity is being measured, three methods were proposed in IEC 60815 as follows:

1) Pollution severity measurements at a site are generally expressed in terms of:

- ESDD and NSDD for Type A pollution;
- Site Equivalent Salinity (SES) for Type B pollution;
- DDGIS and DDGIN for both types.

2) Pollution severity measurements on naturally polluted insulators are generally expressed in terms of:

- ESDD and NSDD for Type A pollution;
- Surface conductivity for Type B pollution.

3) Pollution severity in artificial pollution tests on insulators is generally specified in terms of:

- SDD and NSDD for solid layer methods;
- Fog salinity ( $\text{kg/m}^3$ ) for salt-fog methods.

According to the above mentioned classifications and for the purposes of standardization of the Site Severity Pollution (SPS), five classes of pollution levels, based on the ranges of ESDD and NSDD, characterizing the site severity have been defined as: a) Very light, b) Light, c) Medium, d) Heavy, and e) Very heavy.

Based on field measurements, experiences and pollution tests, the value recorded for the ranges of ESDD/NSDD corresponding to each SPS class is illustrated in figure 2.1 for Pin and Cap reference insulators. The values are the maximum values that can be found from regular measurements taken over a minimum period of one year. As shown in figure 2.1, a particular environment was denoted as  $E_i$  ( $i=1, \dots, 7$ ) corresponding to each mutual range of ESDD and NSDD. Definitions for environments are available in reference [56].

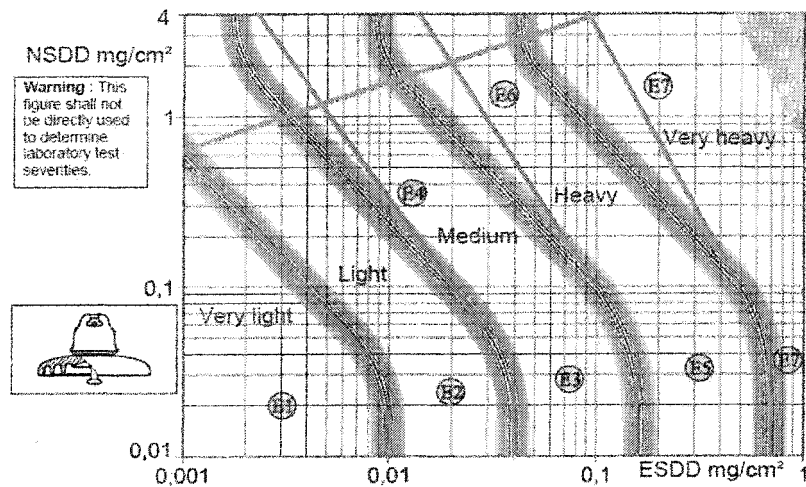


**Figure 2.1** Type A site pollution severity Relation between ESDD/NSDD and Site Pollution Severity SPS for the reference cap and pin insulator [56]

According to the classification mentioned above, appropriate approaches have been proposed for the selection and dimensioning of insulators used in overhead transmission lines in different environmental conditions.

## 2.4 Resistance modeling on polluted surfaces

Following is a brief review of the literature on resistance modeling of polluted surfaces proposed by different researchers. Among several resistance modeling methods, the models with practical and quantitative results are reviewed in this text.

### 2.4.1 Mc Elroy and Woodson model [117]

Mc Elroy and Woodson developed a resistance model for simulating the disc insulator using a model with a circular geometry as shown in figure 2.2. The authors assumed that the resistance of the polluted layer is independent of the arc foot point radius and proposed an imperial expression as:

$$R_p = \frac{Const.}{k_s} (r_o - r_a)^m \quad (2-7)$$

Where  $k_s$  is the surface conductivity of the pollutant, and the Constant and the exponent  $m$  were determined by means of experimental methods as  $1.6 \times 10^{-2}$  and 1.4, respectively.

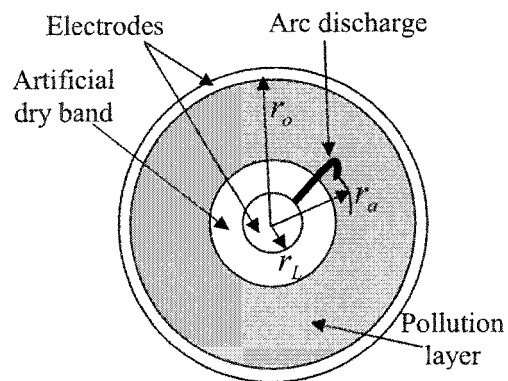


Figure 2.2, McElroy and Woodson circular disc model

Despite dealing with a more likely practical geometry of insulators in McElroy's model compared with the equivalent surface model of Wilkins, the model does not reflect the effect of the electric field strength on the current dispersion at the arc foot point which is indeed a function of the leakage current. Hence, owing to the lack of terms representing the effect of the arc root, it is evident that the formula given by (2-7) yields the same resistance values for two different arcs of the same length but considerably different leakage currents. This fact reveals that the formula given by Wilkins is more realistic than that of Mc Elroy and Woodson.

2.4.2 Wilkins resistance model [116]

In an attempt to calculate the resistance of a polluted surface in the presence of an arc burning at contact points, R. Wilkins considered the geometry as shown in figure 2.3.

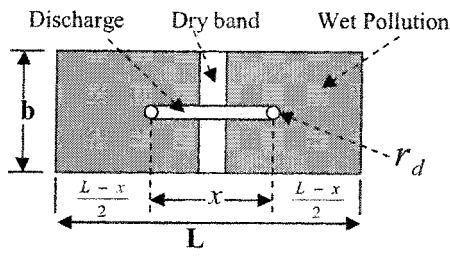


Figure 2.3, Wilkins model for resistance of pollution layer

The problem in the geometry as described in figure 2.3 is a two dimensional Laplace field equation to be solved with specified boundary conditions. The arc feet are considered the source of concentrated electric charges causing current flows through the pollution layer in the direction imposed by the electric field distribution. Depending on the geometry of the

polluted strip expressed as narrow and wide, R. Wilkins proposed two different solutions based on the theory of conjugate functions. The formulas for narrow strips where the length  $L$  is greater than the width  $b$ , and for the wide strip where the width is about three times the length are given by (2-8) and (2-9), respectively.

$$R_p = \frac{1}{2\pi\sigma_s} \left[ \frac{\pi(L-x)}{b} + \ell n\left(\frac{b}{2\pi r_d}\right) \right] \quad (2-8)$$

$$R_p = \frac{1}{2\pi\sigma_s} \left[ \ell n\left(\frac{2L}{\pi r_d}\right) - \ell n\left(\tan \frac{\pi x}{2L}\right) \right] \quad (2-9)$$

Where  $\sigma_s$  and  $r_d$  are the surface conductivity of the pollution layer and the radius of discharge root, respectively. Later, the formulas were expressed in terms of measurable quantities where the arc radius was replaced with the corresponding leakage current using the empirically derived formula:  $r_d = \sqrt{\frac{i}{K\pi}}$ . Where, the constant  $k$  is the current density at the arc foot measured as  $1.45(A/cm^2)$ , and  $I$  and  $r_d$  are measured in (A) and (cm), [116].

#### 2.4.3 Form factor method

The form factor of a certain insulator introduces an effective insulator diameter defined as follows:

$$D_{eff} = \frac{L}{\int_0^L \frac{dl}{D(l)}} \quad (2-10)$$

Where,  $dl$  is the differential element of the leakage path and  $D(l)$  is the insulator diameter at the length  $l$ . The form factor method makes it possible to define an average diameter for complicated geometry of real insulators. Relying on the concept thus described, the Wilkins formula has been applied to the real insulators by replacing the insulator geometry with its equivalent cylindrical surface with diameter of the effective diameter and the length of leakage path of the insulator. The equivalent strip then has a width of  $\pi.D_{eff}$  and a length of  $L$ . [116]

The form factor method was also used by Obenaus and Bohme in their composite models to calculate the resistance of polluted surfaces [5], as well as by Nasser [82], Ghosh and Chatterjee [48] for investigating the performance of practical post and suspension type insulators.

#### 2.4.4 Zhicheng and Renyu model [118]

In a plate model proposed by Zhicheng and Renyu, the surface area of a pin-and-cap insulator was replaced by the model as shown in figure 2.4.

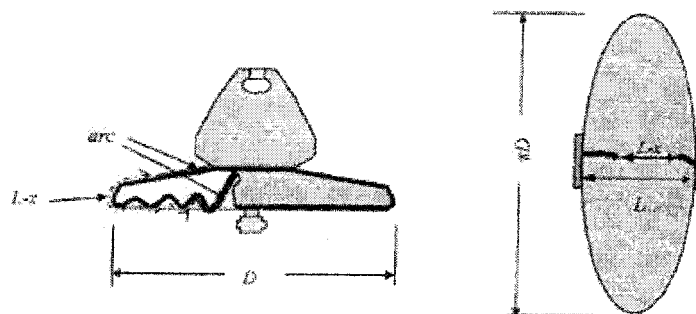


**Figure 2.4** Cap and pin insulator and its equivalent plane model [118].

In Figure 2.4,  $L$  represents the leakage length along the insulator,  $\pi D$  is the circumference,  $D$  is the diameter of the insulator, and  $r_d$  is the radius of the arc root. The resistance of the pollution layer is given as:

$$R_p = \frac{1}{\pi\sigma_c} \ell n \frac{L-x}{r_d} \quad (2-11)$$

Where  $\sigma_c$  is the conductivity of the pollution layer at the flashover moment given in terms of conductivity measured at room temperature  $\sigma$  as:  $\sigma_c = 1.25\sigma$ .

The formula given by (2-11) was derived under certain simplifying conditions relying upon the assumption that the plane model of the insulator is wide enough that the remaining polluted layer between the two arc roots can be expressed as the resistance between two small circular electrodes.

#### 2.4.5 A. Mekhaldi Model

The resistance model given by A. Mekhaldi *et al* [79] deals with a discontinuous pollution layer deposited onto the insulator's surface. The effect of the position of the dry band formed either in the vicinity of HV or ground electrode on the leakage current and the arc length was taken into account in this model. Two formulas were proposed for the resistance of the clean band and the polluted zone, where the total resistance of the discontinuous pollution is given as:  $Z_i(y) = Z_{od}(y) + R_p(y)$ , [84]. This concept is illustrated by the geometry as shown in figure 2.5.

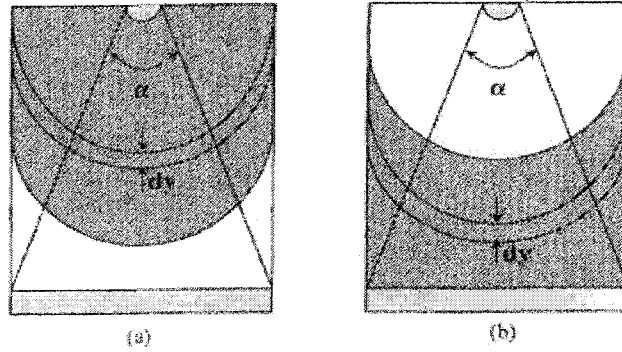


**Figure 2.5** Plane model for pollution layer. a) Near HV electrode, b) Near ground electrode

According to the geometry given by figure 2.5, the total resistance of the pollution layer plus the dry band for the geometries shown in figure 2.5 (a) and (b) are given by (2-12) and (2-13), respectively.

$$Z_t(y) = Z_{od} \left( \frac{L-y}{L} \right)^{0.42} + \frac{K}{\gamma} \ln \left( \frac{\alpha+y}{\alpha} \right) \quad (2-12)$$

$$Z_t(y') = Z_{od} \left( \frac{L-y'}{L} \right)^{0.42} + \frac{K}{\gamma} \ln \left( \frac{\alpha+L}{\alpha+L-y'} \right) \quad (2-13)$$

Where  $y$  and  $y'$  are the radius of polluted bands measured from high voltage electrode as shown in figures 2.5 (a) and (b). The first term in equations (2-12) and (2-13) is an empirically derived formula representing the resistance of the clean band.  $K$  is a constant and  $\gamma$  is the conductivity of the pollution layer.

## 2.5 Static models of pollution flashover

From the literature review, those models of flashover on polluted surfaces with quantitative and sufficient details with their applications are provided here. This review

mainly covers the literature on static modeling of flashover on polluted surfaces as it is the theoretical basis for the present study. However, for the purposes of making a comparison between the main features of dynamic and static modeling of flashover on polluted surfaces, this review includes a brief explanation of dynamic modeling at the end of this section.

## 2.5.1 Direct current models

### 2.5.1.1 Obenaus model

This is the first model in which a quantitative treatment of the pollution phenomenon has been considered for DC voltage. An arc burning in series with a polluted layer is considered as shown in Figure 2.6 [5, 85].

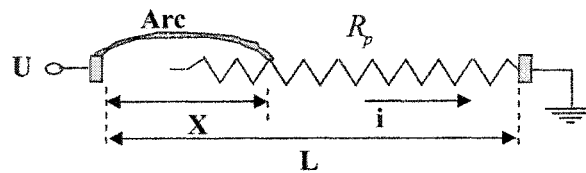


Figure 2.6 Equivalent circuit for Obenaus model

Figure 2.6 shows a schematic view of such a model. The circuit equation for this representation of an electric circuit composed of linear and non-linear elements can be expressed as:

$$U = A \cdot x \cdot i^n + i \cdot R_p \quad (2-14)$$

Where A and n are constants of the static-arc characteristics.

The following main assumptions are made in this model:

- A constant resistance per length is considered for a wet layer.
- The electric field is uniform.

Flashover will occur when the arc is able to bridge the length of the insulator when the arc length is equal to the insulator length and it travels without extinguishing at critical voltage.

The maximum arc length can be found by solving (2-14) for  $x$  and differentiating it with respect to  $i$  and equating the result to zero, thus:

$$i_c = \frac{nU}{(n+1)R_p} \quad (2-15)$$

Equation (2-15) yields the critical leakage current value, from which the critical arc length is given as:

$$x_c = \frac{n^n}{(n+1)^{n+1}} \frac{U^{n+1}}{AR_p^n} \quad (2-16)$$

Obenaus did not solve this equation (2-16) any further. By substituting the value of  $x$  in equation (2-16), the critical value of the voltage  $U = U_c$  for the critical arc length of  $x$  is given as:

$$U_{cx} = \frac{n+1}{n} A^{\frac{1}{n+1}} x_c^{\frac{1}{n+1}} R_p^{\frac{n}{n+1}} \quad (2-17)$$

This model only identifies the necessary conditions for flashover but not the sufficient condition. This means that it identifies the voltage below which no flashover can occur due to discharge extinction, but not the higher value at which the flashover will occur. This model assumes that flashover occurs if the discharge is able to bridge the insulator without extinguishing.

The model is applied to a flat polluted insulator plate, 10 cm long and 1 cm wide, a cylindrical insulator and IEEE insulators.

#### 2.5.1.2 Model of Neumarker [95]

The model of Neumarker was indeed a modified version of the Obenaus model. Neumarker considered a uniform resistance per unit length of the wet polluted layer instead of a fixed resistance of the pollution layer in series with the arc. In this model, the formula relating the minimum voltage required to maintain an arc with a relative length of  $x/L$  was derived, as well as an equation for the critical arc length.

#### 2.5.1.3 Model of L. L. Alston & S. Zoledziowski [2]

The physical test sample used in this model is composed of a cylindrical insulator of the length  $L$  with the electrodes connected at its two sides, as shown in Figure 2.7. An investigation was conducted in this model aiming at analyzing the mechanism of arc extinction. According to this model, the voltage required to maintain the discharge on a polluted insulator may increase with an increase in discharge length, and if this voltage exceeds the supply voltage, the discharge extinguishes without causing a flashover. Based on this mechanism, criteria which define flashover conditions have been developed. Flashover criteria in terms of formulas relating the applied voltage, critical stress, discharge length and resistance have been developed. Flashover is considered impossible if the applied voltage and the initial arc length are less than the critical values defined in this model.

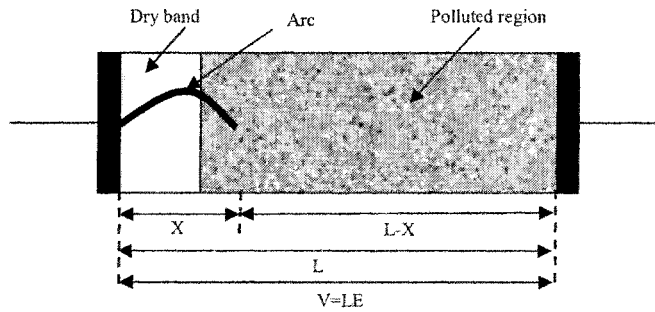


Figure 2.7 Alston cylindrical model

The main formulas representing the salient features of this model are as follows:

$$V = Axi^{-n} + ir_p(L-x) \quad (2-18)$$

Where,  $r_p$  is the resistance of the polluted layer per unit length. For any given arc length  $x$ , the voltage required to maintain this arc can be obtained by  $dV/di = 0$ , and the critical voltage is given as:

$$V_{cx} = (n+1)(Ax)^{1/n+1} \left\{ (L-x)r_p / n \right\}^{n/n+1} \quad (2-19)$$

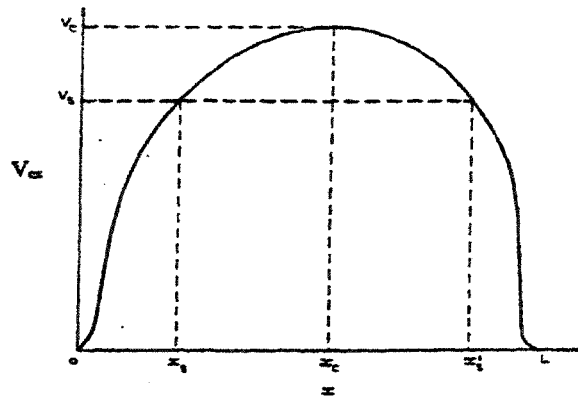


Figure 2.8 Dependence of  $V_{cx}$  on arc length  $x$  [3]

As can be deduced from figure 2.8,  $V_{cx}$  has a maximum value, called critical voltage  $V_c$ . For an applied voltage  $V_s$ , the arc can elongate up to an initial length of  $x_s$ ; as for a length greater

than  $x_s$ , the voltage required to maintain the arc is higher than the supply voltage. On the other hand, if the initial arc was  $x_s'$ , then any increase in the supply voltage would lead to flashover.

#### 2.5.1.4 Model of R. Wilkins [116]

This model also uses the same initial idea used by Obenaus, stating that the arc burns in series with the resistance of the pollution. Pollution can lead to the formation of quasi stable gas discharges which burn in series with the resistive polluted film. The main features of this model are:

- 1) A model for discharge burning on a rectangular plate is presented and uniform pollution is considered. The electrode drop voltage for both cathode and anode is 840 volts and the electrode drop voltage is independent of the discharge current.
- 2) When the voltage is applied to a flat plate with a uniform pollution film, it will heat up uniformly until a part of the film evaporates and the surface conductivity changes. Pollution can lead to the formation of quasi stable gas discharges which burn in series with the polluted resistive layer.
- 3) Based on the geometry illustrated in figure 2.3, the formulas for calculating the resistance  $R_p$  of the polluted layer were derived as given by equations (2-8) and (2-9) for narrow and wide strips, respectively, and the factor which takes into account the change in resistance due to heat is presented as well.

The governing equation on this model is given as:

$$V = xAi^n + V_e + 2iR_p \quad (2-20)$$

Where  $V_e$  is the total voltage drop on the electrodes.

It is assumed that the discharge moves to a position where the rate of energy expenditure is at its maximum. A critical current value may be calculated above which power increases with the discharge length and below which power decreases with the discharge length. For a discharge length of  $x$ , arc propagation will occur if  $dP / dx > 0$ , where  $P$  is the power taken from the source. If the applied voltage is constant during discharge movement, then the propagation criterion is  $di/dx > 0$ . This criterion was first proposed by Hesketh [54].

Based on the formulas derived for polluted strips and the flashover criterion described above, Wilkins calculated the critical voltage as follows:

$$V_c = \frac{i_c}{2\pi\sigma_c} \ln \frac{4L^2 J}{\pi i_c} + \frac{L}{2} A i_c^{-n} + V_e \quad (2-21)$$

Where  $i_c$  is the same critical current as that obtained by Alston and Zoledziowski [2], and  $J$  is the current density measured as  $1.45 \text{ A/cm}^2$ .

## 2.5.2 Alternating current models

Before proceeding with a review of AC models on polluted surface flashover, the physical aspects of the re-ignition phenomenon with relevant mathematical formulas are summarized here in brief, since the re-ignition condition is an additional condition to be satisfied under AC excitation.

### 2.5.2.1 Energy re-ignition model

The basis of the energy re-ignition model is the solution of Mayr's dynamic arc model under a sinusoidal arc current. Under alternating current conditions, the breakdown takes place after current zero condition, since the air gap is no longer able to dissipate the energy absorbed from the power supply as long as the post-zero current in a plasma medium is still conductive. Browne described the dynamic arc in terms of power loss per unit length and proposed a critical condition for breakdown as follows [104]:

$$U_{cx}^2 = KN_{02}R_mx \quad (2-22)$$

Where  $x$  is the arc length,  $R_m$  is the arc residual resistance at current peak,  $K$  is the thermal diffusivity constant and  $N_{02}$  is the power loss per unit length after current zero.

Following Browne, the more quantitative expression for critical energy breakdown was given by Maikapor as [80]:

$$U_{cx} = \frac{2080 x}{I_m} \quad (2-23)$$

Considering the units of  $U_{cx}$ ,  $I_m$  and  $x$  as (V), (A) and (cm), the arc re-ignition constant  $K=2080$  is given in (V.A/cm).

Equation (2-20) states that, in order to maintain an arc with a length of  $x$  cm and a current of  $I_m$  A (Peak), the required applied peak voltage is 2080 V. The following investigations and measurements carried out by Claverie, however, showed that the lower voltage of 940 and even 800 (V.A/cm) is enough to satisfy the critical energy breakdown conditions [14].

#### 2.5.2.2 Dielectric re-ignition model

The mechanism of the arc re-ignition process was analyzed in a fundamentally new approach by Rizk [17], where the residual gap was treated as a hot fluid with a cylindrical geometry. The basis for this assumption relied upon the fact that the electrical conductance of the residual arc is almost zero at current zero where the gap is cooled down due to heat exchange with the medium surrounding gap cylinder from an initial temperature in the order of  $3000^{\circ} K$ . Proceeding with the above mentioned conditions, the author then considered the energy balance equation of the residual plasma expressing the thermal flux function due to Maecker [81] as a partial differential equation in terms of the gap cylinder radius and the time being measured from the point of current zero. Application of initial and proper boundary conditions enabled the author to express a general solution for the energy balance equation along the axis of the residual plasma ( $r=0$  cm) where the temperature is at its highest value. The solution was given as:

$$S(0, t) = \frac{S_0 - S_b}{1 + \frac{a^*}{r_b^2} (S_0 - S_b)t} + S_b \quad (2-24)$$

Moreover, under certain conditions when the temperature is in the range of  $300-3000^{\circ} K$ , the thermal flux was expressed in terms of temperature as  $S = Const \cdot T^{\beta}$ . Based on this relation and further assumptions stating that the dielectric strength of the gap in the absence of ionization is inversely proportional to the absolute temperature, the following expression was given by F.A.M Rizk for the dielectric strength of the residual gap:

$$U_d = U_{da} \left[ \frac{\frac{S_0}{S_b} - 1}{1 + \frac{a^* S_b}{r_b^2} \left( \frac{S_0}{S_b} - 1 \right) t} + 1 \right]^{-1/\beta} \quad (2-25)$$

Where  $U_{da}$  is the dielectric strength of the gap at ambient temperature;  $r_b$  is the cylinder radius at boundary;  $S_0$  and  $S_b$  are the thermal flux at ( $t=0, r=0$ ) and ( $t \geq 0, r = r_b$ ), respectively,  $\beta = 1.573$  and  $a^* = 3.01 \times 10^{-6}$ .

Substituting numerical values for the physical variables in (2-25), the mathematical expression for dielectric re-ignition is given as:

$$U_d = U_{da} \left[ \frac{51.9}{1 + \frac{56.7}{r_b^2} t} + 1 \right]^{-0.636} \quad (2-26)$$

Where  $r_b$  is measured in cm and t in seconds.

### 2.5.2.3 Model of P. Claverie

This model also utilizes the Obenaus discharge concept, which considers an arc in series with a polluted layer (resistance). It is assumed that the arc propagation is due to a thermal phenomenon, i.e. the arc grows due to heat energy as it dries the layer in front of the root. The resistance in series with the arc is a function of the arc root position on the insulator surface. The expression given above describing the mechanism of arc propagation and the nature of residual resistance in series with the arc can be translated into its mathematical form as below:

$$V = AI^{-n} + R_p(x)I \quad (2-27)$$

Where the arc constants A and n were determined as 100 and 0.5, respectively. According to this model,  $R_p(x)$  is the resistance at point "x" and depends on the geometrical structure of the polluted layer, as well as its conductivity which cannot be calculated easily but can be measured.

Moreover, based on experiments, an arc re-ignition criterion was developed given as: [14]

$$V > \frac{940 x}{I^{0.5}} \quad (2-28)$$

Where, V, I and x are given in (V Peak), (A Peak) and (cm), respectively.

The flat plate model and the electrode arrangement used for the experiments is shown in figure 2.9.

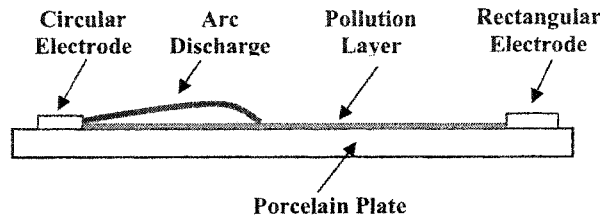


**Figure 2.9** Claverie's model

The method used for calculating the residual resistance proposed in this model is different from all models discussed here so far, where the calculation of the residual resistance was based on an analytical method developed by the authors or deduced from precedent models. This feature of Claverie's model suggests a different method for calculating  $R(x)$ ; in so doing, it first proposes a mathematical relation based on the knowledge of the nature of residual resistance under arcing conditions and then, using a series of measurements of leakage current "I" under several voltages "V", the parameters relevant to the proposed

formula are determined. An empirical formula to calculate the resistance of the polluted layer  $R_p(x)$  was given as:

$$R_p(x_m) = \frac{0.9V}{I_m} \quad (2-29)$$

Where  $x_m$  is calculated when the re-ignition condition is satisfied, i.e.,  $x_m = V(I_m^{0.5})/940$

It is worth mentioning that the measurement of  $R_p$  for disc insulators is more complex than for the plate model [14]. Formulas for critical flashover voltage and arc length were also derived as given by equations (2-30) and (2-31), respectively.

$$d(x^2 F(x))/dx = 0 \quad (2-30)$$

Where  $x_c$  is obtained from the numerical solution of (2-27), so  $V_c$  is then given as:

$$V_c = 90\rho^{1/3}x_c^{2/3}[F(x_c)]^{1/3} \quad (2-31)$$

$F(x)$  is a function that depends on the insulator's geometry and  $\rho$  is the resistance per unit length of the uniform distribution of the pollution layer.

As will be explained later in chapter 4, the method developed by P. Claverie is of a high importance for this study, since the same idea suggesting the use of analytical-empirical approaches based on the identification methods for calculating the residual voltage and the dynamic resistance of unbridged part of insulator was followed in this study.

The literature review provided thus far in this section touched upon the main features of the essential models developed for investigating the flashover of polluted surfaces. Although a survey of the literature reveals a diversity of approaches proposed by different authors on investigating flashover phenomenon and relevant topics, the models discussed

above have served as the theoretical basis for further studies, including this study, carried out with the aim of developing static models capable of predicting the insulators' flashover voltage under different environmental conditions. For the sake of avoiding lengthy elaboration, the following models were reviewed more briefly in this dissertation in order to touch upon their salient features. However, interested reviewers may refer to the original texts for detailed discussions.

#### 2.5.2.4 Model of B. F. Hampton [49]

The main goal of this model was to investigate the mechanism of flashover on a polluted and wet insulating strip used for experiments, where the voltage distribution along the plate was measured. A good explanation of the formation of dry bands was given in this model. Experiments conducted on the water column of constant resistivity indicated that if an arc propagates along the water surface, the arc will burn in an atmosphere of steam. The necessary condition for flashover along the water column is that the voltage gradient in the water column  $E_p$  should exceed that the voltage in the arc  $E_a$ , i.e.:

$$E_a < E_p \quad (2-32)$$

#### 2.5.2.5 Model of G. Zhicheng & Zhang Renyu [118]

In this model, the surface area of a pin-cap insulator is expressed as a two-dimensional plane model having the same area as that of a pin-cap insulator. This concept is illustrated in figure 2.4. Propagation of AC and DC arcs has been recorded for wet polluted surfaces of cylindrical rods by means of a high speed camera. From the experimental results,

it was observed that under DC excitation, the arc elongated along the surface and flashover occurred as soon as it reached a critical length of about 2/3 of the leakage length. AC arcs are more complex because two phenomena were observed: in one case, the arc extinguishes and then reignites when the current passes through zero, and in the second case, the arc does not extinguish but is weakened and shortened when passing through zero. Based on the experimental results, an empirical formula for AC and DC arcs was developed. Moreover, the mathematical resistance model was proposed to calculate flashover voltage.

#### 2.5.2.6 P. S. Ghosh and N. Chatterje model [48]

A mathematical model is presented to predict the flashover voltage of polluted insulators under AC excitation applicable to a static arc. This model takes into consideration the appropriate arc constants for different chemical natures of the pollutants. The critical values of flashover voltage and current are derived based on Renyu's model [118].

#### 2.5.2.7 Model of H. H. Woodson & A. S. McElroy [117]

This model deals with the mechanism of discharge on the surface within the boundary of the two circular electrodes illustrated in figure 2.2. A mathematical model is considered using a simple geometry of a flat plate with concentric circular electrodes. When one or more discharges occur across a dry zone, the width of the dry zone increases by vaporization of water until either the dry zone becomes too wide for the discharge to continue or it attains a critical length beyond which the discharge can rapidly cross the remaining portion of the polluted surface and flashover occurs. The resistance model

proposed by this model was discussed in section 2.3.1 of this chapter. A critical value of surface resistance is suggested, below which flashover may occur and above which flashover may not occur. The model was applied to practical pin-cap insulators.

A selection of static modeling of flashover on polluted surfaces has been provided thus far. The following section touches very briefly upon the main features of selected dynamic models of flashover on polluted surfaces for the purpose of illustrating their analytical basis. In so doing, the differences between static and dynamic models, from the viewpoint of the ways of dealing with issues such as arc modeling and discharge phenomenon, would be easily recognizable.

## **2.6 Dynamic modeling of flashover**

### **2.6.1 Model of F. A. Rizk [96, 94]**

F. A. Rizk *et al* simulated the arc behavior by investigating the discharge phenomenon on polluted surfaces under DC excitation using Mayr's equation (2-5) [78]. The model accounted for the terms of energy loss such as evaporation, condensation and convection, thereby making it possible to calculate the temperature of the electrolyte surface. This temperature value is necessary to calculate the electrolyte thickness in order to obtain the surface resistance. The arc velocity was calculated using a modified version of Al-Baghdadi's equation [1]. The simulation results revealed the satisfactory performance of the model in predicting the characteristics of the DC test source.

### 2.6.2 Model of R. Sundararajan & R S. Gorur [101]

This model investigates arc propagation on real insulator geometry. A mathematical model capable of taking into account the configuration of the insulator profile for DC excitation was proposed. The model is based on Neumarker's model [95], which is a modified version of the Obenaus model [84,5]. The arc voltage was calculated using the same form of Mayr's equation used by F. A. Rizk, while the resistance of the conductive layer was obtained using the form factor concept. The condition of arc propagation is checked based on the Hampton criterion ( $E_p > E_a$ ) [49] at each instant, and when the arc length is almost equal to the insulator leakage length, then the flashover is said to have occurred.

Generally, unlike static models which are capable of providing a quantitative analysis for predicting the critical voltage, the dynamic models provide more precise information about arc states at any given moment during the course of arc propagation. This fact may be considered an advantageous feature for dynamic modeling of flashover over static models. However, the mechanism of the phenomenon initiating the flashover at the final phase of the arc propagation referred to as the final jump is not incorporated into either dynamic or static models.

## 2.7 Physical interpretation of flashover phenomenon

Despite the large number of studies and investigations carried out with the aim of modeling the flashover phenomenon on conductive surfaces, the mechanism of the

conversion of arc propagation to a sudden jump at the final critical moment of arc propagation is still under a shadow of doubt and skepticism. One of the most widely accepted hypotheses ever proposed for explaining the mechanism of arc propagation and the final jump relies upon the effects of external forces pulling the discharge across the surface. Several forces have been suggested including electrostatic forces, electromagnetic attractions, thermal buoyant forces, and steam pressure. In order to have a quantitative idea, it may be worthwhile to review the approximate orders of the above mentioned forces acting on a certain portion of an arc length.

For a discharge current of 100 mA, a polluted surface resistance of  $50k\Omega$  and an arc foot radius  $r_a$  of 0.15 cm, D. C. Jolly [61] calculated the various forces acting on the arc root with the following orders:

$$F_{electrostatic} \cong 1/2\epsilon_0 E^2 r_a^2 = 2.8 \times 10^{-6} \text{ newtons} \quad (2-30)$$

$$\begin{aligned} F_{electromagnetic} &\cong \frac{1}{2} \mu_0 H^2 r_a^2 \\ &= \frac{1}{2} \mu_0 \left( \frac{I}{2\pi r_a} \right)^2 r_a^2 = 1.6 \times 10^{-10} \text{ newtons} \end{aligned} \quad (2-31)$$

$$F_{thermal} \cong \rho_0 g (\pi r_a^2) r_a = 1.3 \times 10^{-7} \text{ newtons} \quad (2-32)$$

By considering the above mentioned calculations, one may immediately conclude that the action of such a small force would be not high enough to step up the arc velocity to a few hundred or even thousand m/s. Hesketh has observed propagation velocities up to 600 m/s [54]. Obenaus and Bohme have also measured velocities in the order of 4200 meters/sec on insulators energized by 220 kV [84,5]. By comparing the order of the forces as discussed

above, the most eligible candidate capable of producing such an arc speed could be the joint effects of electrostatic and thermal forces at the arc tip. In this way, the ultimate phase of the arc propagation was considered to be the electrical-thermal breakdown of air at the arc root.

## 2.8 Conclusion

According to the literature review on arc and resistance modeling, as well as flashover of polluted surfaces presented through different parts of this chapter, the following conclusions may be drawn:

- Generally, two major approaches may be recognized for arc modeling among several methods proposed within studies dealing with arc behavior. The static or empirical approach provides mathematical relations based on E-I characteristics of the arc. This model was widely used in static models of the flashover phenomenon. The dynamic or analytical approach, however, provides instantaneous information about the arc state at any given moment, supplying the theoretical basis for dynamic modeling of flashover or investigating the performance of high voltage circuit breakers.
- Almost all static models have used the imperial arc model proposed by Ayrton, since this model provides a mathematical relation between arc voltage and leakage current fairly suitable to be used in a static model.
- The values determined for the arc constants  $A$  and  $n$  by several investigators cover a wide range of variation because of the different conditions under which these constants were determined.
- The discharge phenomenon takes place in several steps. It starts to with the formation of

dry bands that appear as a result of a non-uniform voltage distribution along the polluted surface and may lead to a flashover of the conductive surface under certain conditions or be extinguished because of the lack of an appropriate condition leading to arc propagation.

- Several models were proposed for calculating the resistance of polluted surfaces.

Some of them have taken into account the effect of the arc root radius allowing for a more realistic calculation of resistance in the presence of an arc.

- Static modeling of flashover makes it possible to calculate the critical flashover voltage of polluted surfaces, however, it does not provide the instantaneous arc states during arc propagation.

- Static modeling of flashover uses the re-ignition criterion for calculating the flashover voltage under AC excitation.

- Two different approaches known as *energy* and *dielectric* re-ignition were proposed for determining the arc re-ignition parameters under AC conditions. The first considers the electrical breakdown as a result of certain conditions immediately after post-current zero, leading to a lack of possibility of dissipating the energy injected by the power supply into the extinguished arc column, whereas the dielectric re-ignition criterion treats the residual gap as a hot gas with a cylindrical geometry and proceeds with the solution of the energy balance equation of residual plasma expressed in terms of a thermal flux function.

- Very few dynamic models were presented to investigate the flashover phenomenon on polluted insulators. The majority of these models have used the Mayr equation to determine the arc state at the moment when the arc propagation condition is checked.

The foregoing conclusion drawn from the literature review of polluted surfaces confirms the serious lack of a comprehensive study on investigating the arc characteristics on polluted surfaces covered with ice. Moreover, the problem of calculating the voltage of unbridged part of insulator (referred to as residual voltage) for this kind of polluted surface and, finally, the establishment of a static model of insulator flashover have remained untouched issues in this field.

# **CHAPTER III**

## **LITERATURE REVIEW OF FLASHOVER ON ICE COVERED INSULATORS**

### **3.1 INTRODUCTION**

As described in the introduction of chapter I, overhead transmission lines and HV substation equipment are subjected to seasonal icing and snowfall in most cold climate countries [6,76,62,20,22,23,32,34,55]. The presence of ice on an insulator's surface leads to a considerable deterioration in the electrical performance of insulators, causing power outages.

Generally, the icing phenomenon has demonstrated itself as a serious problem for the power networks of cold climate countries, since power transmission is accomplished through higher voltages to meet the growing demand on electrical power, hence, phenomena such as partial discharge, air gaps, local melting, etc. has made HV insulators more susceptible to the flashover phenomenon.

In order to overcome the problems caused by atmospheric icing conditions, a large number of studies based on laboratory simulations and field observations have been carried out with the aim of better understanding the nature of the icing phenomenon and the atmospheric factors influencing the electrical performance of HV insulators under icing conditions.

Several efforts have made their contribution to the studies of insulators' performance under icing conditions by touching upon the major relevant topics in this field. This chapter proceeds with providing a brief review of the theoretical studies and experimental

investigations carried out to better understand phenomena such as the mechanism of ice accretion on an insulator's surface, flashover of ice covered surfaces, and the effects of atmospheric parameters on insulator performance. The text will then continue by reviewing the results of studies on determining arc characteristics on an iced surface followed by flashover modeling of insulators covered with ice. Finally, an overall conclusion will close this chapter.

### **3.2 Mechanism of ice accretion on insulator surface and relevant atmospheric factors**

The mechanism of ice accretion on various insulator types was studied by Kuroiwa, investigating the effects of atmospheric factors such as air temperature, wind velocity and liquid water contents on the type of ice formed under icing conditions [66]. Following Kuroiwa, several researchers either in Canada or other countries have conducted comprehensive studies on ice accretion on HV insulators, among which the main authors may be listed according to their precedence as: Khalifa and Morris [67]; Meier and Niggli [77]; Phan et al. [50]; Chisholm, Tam, Erven and Melo [13]; Farzaneh and Melo [76]; Farzaneh et al. [32]; Farzaneh and Kienicki [19]; Farzaneh and Drapeau [18]. It has been concluded that under different atmospheric and environmental conditions, three types of ice were formed on the insulator's surface, or any other energized equipment of the power network, as: 1) Glaze, 2) Hard rime, 3) Soft rime.

Farzaneh, *et al* have proposed an additional terminology as a dry-grown regime for ice classification under certain conditions where all super-cooled water droplets on the impact surface are fully frozen [19]. Both hard rime and soft rime ice was grown in this condition where the temperature is below  $0^{\circ}\text{C}$ . There is also another condition referred to as a wet-grown situation where the super-cooled water droplets are not completely frozen on the

impact surface leading to runoff water during the course of icicle formation. Glaze ice is grown in a wet-grown regime.

**Table 3.1** Ice types' characteristics [66]

	Surrounding Air Temperature (°C)	Wind Velocity (m/s)	Water Droplet Diameter (µm)	Density (g/m <sup>3</sup> )
Glaze	0 to -3	1 to 20	500 to 6000	(0.8 to 0.9) x10 <sup>6</sup>
Hard Rime	-3 to -15	5 to 20	5 to 20	(0.6 to 0.87) x10 <sup>6</sup>
Soft Rime	-5 to -25	5 to 20	5 to 20	<0.6x10 <sup>6</sup>

Table 3.1 summarizes the main characteristics of the above mentioned ice types.

In addition to the above mentioned atmospheric conditions, the ice formation on energized insulators is considerably affected by electrical phenomena such as partial discharges, corona discharge, leakage current, etc.

In order to investigate the mechanism of ice formation under the above mentioned conditions, a comprehensive study based on laboratory simulations, as well as field observations of the icing phenomenon was initiated under the framework of a joint program between the University of Quebec in Chicoutimi and Hydro-Quebec in 1989. The ice accretion studied under certain conditions such as freezing rain accumulation with different thicknesses under an air temperature from -4 to -1 °C and curtain accretion resulted from the condition of precipitation of 30 to 40 mm freezing rain at an ambient temperature of -1 °C . [18].

The extent of the studies of the icing phenomenon has also covered the investigations of insulators' electrical performance. For the purpose of investigating the flashover of ice covered insulators, a variety of ice types was formed in the climate chamber of the high

voltage laboratory of CIGELE, UQAC. Table 3.2 summarizes the ice types used for flashover tests [18,19].

**Table 3.2** Ice accumulation regimes and ambient conditions [66]

Accumulation Regime	Air Temperature (°C)	Wind Velocity (m/s)	Water Droplet Diameter (µm)	Liquid Water Content (g/m <sup>3</sup> )
Dry	-12	3.3	15	6.8x10 <sup>6</sup>
Wet	-12	3.3	80	6.8x10 <sup>6</sup>

### 3.3 Flashover of ice covered insulators

The influence of ice accretion on the electrical performance of high voltage insulators in cold climate countries has always been a challenging topic in power system networks so that this phenomenon has been investigated in several research centers and industrial laboratories. Following is a brief review of these studies.

The electrical performance of high voltage porcelain and composite insulator strings under icing conditions was studied by Khalifa and Morris [67]. Under various atmospheric conditions simulated in the laboratory, the influence of ice density and conductivity on the flashover voltage of ice covered insulators was investigated. The ice was formed by spraying freezing water on vertically installed insulator strings in the cold room within the temperature range of -12 to -7°C. It was concluded that the critical leakage current leading to flashover was less than that of polluted insulators under alternative excitation.

In an outdoor test arrangement under field conditions, the performance of glass, suspension and substation insulators under DC excitation was studied by Renner and Ratz in

the United States [93]. Ice was formed by spraying water on the surface of the insulators. This study resulted in the determination of the electrical performance of the above mentioned insulators, stating that for a vertically installed insulator string with an ice thickness of less than 0.5 cm, the insulating performance of a single string was better than that of double strings; however, for higher ice thickness there was no difference between single and double string insulators. It was also found that the minimum flashover voltage was a little higher for positive DC voltage than negative.

The standard and anti-fog porcelain insulator was studied using an artificial ice test method on transmission lines under field conditions by Schneider [105]. Ice was formed by spraying water with a conductivity of  $29 \mu S/cm$  at night time when the temperature was below  $-2.8^{\circ}C$  under high voltage excitation. By performing certain flashover test methods, it was concluded that the insulating performance deteriorated with the quantity of ice accumulation. It was also found that the V type insulator string had a better performance than the vertical one, capable of withstanding up to 70% higher ice accumulation in this study.

The phenomenon of non-uniform voltage distribution along ice-covered insulators leading to a strong corona discharge while a constant AC voltage was applied in the course of ice accumulation was studied by Kawai [62] in a cold climate room, as well as under site conditions. For a maximum ice thickness of 4 mm, it was concluded that the insulation performance was a non-linear function of the arcing distance.

A comparative study on the electrical performance of porcelain insulators under icing and contamination conditions in mountain areas was carried out by Watanabe in Japan [114]. Freezing water with a conductivity of  $100 \mu S/cm$  was used for ice formation on the

insulator's surface. The results highlighted the fact that the effect of wet-grown ice was more significant than that of pollution. Based on the results of this study, the design criterion was suggested for AC&DC and impulse voltages of 75 and 200, kV/m. However, another comparative study conducted by Fujimura, *et al* indicated that the AC and DC withstand voltages of ice-covered insulators were higher than those of polluted insulators with an ESDD level producing the same conductivity of melting water measured in the course of the experiments [44].

The joint effect of pollution and ice accretion on 3 units of IEEE standard insulators was studied by Shu, Sun, Zhang and Gu in China. The effect of a pollution layer on ice film conductivity during the melting period, as well as on the maximum flashover voltage, was investigated. It was concluded that the maximum withstand voltage decreases with an increase in the pollution level up to an ESDD of  $0.09 \text{ mg/cm}^2$  and remains constant for higher levels of ESDD [100].

In an attempt to investigate the variations of surface resistance as a function of time for various ice types in the course of accumulation, Sugawara *et al* carried out a series of experiments on two types of insulators, a string of three IEEE standard and long rod insulators. It was confirmed that the insulation resistance depends on both ice type and the geometry of insulators. Hard rime and glaze ice accretions showed the same behaviour during the icing and de-icing periods, whereas the insulation resistance for soft rime ice accretion decreased relatively more during the de-icing period than the icing period [106].

### 3.3.1 The influence of atmospheric parameters on electrical performance of high voltage insulators under icing conditions

A series of systematic studies of the electrical performance of high voltage insulators under icing conditions under several atmospheric conditions has been conducted by Professor Farzaneh at NSERC / Hydro-Quebec / UQAC Industrial Chair on Atmospheric Icing of Power Network Equipment (CIGELE). [19,18,20].

The facilities of the high voltage laboratory in UQAC made it possible to form a variety of artificial ice types in climate rooms as those observed in field conditions. In order to simulate the freezing rain precipitation found in field conditions, wet grown ice deposits were formed within the experimental conditions. From the results of laboratory investigations it was confirmed that the wet grown ice leads to the lowest flashover voltage for the same freezing water conductivity used in different ice types.

A survey of the literature on flashover on iced insulators presented throughout the preceding sections shows that flashover of ice covered insulators was studied by researchers from different countries under conditions of certain test methods where the results were expressed under specific standards pertaining to the corresponding conditions under which the tests were performed. Hence, in spite of all the comprehensive studies resulting in precious information, the lack of a unique standard for test procedures made it difficult to compare the obtained results. This fact had highlighted the necessity of an official standard as an inevitable part of studies conducted in the field of flashover of ice covered insulators.

Based on the test methods described in the IEC 60507 standard for polluted insulator flashover, two test methods were developed for insulators under icing conditions at UQAC [18,19] titled as: 1) Maximum withstand voltage, and 2) 50% withstand voltage.

In conformity with the above mentioned standards and using short strings of IEEE standard insulators from 1 to 6 units, the influence of several factors, such as ice uniformity, ice thickness, and freezing water conductivity, as well as the effect of atmospheric parameters on the withstand voltage of insulators, was investigated at UQAC [18,22,23]. In addition to the above mentioned parameters, the appearance of the electric field and its effects on ice accretion, as well as the effect of ionic winds, were the main topics of these studies [89].

According to the results obtained from the experiments, it was confirmed that the uniformity of the ice accreted on the insulator surface is a decisive factor for the electrical insulation level, i.e. the more uniform the ice accretion along an insulator string, the lower the maximum withstand voltage. Moreover, wind velocity influences the deviation angle of icicles determining the degree of uniformity of ice accretion. It has been observed that for a given freezing water content, for the icicles formed under lower wind velocity (less than 3.3 m/s) the accreted ice was almost uniform, whereas the ice formed under higher wind velocities (above 6.4 m/s) resulted in non uniform ice accretion along the insulator string [22,23]. It was also noted that the presence of air gaps, mostly formed in the vicinity of the high voltage and ground electrodes, is the consequence of the complexity of the ice accretion process in the presence of a high and non-uniform electric field along the insulator surface. The heat dissipation due to partial arcs causes local melting on the ice accumulation, forming

air gaps [22,34,50,51]. Further discussions about the formation of air gaps and local arcs will be given later throughout the following sections.

Ice thickness also has a considerable effect on the maximum withstand voltage of ice covered insulators. The increase in ice thickness tends to decrease the maximum withstand voltage up to a certain value, above which, it has no considerable effect on the flashover voltage. The level of the maximum withstand voltage then seems to be a function of shed or unit diameter, shed spacing, and the type of insulator. This limiting value of ice thickness was obtained as 20 mm and 25 mm for glass and cap-and-pin insulators, respectively.

[18,19 and 87].

As can be noted from the brief review given above, it is evident that several factors influence the flashover phenomenon of ice covered insulators. These factors are mostly related to the mechanism of ice formation under different circumstances, ambient conditions and the type of applied voltage under which the ice accumulation process is accomplished. Following are further discussions in brief on the individual effect of the parameters summarized above.

#### 3.3.1.1 Air gaps and partial arcs

It has been confirmed by very early studies that the presence of air gaps is the main origin of the formation of partial arcs along the insulator's surface as they provide a susceptible geometry for the initiation of partial discharges [22,34,51]. It has also been concluded from field observations and laboratory records that the formation of air gaps takes place at the beginning of the ice accretion period [112].

The air gaps may be formed either due to a sudden fall of a piece of ice leaving a part of the insulator's surface free from ice, or as a result of icicle elongation downward along the insulator's surface as shown in figure 3.1.

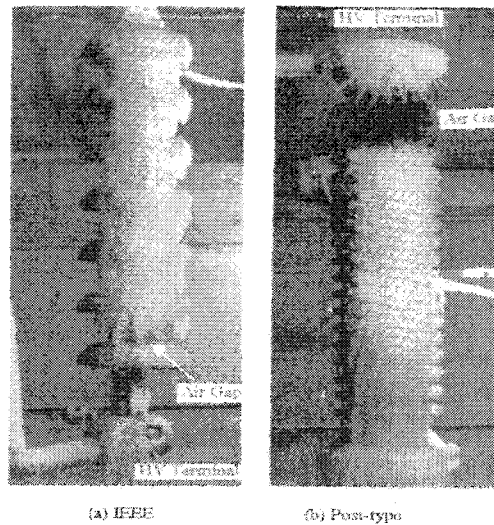


**Figure 3.1** Air gaps formed on IEEE suspension and post-type insulators covered with artificial ice [29]

The latter takes place when an icicle continues to elongate toward the next insulator skirt below until it reaches a certain distance where an electric arc appears between the tip of the icicle and the insulator and terminates any further icicle elongation. Under such a condition, in some critical conditions if the applied voltage tends to increase the electric field across the air gaps consolidating the local arcs and their elongation process, the situation may pave the way toward the completion of a flashover [26].

Electrical breakdown takes place when the electric field strength across an air gap exceeds the onset level, which is determined by the air gap length and the characteristics of the surrounding air across the gap, as well as the geometry of the electrodes. Studies carried out

on developing a mathematical relation between air gap length and electric breakdown have yielded the following expression [26, 29]:

$$V_b = 4.10d + 3.8 \quad (3-1)$$

Where  $d$  is the air gap length measured in cm and  $V_b$  is the breakdown voltage in  $kV_{rms}$ . Equation (3-1) was proposed for air gap geometry where the ice deposit is on one side of the electrode with a cylindrical shape during the melting period [26].

### 3.3.1.2 Freezing water conductivity

One of the major parameters influencing the flashover of ice covered insulators is the conductivity of the freezing water [18, 23,87]. Natural rain which is the origin of icing on the insulator's surface is not pure water. Its conductivity depends on several environmental and geological characteristics of the regions where overhead transmission lines pass, which may vary as a function of different air pollutants, as well as air temperature [89]. Due to the dependency of freezing water conductivity on air temperature, its value is expressed corresponding to the temperature of  $20^\circ C$  and then adapted according to different temperatures using correction factors [18,22, 34].

The studies of the effect of freezing water conductivity on the maximum withstand stress of ice covered insulators reveal that freezing water with higher conductivity leads to a lower flashover voltage [18, 23, 87]. The decrease in maximum withstand stress of the short string of IEEE standard insulators covered with wet-grown ice was given as [22]:

$$E_{ws} = 165.3\sigma^{-0.18} \quad (3-2)$$

Where  $\sigma$  is the freezing water conductivity measured in  $\mu S cm^{-1}$  and  $E_{ws}$  in  $kV m^{-1}$ .

This means that the air gap breakdown plays a significant role in the flashover process.

#### 3.3.1.3 Dry arc distance

The dependency of the flashover voltage on dry arcing distance is actually determined by the geometrical characteristics of the ice formed on the insulator's surface. In cases where the sheds are bridged by icicles, the flashover voltage can be expressed as a linear function of the dry icing distance for short string insulators [23,87]. However, for long insulators this function becomes non-linear [107]. The factors characterizing the non-linearity of this function may be the non-uniform ice distribution along the insulator, change in physical properties of melting ice such as surface water conductivity, and physical discharge phenomena [107].

#### 3.3.1.4 Applied voltage type

Studies of electrical performance of ice covered insulators under different applied voltages revealed that voltage type and polarity are also a decisive factor for the maximum withstand stress of ice covered insulators [36].

Under DC excitation, ice covered insulators showed different performance under different polarities, so that the maximum withstand voltage of a short suspension insulator string under positive DC was about 17% less than that of negative DC, which is almost the same as the effective AC value.

It was also concluded that the performance of ice covered insulators under lightning impulse voltages is the same as dry or clean insulators where the rise time of the front part of the surge is very short ( $1.2 \mu s$ ). However, under a switching impulse voltage with a relatively

slow rise in the front part of the surge (around a few hundred  $\mu s$ ), there was a decrease of about 50% in the minimum flashover voltage,  $V_{MF}$ , in comparison with that of dry or clean insulators [34]. Table 3.3 summarizes the maximum withstand stress of ice covered insulators under different types of applied voltages.

**Table 3.3** Maximum withstand stress of short string of IEEE standard insulators under wet-grown ice [34]

Type of voltage	$E_{WS}$ (kV/m)
DC+	86
DC-	71
AC	85

### 3.3.1.5 Air pressure

Air pressure is an important factor with a drastic effect on the electrical performance of ice covered insulators, as it is the main parameter influencing the onset voltage of partial discharges, as well as the arc voltage [97]. The effect of air pressure is expressed as the air density reduction factor known as  $K_d$  through a linear relation between the critical flashover voltage  $V_c$  at any pressure and that at standard sea level  $V_0$  as [73]:

$$V_c = K_d V_0 \quad (3-3)$$

The air density reduction factor, however, depends on a number of factors such as insulator profile, pollution severity and type of voltage [74].

### 3.4 Modeling of electrical arc on ice surface

The main objective of this section is to touch upon the salient features of the systematic and comprehensive studies carried out at NSERC / Hydro-Quebec / UQAC Industrial Chair on Atmospheric Icing of Power Network Equipment (CIGELE) dealing with a variety of factors characterizing the flashover phenomenon on ice covered surfaces. These studies have covered the determination of arc characteristics, the mechanism of the arc propagation on ice surfaces and relevant factors, ice surface conductivity during the melting period, as well as developing the mathematical models for predicting the flashover voltage of ice covered insulators.

#### 3.4.1 Ice surface conductivity

The ice surface conductivity was determined during the de-icing period and flashover [27, 28,29]. Using a cylindrical ice sample and assuming that the main path for the leakage current is provided by the outer ice surface when a partial arc occurs, the equivalent surface conductivity  $\gamma_e$  was given for different applied voltages as:

$$\text{For positive voltage: } \gamma_e = 0.061 \cdot \sigma + 5.6 \quad (3-4)$$

$$\text{For negative voltage: } \gamma_e = 0.063 \cdot \sigma + 5.8 \quad (3-5)$$

$$\text{For ac (AC) voltage: } \gamma_e = 0.067 \cdot \sigma + 5.6 \quad (3-6)$$

Where  $\gamma_e$  is expressed in  $\mu S$  and  $\sigma$  in  $\mu S / cm$  (at  $20^\circ C$  ).

#### 3.4.2 Arc constants and re-ignition parameters on ice covered surface

In order to determine the arc constants and re-ignition parameters, a series of tests was carried out using wet-grown ice formed on cylindrical samples. The method for determining the AC arc constants is described in brief here.

The length of the arcs was adjusted to values varying in the range of 0.015 to 0.15 m for an ice sample with an arcing distance of 0.3 m.

For each arc length chosen  $x$ , the applied voltage  $V_1$ , the voltage on the measuring electrode  $V_2$ , and the leakage current  $I$ , were recorded simultaneously using a Data Acquisition System (DAS). The typical waveforms of  $V_1$ ,  $V_2$ , and  $I$  under AC voltage are shown in Figure 3.2. As it can be noticed, before the arc reaches the measuring electrode,  $V_2$  is the sum of the local arc voltage, the electrode voltage drops and the voltage on the remaining ice surface between the foot of the arc and the measuring electrode.  $V_2$  increases with the increase of the applied voltage  $V_1$  until when the arc reaches the measuring electrode. At this moment the arc voltage  $V_2$  drops suddenly and is the sum of the voltage across the arc and the electrode voltage drops (Point P2).

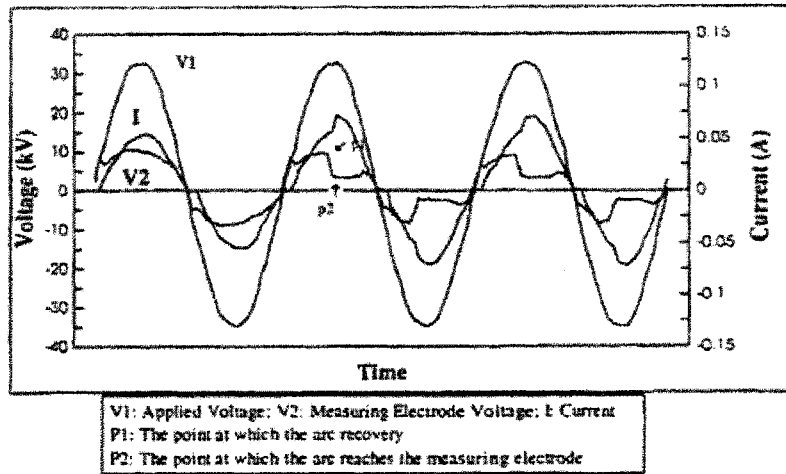


Figure 3.2 Typical waveform used for determining arc constants [29]

The arc constants were determined for different types of applied voltages as [27]:

$$\text{For positive voltage: } E_{arc} = 169I^{-0.59} \quad (3-7)$$

$$\text{For negative voltage: } E_{arc} = 213I^{-0.53} \quad (3-8)$$

$$\text{For AC voltage: } E_{arc} = 152I^{-0.52} \quad (3-9)$$

Where,  $E_{Arc}$  and  $I$  are given in V/cm and (A), respectively.

The arc re-ignition condition was also determined on wet-grown ice surfaces [29]. The parametric representation of re-ignition condition is given as:

$$V_m \geq \frac{Kx}{I_m^b} \quad (3-10)$$

Where  $V_m$  and  $I_m$  are the peak value of the applied voltage and the leakage current, respectively, and  $x$  is the arc length.

For different ice samples made from freezing water with various conductivities, the peak values of the leakage current ( $I_m$ , in A), the applied voltage ( $V_m$  in V), and the corresponding voltage ( $V_p$  in V) across the arc  $x$  cm in length were measured. The method used for determining the AC arc re-ignition parameters is similar to that of explained for arc constants, where for each arc length, the applied voltage  $V_m$  was adjusted to cause the arc recovery to occur at its peak value. The critical arc re-ignition condition is obtained as [11]:

$$V_m \geq \frac{1258.6x}{I_m^{0.51}} \quad (3-11)$$

#### 3.4.3 Supplementary studies on arc behaviour on ice surfaces

In addition to the determination of the principal factors for the modeling of electrical arcs on ice surfaces as mentioned above, the extent of these studies have also covered a

series of supplementary investigations for better understanding the nature of the electrical arc, as well as the mechanism of its propagation under different applied voltages.

Using the high speed camera, a large number of tests on arc development on ice surfaces was carried out. The relationships between arc radius  $r_0$  and arc current  $I_m$  under different applied voltages have been expressed as [30]:

$$\text{Positive arc: } r_0 = \sqrt{\frac{I}{1.75 \pi}} \quad (3-12)$$

$$\text{Negative arc: } r_0 = \sqrt{\frac{I}{1.67 \pi}} \quad (3-13)$$

$$\text{AC arc: } r_0 = \sqrt{\frac{I}{2.04 \pi}} \quad (3-14)$$

Where,  $r_0$  and  $I$  are given in cm and A, respectively.

Moreover, the technical facilities of the high speed camera made it possible to investigate the arc propagations of AC and DC arcs on ice surfaces [28,29] Based on the results of these investigations, it was concluded that, during the DC flashover process, the arc may propagate outside or inside the ice on the triangular ice samples. The propagation of the arc on the ice surface can be divided into two stages. In the first stage, which covers a distance of about 45% to 60% of the total leakage distance, the velocity is relatively low, varying between 0.05 to 0.3 m/s. In the second stage, the propagating arc velocity is about 20 to 50 m/s for an outer arc, and only about 3 to 7 m/s for an inner arc. The maximum velocities reach about 100 m/s and 50 m/s for outer and inner arcs respectively, just before flashover [28]. The radius of both inner and outer arc is proportional to the square root of the leakage currents as given by equations (3-12) through (3-14). Under AC conditions and for rectangular ice samples, the partial arc on ice surfaces extinguishes and reignites with the cyclical variation of the applied voltage. There is a delay of about 1 mSec between the variations of arc length and voltage

[28]. Generally, the arc propagation process was found to be similar to that of a DC arc. However, the maximum velocity of arc propagation before flashover under AC was about 4 times that under DC+ and DC- [28,29].

### 3.5 Modeling of flashover on ice covered surfaces

#### 3.5.1 Static models

Based on the results obtained from the studies reviewed through section 3.4 of this chapter, mathematical models were developed for modeling flashover on ice surfaces under DC and AC excitations.

##### 3.5.1.1 DC flashover model

This model was established on the basis of the Obenaus concept of arc discharge in series with a residual resistance. The principal circuit equation of the model reads as:

$$V = xAI^{-n} + R(x)I + V_e \quad (3-15)$$

The residual resistance in this model was calculated based on the R. Wilkins resistance model given for a conductive layer of narrow strip geometry, where the equivalent surface concept was used to apply the formula to cylindrical samples as well as the practical insulators.

$$R_p = \frac{1}{\pi\gamma_e} \left[ \frac{\pi(L-x)}{w} + \ln\left(\frac{w}{2\pi r_0}\right) \right] \quad (3-16)$$

Where  $w = \pi D$  is the equivalent width of the wet-grown ice surface on a cylindrical model.

By recalling equations (3-4) through (3-6) and (3-12) through (3-14), the values for  $\gamma_e$  and  $r_0$  can be substituted with respect to the applied freezing water conductivity and the leakage current, respectively. In order to calculate the critical current  $I_c$ , arc length  $x_c$  and flashover voltage  $v_c$ , the same analysis was made as that of Alston and Zoledzioski [3] (Section 2.4.1.3), where the value of  $v_c$  for a given arc length  $x$  can be obtained from equation (3-15) by equating the first derivative of voltage  $V$  with respect to  $I$  to zero:

$$\frac{dV}{dI} = 0 \quad (3-17)$$

The critical arc length is also obtained from equation (3-18) as:

$$\frac{dV}{dx} = 0 \quad (3-18)$$

The simultaneous solution for the set of equations (3-15), (3-16) and (3-18) yields the critical voltage, arc length and leakage current for ice samples under DC conditions.

### 3.5.1.2 AC flashover model

The basis of the AC static model is also the Obenaus concept of arc discharge in series with a residual resistance, so the model can be expressed by equation (3-15) for the peak values of applied voltage  $V_m$  and leakage current  $I_m$ . Under AC excitation, arc re-ignition conditions also must be satisfied for the arc to sustain itself and continue to propagation. The re-ignition condition was determined as:

$$V_m = \frac{Kx}{I_m^b} \quad (3-19)$$

The combination of (3-15) and (3-19) yields a non-linear relation between critical flashover voltage  $V_c$  and arc length  $x$  as:

$$V_m = Ax\left(\frac{Kx}{V_m}\right)^{\frac{-n}{b}} + U_e + R(x)\left(\frac{Kx}{V_m}\right)^{\frac{1}{b}} \quad (3-20)$$

Equation (3-20) presents a non-linear relationship between  $V_m$  and the length of arc  $x$ .  $V_m$  reaches its maximum value denoted as  $V_c$  when  $x$  varies in the range of  $[0 L]$  which determines the flashover voltage and the corresponding arc length and leakage current are referred to as critical arc length  $x_c$  and leakage current  $I_c$ , respectively.

This model along with the DC model described in section 3.5.1.1 has been applied to wet-grown cylindrical ice samples of various arcing distances. Figure 3.3 shows a comparison between the calculated and experimental results of the application of these models to wet-grown ice samples 0.3 m in length.

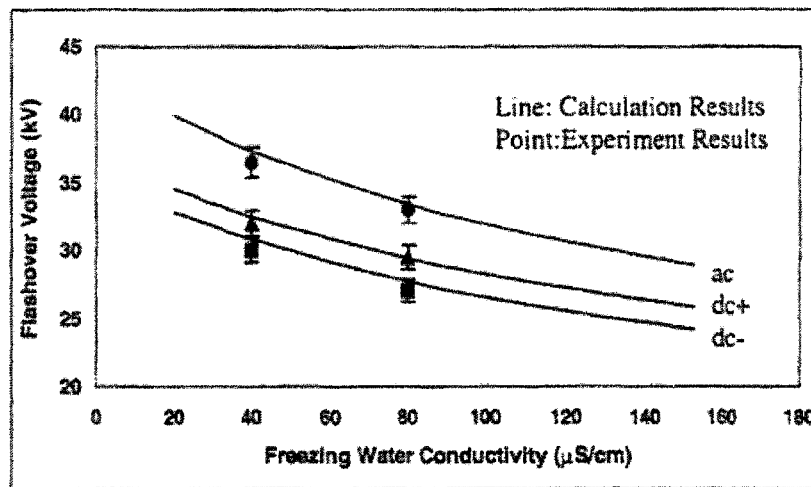


Figure 3.3 Calculated and experimental results of flashover voltages for wet-grown ice sample of 0.3 m length [11]

The AC static model was also successfully applied to a short string of 5 IEEE standard units insulators and the critical flashover voltage was calculated. The experimental as well as the calculated values of the 50% flashover voltage from the model are presented in figure 3.4.

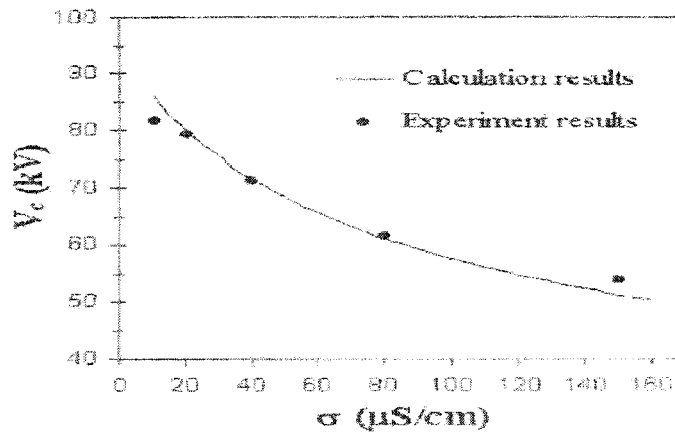


Figure 3.4, Calculated and experiment results of flashover voltage with 5 units of IEEE insulator [29]

### 3.5.2 Dynamic modeling of flashover on ice covered insulators

In an attempt to analyze the dynamics of arc propagation and the flashover phenomenon on ice covered surfaces, comprehensive studies started at NSERC / Hydro Quebec / UQAC Industrial Chair on Atmospheric Icing of Power Network Equipment (CIGELE) in 2000. These comprehensive studies resulted in the development of a dynamic model of flashover on ice covered surfaces.

The simplified dynamic arc model developed for flashover on ice covered surfaces by Farzaneh *et. al* [36,38] is based on Mayr's dynamic arc equation [78]. The equivalent circuit representation proposed for arc propagation in this model is shown in figure 3.5. In this figure, the arc is simulated by a time variant resistance  $R_{arc}$  in series with an inductance  $L_{arc}$

and capacitance  $C$  between the arc tip and the ground. As shown in figure 3.5, all parameters are time variant according to the arc characteristics and discharge geometry, where the instantaneous states of the circuit elements are updated according to the time dependent formulas given for each element [35,37].

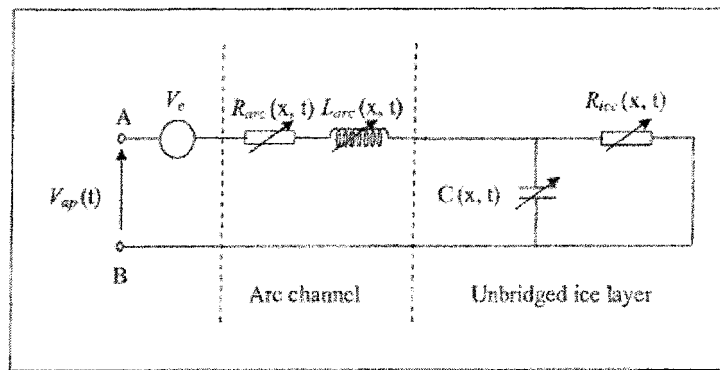


**Figure 3.5** Equivalent circuit used for modeling arc propagation on iced surfaces [37]

The formulas were also derived based on the simulation results, as well as the experiments carried out by Ishii *et al.* [117], in order to take into account the arc temperature as a function of the applied voltage level for DC+ and DC- [35].

In a general consideration, this model is capable of predicting the leakage current and the corresponding charges; arc channel radius, trajectory and electric stress; propagation velocity and energy injected into arc gaps; and the critical flashover of an ice-covered surface [37].

The model was successfully applied to a short string of five IEEE standard insulators covered with wet-grown ice and the calculated results were in good agreement with the experimental data [35].

Moreover, based on the same concepts of dynamic arc behaviour on ice covered surfaces as considered for modeling DC arc propagation as described above, the arc propagation of a dynamic arc under AC excitation was also developed by Farzaneh *et. al* [108]. The mechanism of the flashover phenomenon was divided into three separate stages, where each stage was simulated under dynamic arc analysis according to the phenomena characterizing the physical status of discharge. The first stage is recognized as the establishment of a white arc following the appearance of the first water droplets on the surface of the ice leading to the initiation of the leakage current in the order of 25 mA [54]. The second stage starts at the instant when the established white arc tends to elongate itself, manifesting the first indications of propagation. This moving arc extends itself up to 45-60% of the total insulator length and the leakage current reaches a magnitude of a few hundred mA [120]. The final stage begins when the arc has already traversed above 60% of the insulator length, paving the way toward completion of a flashover. This event normally takes place when the applied voltage is around its maximum peak value.

### 3.6 Conclusion

- High voltage equipment in cold climate regions is subjected to atmospheric ice precipitations seasonally. This type of precipitation generally decreases the electrical performance of the equipment and may cause a flashover with subsequent system failure.

- Wet-grown ice or glaze, which has a relatively high density, is the most dangerous type of ice from an electrical point of view. Certain climate conditions result in wet-grown ice accretion on insulator surfaces and this type of ice may be produced at a rapid speed in the laboratory by imposing controlled climate conditions.
- Several main parameters have a certain amount of influence on the insulating performance of high voltage insulators. Among them may be counted insulator geometry, applied water conductivity, ice type and amount, as well as climate conditions. In general, shorter insulator length, larger insulator diameter and higher applied water conductivity may each result in a lower flashover voltage.
- The creeping distance of the arc in the presence of ice formed at a low air velocity may decrease to as low as the dry arcing distance of the insulator. Ice formation under the applied voltage is accompanied by the formation of air gaps.
- The flashover process is triggered by the presence of a highly conductive water film on the surface of the ice, which results in intense electric stress along the air gaps. This high electrical stress initiates the ionization of the air inside the air gaps thereby leads to the creation of the corona discharges. The small violet corona discharges lead to formation of a high-current white arc. The latter may lead to a sudden flashover under sufficiently high applied voltages.

- Both static and dynamic flashover models conceptually rely on the Obenaus model considering an arc in series with a residual resistance. However, the static models utilize Ayrtton's arc model dealing with a comparatively easier mathematical model than Mayr's equation used in the dynamic models. The static model provides more quantitative results for flashover voltage prediction whereas the dynamic models provide more precise results about instantaneous arc states and arc propagation speed.

# **CHAPTER IV**

## **THEORETICAL DEVELOPMENT AND MODELLING OF FLASHOVER PHENOMENON ON CONTAMINATED INSULATORS COVERED WITH ICE**

### **4.1 INTRODUCTION**

A survey of the literature on flashover of polluted or ice covered insulators as provided in chapter II and III confirms the lack of mathematical model correlating the effect of the major parameters influencing the electrical performance of insulators subjected to pollution accompanied by icing condition. Few publications are available on comparative investigations of electrical performance of high voltage insulators subjected to contamination or icing. Farzaneh and Kiernicki have conducted a comparative study on severities of ice and salt contamination. It was concluded that the wet-grown ice accreted on a clean insulator string causes the same deteriorating effect on withstand voltages as that of ESDD of 0.15 mg/cm<sup>2</sup> [22]. Some other authors from different countries have also made their own contributions to this field, amongst which are Watanabe in Japan [114]; Fujimura, Naito, Hasegawa and Kawaguchi, Japan [44]; and Shu, Sun, Zhang and Gu, China [100]. Although all of these studies have touched upon this topic from different points of view, the extent of these studies was restricted to some limited reports. Therefore, the literature review highlights the necessity of a comprehensive study on modeling the flashover phenomenon on contaminated insulator surfaces covered with ice.

This chapter covers the theoretical basis of this study carried out with the aim of modeling the flashover phenomenon on contaminated insulators covered with ice. The

structure of the model will be primarily explained in the following section, where the main parameters and variables characterizing the static AC model are introduced. The text will then continue with the explanation of the methods used for determining the relevant parameters and variables.

#### 4.2 Static AC modeling of flashover on contaminated insulators covered with ice

As described in chapter I, the present Ph.D program was mainly intended to develop a mathematical model for predicting the flashover voltage of contaminated insulators covered with ice. More specifically, this study has primarily dealt with the joint effects of the major parameters influencing the arc characteristics on contaminated surfaces covered with ice, such as ice thickness,  $\delta$  ; freezing water conductivity,  $\sigma$  ; ambient temperature,  $\theta$ ; and the salt deposit density, SDD. The arc characteristic is determined based on the results obtained from a series of experiments carried out on cylindrical laboratory samples. Following the determination of the arc characteristic, the V-I characteristic of the residual part of real insulators depicted in figure 4.1 as  $V_{Res}$  was determined in this study, which may be denoted as the most challenging part of this research. The results were then served to the mathematical representation of the static AC model as expressed through the set of equations given by (4-1) and (4-2). The set of equations characterizing the mathematical expression of the model reads as:

$$\left\{ \begin{array}{l} V_m = A_p \cdot x \cdot I_m^{-n_p} + V_{Res}(x, SDD, \sigma, I_m) \quad (4-1) \\ V_m \geq \frac{x \cdot K_p}{I_m^{b_p}} \quad (4-2) \end{array} \right.$$

Where  $V_m$ ,  $A_p \cdot x \cdot I_m^{-n_p}$  and  $V_{Res}$  in (4-1) are the applied voltage, the arc voltage and the voltage of the un-bridged part of the insulator (referred to as residual voltage), respectively. The arc re-ignition condition which must also be satisfied under AC excitation is expressed by equation (4-2), where  $K_p$  and  $b_p$  are arc re-ignition parameters.

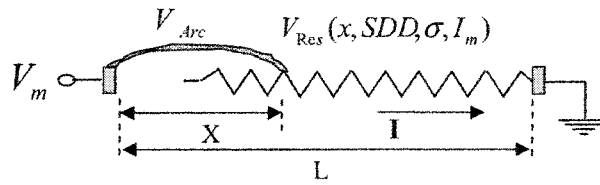


**Figure 4.1** Circuit representation of static model

Figure 4.1 illustrates the circuit representation of the model describing an arc discharge in series with the unbridged part of the insulator. The arc constants  $A_p$  and  $n_p$ , as well as the arc re-ignition parameters  $K_p$  and  $b_p$  in equations (4-1) and (4-2), were determined according to the method used by Farzaneh *et al* [27,28,29,30] under conditions of joint effects of contamination and icing.

As it can be noted from equation (4-1), unlike almost all previous static models proposed for predicting the flashover voltage of either a polluted or an ice covered insulator, this model primarily proceeds with the definition of a mathematical expression for the residual voltage of the insulator and provides a mathematical formula obtained from the application of identification methods. In so doing, instead of dealing with direct calculation of residual resistance, which seems to be extremely difficult in this case, the model introduces a mathematical formula for the voltage of the residual part of the insulator that eliminates the need for direct calculation of residual resistance, which was the key point for calculating the

flashover voltage based on previous models proposed until now. The dynamic resistance is then calculated from V-I characteristic of the residual part of the insulator. The situation compelling us to deal primarily with residual voltage instead of residual resistance is described in the following section, where the complex nature of the residual resistance of contaminated insulators covered with ice is discussed in detail.

#### **4.2.1 Complicated nature of residual resistance under condition of joint effect of contamination and icing**

##### **4.2.1.1 Non uniform ice accretion and pollution layer**

Several factors influence the pre-contamination of the insulator's surface, leading to formation of a non uniform pollution layer. Wind speed and its direction are two major factors influencing this process [88]. Moreover, some parts of the insulator's surface may be washed up during the seasonal raining phenomenon.

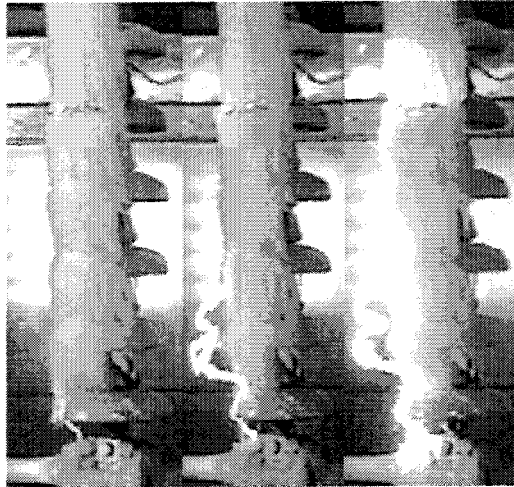


**Figure 4.2** Ice covered insulator at three steps of arc propagation. [30].

In addition to these factors, the formation of local arcs during dry seasons of the year leads to non uniformity of the pollution layer.

The icing process is affected not only by the factors mentioned above, but also the effect of icicles, as well as other atmospheric parameters described in section 3.2.

In such conditions, when the effects of the electrical field and the complexity of the insulator geometry accompany the environmental parameters, the physical appearance of insulators covered with ice resembles that shown in figure 4.2. This figure depicts a typical ice accretion on a practical insulator's surface.

#### 4.2.1.2 Local melting phenomenon

As a result of investigations with the aim of determining the arc temperature, Farzaneh *et al* have concluded that the arc temperature at atmospheric pressure is above  $4000^{\circ}K$ . [27]. As shown in figure 4.2, such a high temperature at the arc foot contact can lead to immediate melting and even vaporization of the melted water. A portion of this thermal energy can be transferred immediately to the insulator's surface leading to a sudden increase in the mobility of pollutants already deposited on the insulator's surface. Moreover, recalling the analysis made by D. C. Jolly [61] on calculating the buoyant forces of thermal energy proves that the thermal energy injected by the arc foot inside the ice accretion is capable of digging the solution composed of melted ice and pollutants onto the ice surface in the form of liquid and even vapour. Therefore, the physical as well as chemical characteristics of this kind of contamination change from the very early moments of arc discharge initiation. The complex nature of pre-contaminated long insulators covered with ice and the unusual behaviour of the leakage current during arc propagation was also

concluded among the reports of joint studies between CIGELE and Hydro-Quebec on flashover of pre-contaminated long insulators covered with ice [40].

#### 4.2.1.3 Non linearity of potential and electric field distribution along insulator

In order to have a quantitative idea of electric potential and field distribution in the presence of arc discharge along the conductive layers in the boundary of two electrodes with a relatively high potential difference (80 kV), a very thin rectangular strip of porcelain in parallel with conductive layers of salt and ice was analyzed as shown in figure 4.3. It should be mentioned that the main purpose of this analysis is merely to examine the electrical potential and field distribution in a very simple geometry in the presence of arc discharge in the vicinity of different conductive layers.

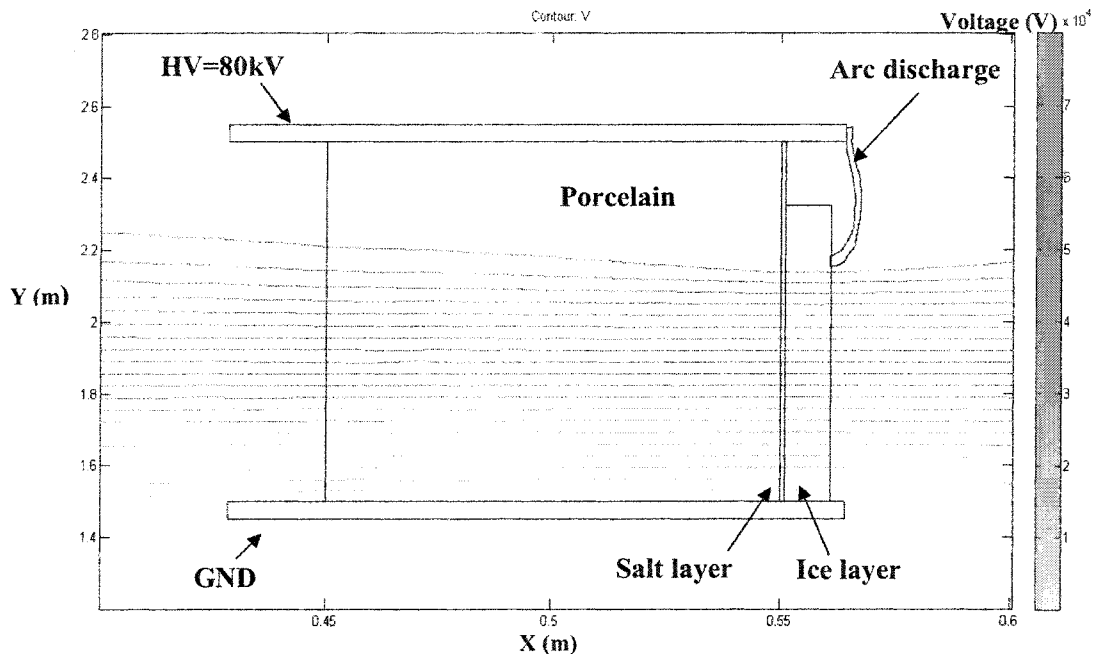


Figure 4.3 Electric potential distribution along tiny porcelain surface in parallel with salt and ice strips.

The electrical properties of Aluminum were adopted for simulating the electrical arc as a very highly conductive material with electrical characteristics as described in Table 4.1. The finite element method was used in order to calculate the electric potential and field distribution in the boundary of two electrodes.

The simulation of the arc in three dimensional and complex geometries is not as easy as it is done here. Therefore, it was assumed that the arc burns on the same plane containing the porcelain and two conductive salt and ice layers. The results shown in figures 4.3 through 4.5 were obtained using PDE (Partial differential equation) finite element tool-box of MATLAB software. As shown in figure 4.4, the infinity was mapped to an elliptic boundary with Neumann conditions where the electric field is tangent to any point of this boundary. In order to have an acceptable degree of precision in the calculated results, it is enough to choose this boundary of about three times the average dimension of the geometry in which the Laplace or Poisson equation are supposed to be solved [92].

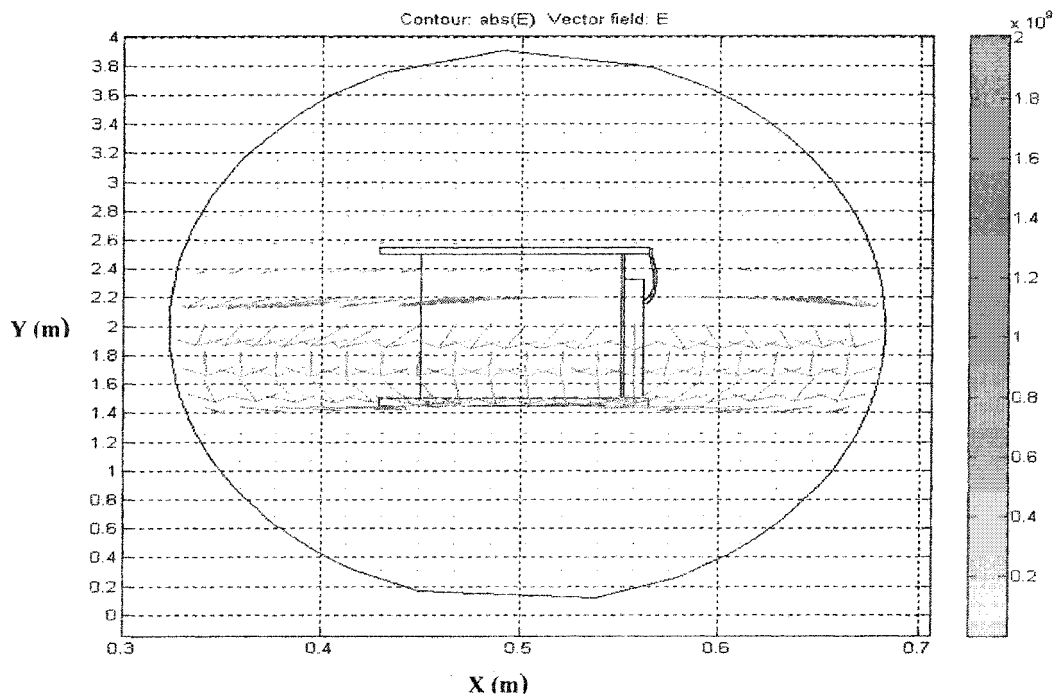
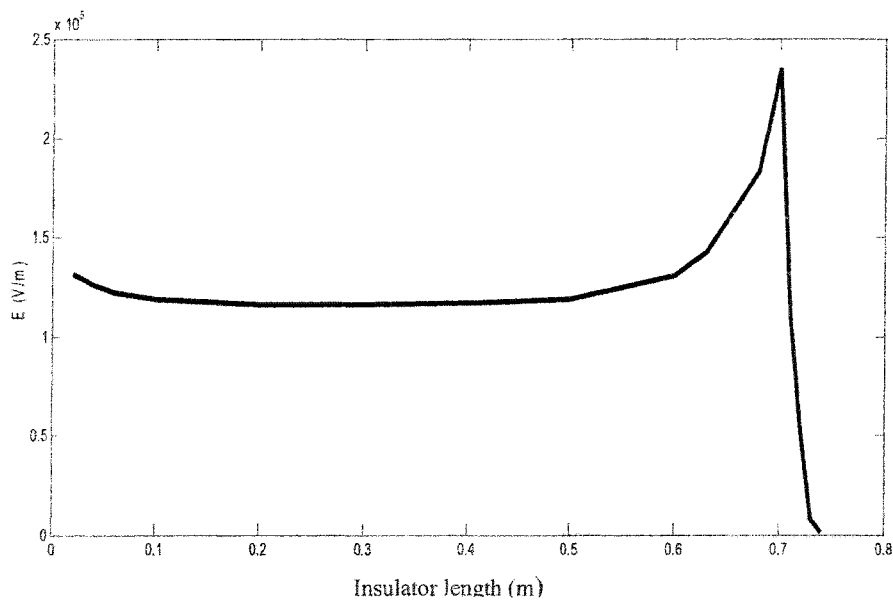


Figure 4.4 Electric field distribution.

In figure 4.3, the coloured contours indicate the electric potential distribution between two electrodes. As can be seen, almost all applied voltage appeared along the un-bridged part of the parallel strips. Figure 4.4 shows how the electric field is dispersed in the vicinity of the arc foot. The variation of the electric field over the ice surface starting from the ground electrode toward the arc foot is also shown in Figure 4.5. It can be noted that the electric field tends to decrease starting from the ground electrode and remains almost constant until it approaches the arc tip and then it increases rapidly as it gets closer to the arc foot. The electric field gains its maximum value in the vicinity of the arc foot and then decreases immediately to almost zero in the zone bridged by the arc (referred to as the iso-potential area). This fact has already been concluded by Volat and Jaiswal, [112,59].



**Figure 4.5** Electric field distribution along ice surface.

The electrical characteristics of the materials used in the above simulation are summarized in table 4.1 [69].

**Table 4.1** Electrical properties of materials [69,63]

Material	Relative electrical permittivity $\epsilon_r$	Conductivity $\sigma$ ( $\Omega^{-1}m^{-1}$ )
Ice	81	$\approx 10^{-4}$
Moisturized Salt	3-15 ( $\approx 9$ )	$\approx 4$
Porcelain	3-5	0
Arc discharge (Aluminum)	$\approx 1300$	$\approx 40 \times 10^6$

The foregoing discussions about the complex nature of the residual resistance of contaminated insulators covered with ice reveals that any analytical approach aimed at developing a formula for residual resistance seems to be extremely difficult. Nevertheless, being inspired by the power of the finite element method, one may think about calculating the electric field using a sophisticated finite element software within very complex

geometries in the presence of arc discharge. The electric field so calculated by this method could be substituted into equation (4-3) leading to calculate the residual resistance as:

$$R_{Res} = \frac{\int E \cdot dl}{\oiint \sigma E \cdot ds} \quad (4-3)$$

A numerical solution of equation (4-3) may lead to some impressive results with calculation of residual resistance; however, it should be kept in mind that the value of the electric field  $E$  and the conductivity of the medium  $\sigma$  is the function of the position and the temperature at the points at which it is calculated. In addition to these, the effect of melting, as well as the change in the conductivity of pollutants in different parts of the residual resistance should somehow be taken into account, which is an additional challenge of such a method.

The foregoing illustration of geometrical and physical characteristics of the ice covered contaminated insulators confirms the complexities which any efforts pursuing the goal of direct calculation of resistance based on analytical methods may face under this condition.

In spite of several resistance models given for polluted surfaces by different authors as reviewed through chapter II of this dissertation [95,48,116,118,117,79], none of them is applicable to the situation of pre-contaminated insulators covered with ice. In the case of ice covered insulators, Farzaneh and Zhang [29] have employed the R. Wilkins resistance model [116], assuming the conductive surface in series with the arc is composed of a very thin water film on the surface of the ice accretion. The authors then replaced the surface of ice accumulation with an equivalent rectangular plane surface, thereby applying the Wilkins formula for calculating the series resistance of ice covered insulators.

Generally, the common feature of the models proposed by the authors listed above was to reduce the complex geometry of the residual resistance, by leaning on simplifying assumptions and viewing it as a uniformly distributed single conductive layer.

Unlike either a single polluted layer or ice accretion, the physical nature of contaminated insulators covered with ice, as explained above, is characterized by the joint effects of several parameters such as the interaction of different pollutants initiated by the local melting phenomenon due to the hot arc propagation; non-uniform ice accretion and the pollution layer on the insulator surface; and the non-uniformity of the electric field along the insulator's surface. It is quite evident that the simplifying assumptions allowing the residual resistance to be considered as a single and uniform conductive surface are definitely not permitted in the situation described above.

#### **4.3 New approach for determining V-I characteristics of residual part of insulator**

Claverie in his model of flashover on electrolytic surfaces has stated: "The resistance in series with the arc is a function of the arc root position on the conductive surface.  $R(x)$  is the resistance at point "x" and depends on the geometrical structure of layer and its conductivity which can not be calculated easily but can be measured. The resistance  $R(x)$  can be determined by measurements of the leakage current  $I$ , under several voltages  $V$  [14].

The general aspects of the approach followed in this study for calculating the residual voltage was conceptually somewhat similar to that proposed by Claverie, where the basis of the method was the observation of the system's behaviour under different test conditions.

This information, sometimes referred to as priori knowledge, thus suggests a parametric mathematical model representing the V-I characteristics of the un-bridged part of the insulator to be verified by validation tests. The mathematical expression describing V-I characteristics of the residual voltage then made it possible to calculate the dynamic or differential resistance of the un-bridged part of insulator as it will be explained later in this chapter.

#### **4.3.1 The identification procedure**

The problem of determining a mathematical model for an unknown system (or target system) by observing its input-output data pairs is generally referred to as system identification. System identification involves two steps referred to as: 1) Structure identification and 2) Parameter identification [98]:

##### **4.3.1.1 Structure identification**

In this step, we need to apply a priori knowledge about the target system to determine a class of models within which the search for the most suitable model is to be conducted. Usually this class of model is denoted by a parameterized function  $\hat{y} = f(u; p)$ , where  $\hat{y}$  is the model's output,  $u$  is the input vector, and  $p$  is the parameter vector. The determination of the function  $f$  is a problem-dependent procedure, and the primarily proposed function is based on the designer's experience, intuition and the knowledge of the natural laws governing the behaviour of the target system.

#### 4.3.1.2 Parameter identification

In the second step, the structure of the model is known and all we need to do is to apply optimization techniques to determine the parameter vector  $p = \hat{p}$  such that the resulting model  $\hat{y} = f(u; \hat{p})$  can appropriately describe the system with the minimum possible error level.

If we do not have a priori knowledge about the target system, then the structure should be determined by trial and error.

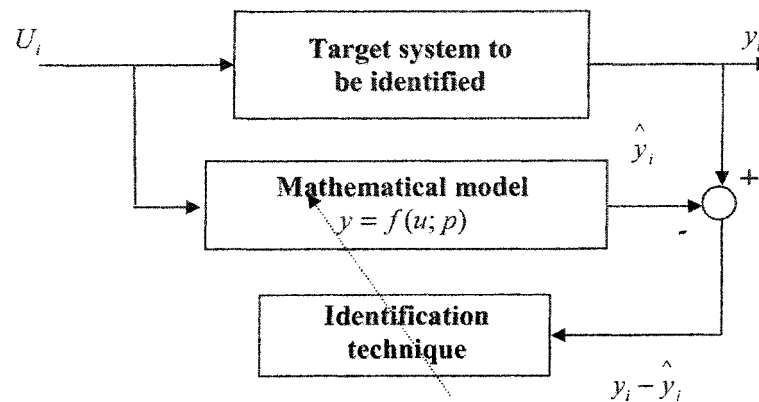


Figure 4.6 Block diagram of parameter identification procedure

Fortunately, as described throughout the preceding parts of this chapter, the major variables characterizing the nature of V-I characteristics of the residual part of the insulator are well known, so there is no need to perform a trial and error procedure to identify the class of the parameterized function that can best describe the target system.

Figure 4.6 illustrates a schematic diagram of parameter identification, where the input  $u_i$  is applied to both system and model, and the resulting error measured between the target system output  $y_i$  and that of model  $\hat{y}_i$  is used in an appropriate manner to update a parameter

vector  $p$  to reduce this difference. The data set composed of  $m$  desired input-output pairs  $(u_i; y_i)$ ,  $i=1, \dots, m$  is often called the training dataset or sampled dataset. In the most general case,  $u_i$  and  $y_i$  represent the desired input and output vectors, respectively. In figure 4.6 the target system is the actual pre-contaminated insulator covered with ice with the input vector  $u$  containing the following variables:

The salt deposit density (SDD), the freezing water conductivity ( $\sigma$ ), the leakage current  $I$  and the arc length  $x$ . In each data acquisition, the vector of the above-mentioned variables  $[SSD_i, \sigma_i, I_i, x_i]$  is the input data vector applied to both target system and mathematical model  $\hat{y}$ , so the nomenclature of the variables shown in figure 4.6 can be given as:

$$u_i = [SSD_i, \sigma_i, I_i, x_i] \quad (4-4)$$

$$\hat{y}_i = f(u_i, p_i) \quad (4-5)$$

$$y_i = V_{app} - A_p \cdot I_i^{-n_p} \cdot x_i \quad (4-6)$$

In general, system identification is not a one-pass process; it needs to repeat both structure and parameter identification throughout the following steps until a satisfactory model is found:

1. Specify and parameterize a class of mathematical models representing the system to be identified.
2. Perform parameter identification to choose the parameters that best fit the training data set.

3. Conduct validation tests to see if the model identified responds correctly to an unseen data set. (This data set is disjointed from the data set and is referred to as test, validating, or checking data set)
4. Terminate the procedure once the results of the validation test are satisfactory. Otherwise, another class of models is selected and steps 2 through 4 are repeated.

#### 4.3.2 Determination of the parameterized model of residual voltage

The type and also the degree of the complexity of the function we choose as the parametric function mainly depend on the physical nature of the target system. In some cases we may be required to try several functions to find out which one can best imitate the target system over a wide range of variations of input variables with minimum error.

The mathematical model representing the voltage of the residual resistance is expressed as a function of SDD,  $\sigma$ , I and x.

$$\hat{V}_{Res} = f(SDD, \sigma, I, x) \quad (4-7)$$

The first two of three variables SDD and  $\sigma$  appearing in the argument of  $V_{Res}$  always have a decreasing effect on the voltage of the residual part but the leakage current has both an increasing and a decreasing effect. The increasing effect is deduced from the linear nature of a passive electrical circuit element where the voltage drop across such an element is proportional to the leakage current, whereas the decreasing effect reflects the effect of the local melting phenomenon during the arc discharge process leading to a significant increase in the conductivity of both pollution and ice accretion. Concerning the variable x denoting the arc length, it was assumed that the residual voltage varies proportionally with respect to

its length (L-x). This knowledge about the nature of the residual voltage immediately inspires us to think about a fractional function that incorporates all variables mentioned above in the following form:

$$V_{Res}(I) = \frac{(L-x)I}{p_1 \cdot f_1(ESDD) + p_2 \cdot f_2(\sigma) + p_3 \cdot f_3(I)} \quad (4-8)$$

Equation (4-8) proposes the first trial function representing the V-I characteristics of the residual part of insulator. Once we can define such a function, we have completed the structure identification process and therefore we can proceed with the second step which is the parameter identification process.

The form of the mathematical model is not unique, so that, after performing the training process, the results will confirm whether the structure identification step was successful or not. Depending on the obtained results, we may be required to make some changes to the form of the mathematical model and proceed again with the parameters identification process until satisfactory results are obtained.

#### 4.3.2.1 Least-squares estimator

In the case of using Least Square Estimator (LSE), the block referred to as Identification technique in figure 5.4 is replaced by the least-square estimator. In a general least-square problem, the output of a linear model  $y$  is given by the linearly parameterized expression as [98]:

$$\hat{y} = p_1 f_1(u) + p_2 f_2(u) + \dots + p_n f_n(u) \quad (4-9)$$

Where  $u = [u_1, \dots, u_n]^T$  is the model's input vector,  $f_1, \dots, f_n$  are predefined functions of  $u$  and  $p_1, \dots, p_n$  are unknown parameters to be estimated. In statistics, the task of fitting data using a linear model is referred to as linear regression where  $p_i$ s are often called the regression coefficient to be identified. Usually we have to perform a series of experiments to obtain a training dataset composed of data pairs  $\{(u_i; y_i), i = 1, \dots, m\}$ ; they represent the desired input-output pairs of the target system to be modeled. By substituting each data pair into equation (4-9), a set of  $m$  linear equations will be obtained as:

$$\begin{cases} f_1(u_1)p_1 + f_2(u_1)p_2 \dots + f_n(u_1)p_n = y_1 \\ f_1(u_2)p_1 + f_2(u_2)p_2 \dots + f_n(u_2)p_n = y_2 \\ \vdots \\ f_1(u_m)p_1 + f_2(u_m)p_2 \dots + f_n(u_m)p_n = y_m \end{cases} \quad (4-10)$$

Using matrix notation, we can rewrite the preceding equations in a concise form:

$$Ap = y \quad (4-11)$$

Where  $A$  is the  $m \times n$  matrix (sometimes called the design matrix):

$$A = \begin{bmatrix} f_1(u_1) & \dots & f_n(u_1) \\ \vdots & \vdots & \vdots \\ f_1(u_m) & \dots & f_n(u_m) \end{bmatrix} \quad (4-12)$$

$p$  is the  $n \times 1$  unknown parameters vector:

$$p = [p_1, \dots, p_n]^T \quad (4-13)$$

and  $y$  is the  $m \times 1$  output vector:

$$y = [y_1, \dots, y_m]^T \quad (4-14)$$

In order to uniquely identify the unknown vector  $p$ , it is necessary that  $m \geq n$ . If  $A$  is square ( $m=n$ ) and non-singular, then we can solve  $x$  from Equation (4-11) by:

$$p = A^{-1}y \quad (4-15)$$

Generally, however,  $m$  is greater than  $n$ , indicating that we have a higher number of data pairs than of fitting parameters. In this case, an exact solution satisfying all the  $m$  equation is not always possible, since the data might be contaminated by noise, or the model might not be appropriate for describing the target system. Thus Equation (4-11) should be modified by incorporating an error vector “ $e$ ” to account for random noise or modeling errors, as follows:

$$Ap + e = y \quad (4-16)$$

If  $A^T A$  be a non-singular matrix, the error “ $e$ ” is minimized when the parameter vector is given as [62]:

$$\hat{p} = (A^T A)^{-1} A^T y \quad (4-17)$$

In order to recapitulate the foregoing explanation of the structure and parameter identification procedure used in this study, a block diagram representing the necessary steps to be taken to fulfill our goal is shown in figure 4.7

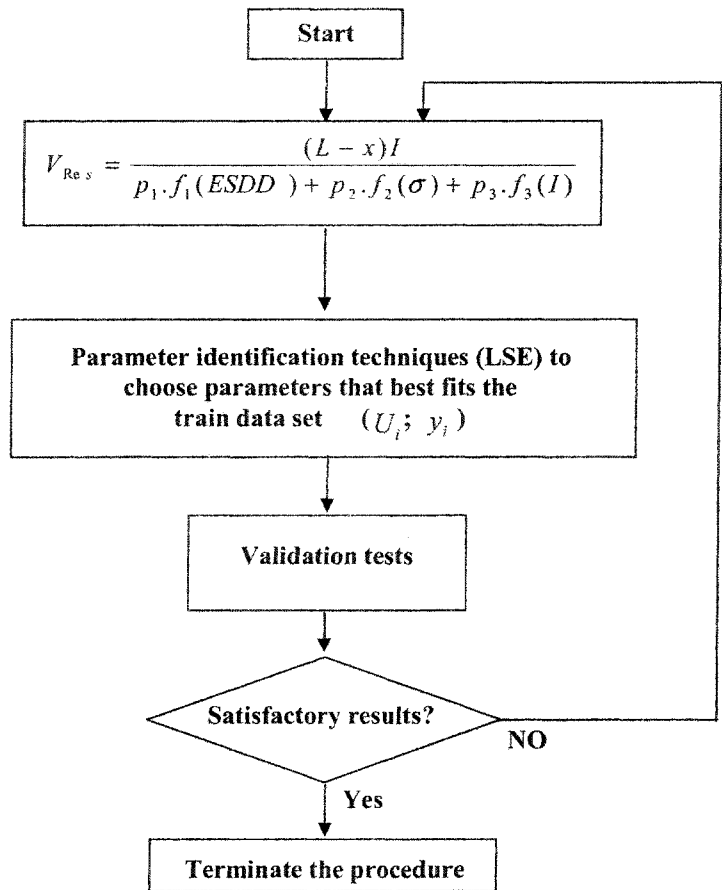


**Figure 4.7** Flowchart representation of structure and parameter determination process.

At first, a class of parameterized function is proposed to be fitted using the training dataset and after taking the parameter identification step, the parameterized function is checked using a test dataset to find out whether the function can best fit the test dataset or not. If the result was satisfactory then the identification process is said to be complete; otherwise the process should be repeated with a different parameterized function.

#### 4.3.2.2 Adaptive Neuro-Fuzzy Inference System (ANFIS)

In the case of employing intelligent identification models, we are not required to perform the system structure identification step, so the block denoted as mathematical model in figure 4.6 is replaced with an Adaptive Neuro-Fuzzy Inference System (ANFIS) and the block diagram shown in figure 4.6 will be modified as shown below:

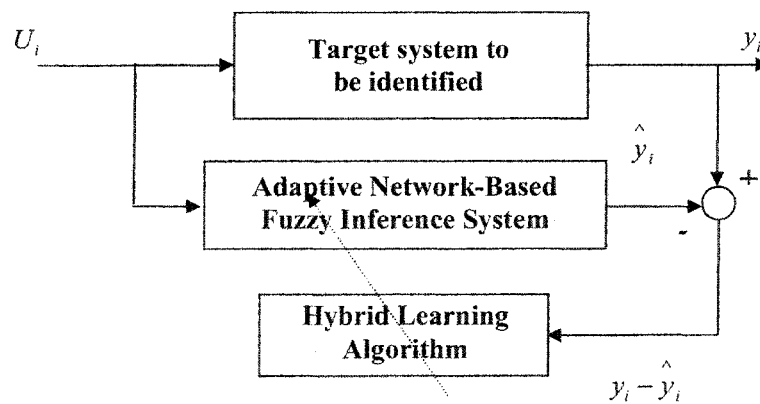


Figure 4.8 ANFIS based system identification

The architectures and learning rules of these kinds of adaptive networks have been discussed in detail in reference [98]. Because of its flexibility, an adaptive network can be employed directly in a wide variety of applications on modeling, decision making, signal processing, and control [98].

A class of adaptive networks that is functionally equivalent to fuzzy inference systems is proposed here. For the purpose of clarifying the structure of ANFIS, the architecture of this network is briefly described in the following section; however, this section may be skipped by those reviewers who are familiar with this kind of network.

#### 4.3.2.2.1 ANFIS architecture

For the sake of maintaining the simplicity of description, we assume that the fuzzy inference system has two inputs  $x_1$  and  $x_2$  and a single output  $z$  as described in figure 4.6 (a).

However, the network used in this study accepts four inputs signals as:

$$[x_1, x_2, x_3, x_4] = [SDD, \sigma, I, (L - x_{arc})] \quad (4-18)$$

Where  $(L - x_{arc})$  represents the length of the residual part of the insulator for a given arc length  $x_{arc}$ .

Functionally, ANFIS performs a first-order fuzzy inference operation proposed by Sugeno with two fuzzy “if-then” rules as follows [ ]:

$$\text{Rule 1: If } x_1 \text{ is } A_1 \text{ and } x_2 \text{ is } B_1, \text{ then } f_1 = p_1x_1 + q_1x_2 + r_1$$

$$\text{Rule 2: If } x_1 \text{ is } A_2 \text{ and } x_2 \text{ is } B_2, \text{ then } f_2 = p_2x + q_2y + r_2$$

Figure 4.9 (a) illustrates the reasoning mechanism for this model; the corresponding equivalent ANFIS architecture is also shown in Figure 4.9 (b), where nodes of the same layer have similar functions. Here the output of the  $i$ th node in layer  $i$  is denoted as  $O_{i,i}$ , where, each layer performs a specific operation on incoming signals as described below:

*Layer 1* Every node  $i$  in this layer is an adaptive node with a node function as:

$$\begin{aligned} O_{i,i} &= \mu_{A_i}(x_1), & \text{for } i=1, 2, \text{ or} \\ O_{i,i} &= \mu_{B_{i-2}}(x_2), & \text{for } i=3, 4, \end{aligned} \quad (4-19)$$

Where  $x_1$  and  $x_2$  are the inputs to node  $i$  and  $A_i$  (or  $B_i$ ) is a linguistic label describing a quantity such as “small” or “large” associated with this node. In other words,  $O_{i,i}$  is the

membership grade of fuzzy set A ( $= A_1, A_2, B_1$  or  $B_2$ ) and it specifies the degree to which the given input  $x_1$  and  $x_2$  satisfies the quantifier A or B.

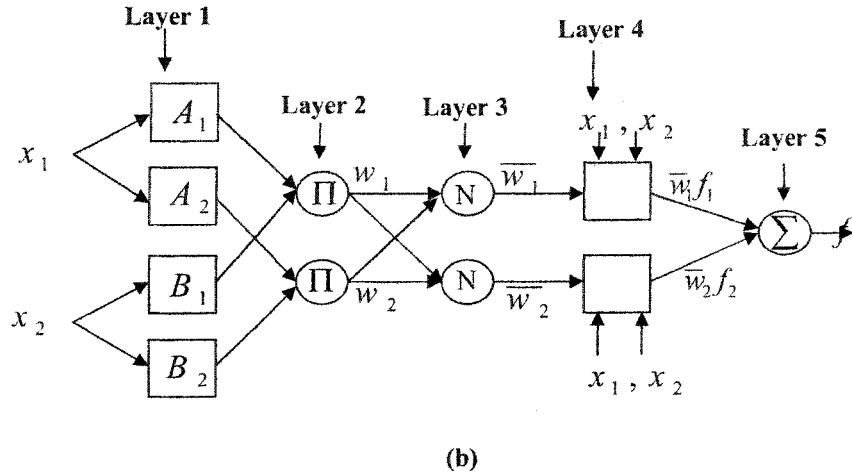
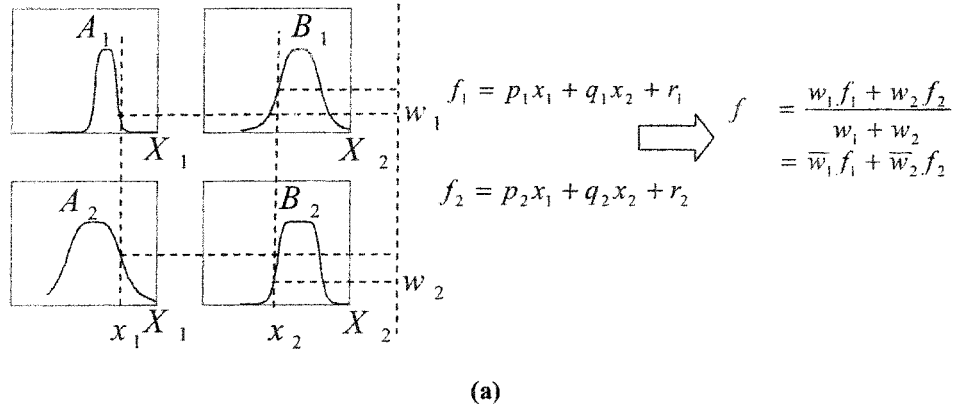


**Figure 4.9,** a) A two-input first-order Sugeno fuzzy model with rules;  
b) Equivalent ANFIS architecture

Here the membership function for A or B can be any appropriate parameterized membership function such as a generalized bell function given as:

$$\mu(x) = \frac{1}{1 + \left| \frac{x - c_i}{a_i} \right|^{2b}} \quad (4-20)$$

Where the set of  $\{a_i, b_i, c_i\}$  is the parameters related to each membership function associated with this layer. As the value of these parameters changes, the bell-shaped function varies accordingly, thus exhibiting various forms of membership functions for the fuzzy set. The parameters in this layer are referred to as “premise parameters”.

*Layer 2* Every node in this layer is a fixed node labelled  $\Pi$ , whose output is the product of all the incoming signals:

$$O_{2,i} = w_i = \mu_{A_i}(x_1) \cdot \mu_{B_i}(x_2), i = 1, 2. \quad (4-21)$$

Each node output represents the firing strength of a rule. In general, any other T-norm operators that perform fuzzy AND operation can be used as the node function in this layer.

*Layer 3* Every node in this layer is a fixed node labelled N. The *i*th node calculates the ratio of the *i*th rule’s firing strength to the sum of all rules’ firing strengths:

$$O_{3,i} = \bar{w}_i = \frac{w_i}{w_1 + w_2}, i = 1, 2. \quad (4-22)$$

The outputs of this layer are called normalized firing strengths.

*Layer 4* Every node *i* in this layer is an adaptive node with a function as:

$$O_{4,i} = \bar{w}_i f_i = \bar{w}_i (p_i x_1 + q_i x_2 + r_i) \quad (4-23)$$

Where  $\bar{w}_i$  is a normalized firing strength from layer 3 and  $\{p_i, q_i, r_i\}$  is the parameter set of this node. Parameters in this layer are referred to as “consequent parameters”.

Layer 5 The single node in this layer is a fixed node labelled  $\sum$ , which computes the overall output as the summation of all incoming signals:

$$O_{5,1} = \sum_i \bar{w}_i f_i = \frac{\sum_i w_i f_i}{\sum_i w_i} = V_{Rc,5} (ESDD, \sigma, I, L - x) \quad (4-24)$$

#### 4.3.2.2.2 Learning algorithm

Concerning the learning algorithms, it should be noted that a hybrid learning method utilizing two types of learning algorithm was used for this network, where, using LSE in parallel with the gradient-descent back propagation method, the consequent parameters and premise parameters were determined, respectively. Table 4.2 summarizes the learning procedures performed for this network.

**Table 4.2.** Two passes hybrid learning procedure of ANFIS [98]

	Forward pass	Backward pass
Premise parameters	Fixed	Gradient descent
Consequent parameters	Least-square estimator	Fixed
Signals	Node outputs	Error signals

#### 4.4 Mathematical model developed for flashover on contaminated insulators covered with ice

As described in the preceding sections of this chapter, based on LSE and ANFIS identification methods, two different approaches for calculating the voltage of the residual part of the insulator were proposed. The results were then served to the set of equations given by (4-1) and (4-2), whereby the required mathematical representation for flashover modeling of contaminated insulators covered with ice is completed. The mathematical expression of flashover will then read as follows:

$$V_m = A_p \cdot x \cdot I_m^{-n_p} + V_{Res} \quad (4-26)$$

$$V_m \geq \frac{K_p \cdot x}{I_m^{b_p}} \quad (4-27)$$

$$\left\{ \begin{aligned} V_{Res} &= \frac{(L-x)I}{p_1 \cdot f_1(SDD) + p_2 \cdot f_2(\sigma) + p_3 \cdot f_3(I)} & (4-28) \\ &= F_{Res}(SDD, \sigma, I, x) & (4-29) \end{aligned} \right.$$

Where,  $V_{Res}$  introduced in equation (4-26) is replaced by one of the expressions given by (4-28) or (4-29). The quantitative results and discussions of the model proposed in this study are provided in chapter 5, where the experimental facilities, test procedures and results are presented in detail.

#### 4.5 Dynamic or differential resistance of contaminated insulators covered with ice

Although the dynamic resistance as calculated here was not incorporated into static model proposed in this study, but it is worthwhile to introduce the definition of dynamic resistance and its possible applications. The dynamic resistance thus calculated here can be used in any future study aimed at developing the dynamic model of flashover phenomenon on contaminated insulators covered with ice in which the arc propagation criterion is required. The arc propagation and electrical stability criterion proposed by Nacke is given by equation (30) as: [95]

$$R_p \geq -\frac{\partial V_{arc}}{\partial i} \quad (30)$$

Where,  $R_p$  is the resistance of polluted surface and  $\frac{\partial V_{arc}}{\partial i}$  is the dynamic resistance of electrical arc. This criterion is applicable to the condition when the arc propagation is deemed to be analyzed on contaminated and ice covered insulators if the dynamic resistance

of the residual part is known. Knowing the V-I characteristics of the residual part of the insulator makes it possible to determine the dynamic resistance. According to our knowledge about the theories of the electric circuits, for a non-linear electrical element described in the form of  $V = f(I)$ , the dynamic resistance is obtained by taking the first derivative of the voltage (V) with respect to the current (I) at a given point ( $I_0$ ), or in mathematical expression it reads as:

$$R_{dyn} = \left. \frac{\partial V_{Res}}{\partial I} \right|_{I=I_0} \quad (4-31)$$

By substituting the  $R_{dyn}$  as given by (31) into equation (30) the arc propagation and electrical stability criterion proposed by Nacke can be given as:

$$\frac{\partial V_{Res}}{\partial i} \geq -\frac{\partial V_{arc}}{\partial i} \quad (4-32)$$

Considering the V-I characteristics derived from the LSE identification method introduced by equation (4-8), the dynamic resistance can be given as:

$$R_{dyn} = (L-x) \cdot \frac{p_1 \cdot f_1(SDD) + p_2 \cdot f_2(\sigma) + p_3 \cdot f_3(I) - p_3 \cdot f_3'(I) \cdot I}{[p_1 \cdot f_1(SDD) + p_2 \cdot f_2(\sigma) + p_3 \cdot f_3(I)]^2} \quad (4-33)$$

Equation (4-33) is the general form of dynamic resistance illustrating the contribution of different variables SDD,  $\sigma$  and I to the overall value of the residual resistance of combinational pollution.

In the case of utilizing ANFIS, the dynamic resistance can be determined from either the V-I characteristic given by (4-23) or a direct determination of resistance based on the training dataset in the form of  $(\Delta V_i, \Delta I_i)$ . This concept is illustrated in detail throughout chapter 5

where the results obtained from experimental data using both LSE and ANFIS methods are presented.

#### **4.6 Conclusion**

Based on the foregoing discussions illustrating the joint effect of relevant parameters influencing the V-I characteristic of the residual voltage of insulators under conditions of contamination and icing, as well as the theoretical basis of the new approach proposed in this study for flashover modeling of a contaminated insulator covered with ice, the following conclusions may be drawn:

- The theoretical basis of a static AC modeling of flashover based on Obenaus discharge model was proposed for contaminated insulators covered with ice.
- The local melting phenomenon leading to interaction of different pollutants during arc propagation on the surface of a real insulator was discussed. It was concluded that the equivalent surface criterion for calculating the residual resistance is not applicable to the complex geometry of combinational pollution on the real insulator surface.
- The electrical field calculation along a two dimensional geometry composed of the materials with different electrical properties in presence of an arc was carried out. The results revealed a highly non-linear distribution of the electrical field between high and low voltage electrodes.
- The presence of a very high electrical field accompanied by a considerably high temperature of the arc at the contact point can easily mobilize the different pollutants, thereby paving the way toward the change in physical properties of the equivalent conductive layer during arc discharge.

- A new approach based on identification methods for determining the voltage of the residual part of contaminated insulators covered with ice is proposed in this study. The method is applicable to either contaminated insulators under field conditions or artificially made in the laboratory in conformity with IEC 60507
- The application of the LSE identification method made it possible to derive a mathematical representation of residual voltage as a function of major variables influencing the V-I characteristic of the residual voltage.
- The V-I characteristic of the residual part of the insulator was also determined using the Adaptive Network-Based Fuzzy Inference System (ANFIS).
- The dynamic resistance of a real contaminated insulator covered with ice was determined using both LSE and ANFIS identification methods.

# CHAPTER V

## EXPERIMENTAL FACILITIES, TEST PROCEDURES AND RESULTS

### 5.1 INTRODUCTION

The theoretical basis of this study, as described in detail in chapter 4, deals with the major parameters and variables characterizing the static AC model proposed for flashover voltage prediction of contaminated insulators covered with ice. The mathematical representation of the model was given in parametric form, where the parameters to be determined are the arc constants ( $A_p$  and  $n_p$ ) and re-ignition parameters ( $K_p, b_p$ ), and the V-I characteristic of residual voltage  $V_{Res}$ . The results of this study have also contributed to the calculation of dynamic resistance of the un-bridged part of contaminated ice covered insulators which has been remained an untouched topic in this field until now. In order to express the model in a quantitative form, it is necessary to perform a series of experiments required to determine the parameters as described above. For this purpose, the facilities of the High Voltage laboratory in CIGELE were used to perform all necessary tests to fulfil the final part of this study. This chapter proceeds with a brief explanation of the facilities of the High Voltage laboratory in CIGELE, followed by a presentation of the test procedures for determining the parameters and the relevant experimental results. The final part of this chapter provides the experimental results obtained from flashover tests performed on IEEE standard insulators.

## **5.2 Facilities of High voltage laboratory**

### **5.2.1 High voltage equipment**

Considering the estimated voltage level required for these particular experiments, a single-phase test voltage transformer of 120 kV (maximum), 240 kVA and 60 Hz was used. The input voltage of this equipment is 600 V. A regulator is used to make it possible to vary the output voltage from 0 to 120 kV. The voltage control is fulfilled either manually or automatically at an approximately constant rate of 3.9 kV/s. Since high voltage experiments on ice-covered insulators are carried out in a closed area, and the transformer is kept outside that area, the security system set in place for this type of experiment is of vital importance. Two circuit-breakers and an accurate relay which interrupts the voltage instantaneously on demand are a part of this security system. The system may be adjusted to cut off the voltage and de-energize automatically in the case of personnel entering any of the test zones. High voltage bushing conducts the applied voltage through the walls of the cold climate room.

### **5.2.2 Climate Room**

The most dangerous ice type formed under a wet-grown regime was used in all experiments carried out in this study [18]. In the climate room, wet-grown ice was formed from super-cooled droplets sprayed onto the test object. This kind of ice is similar to the ice accumulated on actual insulators in field conditions [18]. This climate room, shown in figure 5.1, is a thermally isolated room equipped with sufficient facilities to meet the standard clearances required by IEC60507 [18,19,57]. The room temperature is controlled with a precision of  $\pm 0.2$  °C. The room is equipped with such appropriate facilities as a wind

generator and a water-droplet spray system. Super-cooled droplets are generated by oscillating nozzles which are of the air-atomizing type. Each nozzle produces a mix of water droplets and compressed air. The air pressure is controlled and set to remain constant. The water flow is also controlled by flow meters which were maintained at a rate of 200 mL/s/Nozzle.

The ice type and the ambient conditions of the climate room are summarized in table 5.1

**Table 5.1** Ice type and ambient conditions

Ice Type	Glaze
Ambient temperature	-12 (°C)
Droplet Size	80 (µm)
Wind Velocity	3.3 (m/s)
Air pressure	10 (psi), 70 (Kpa)

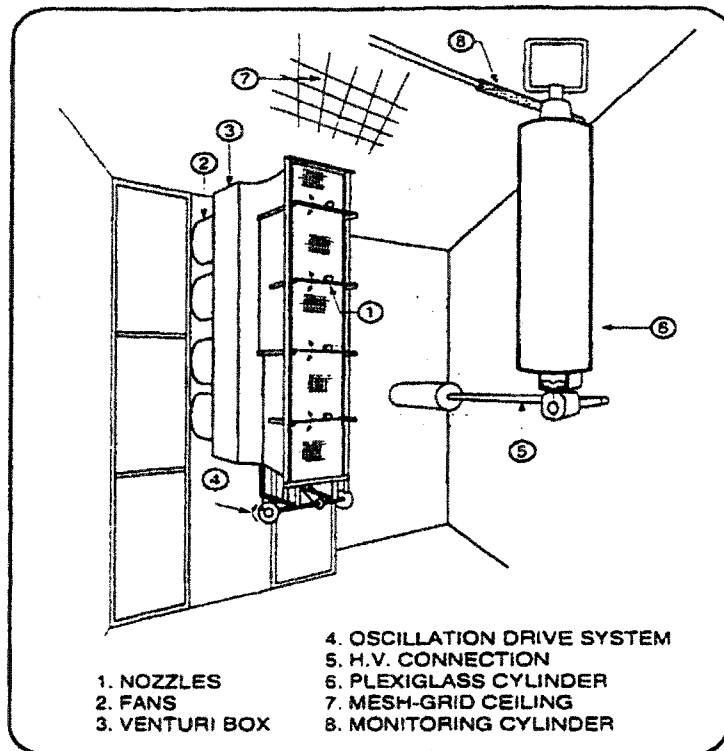


**Figure 5.1** Climate room [21]

### 5.2.3 Data Acquisition System

Dynamic modeling of the arc leads to the temporal evolution of a number of parameters. In order to be able to compare these curves with the ones produced experimentally, the laboratory data should be acquired at a relatively rapid frequency. A LabVIEW graphical software program was used to acquire high quality data. The voltage signal was attenuated by using a capacitive voltage divider. The current signal was transferred to a voltage signal using a low resistance shunt of  $10\Omega$ . The test signals were connected to a measuring set through a conditioning box providing protection and insulation. A NI-DAQ device, model PCI-6035E, was used for this purpose. Using the LABVIEW user-interface features, a visual program was specifically designed and developed for these experiments to acquire and save data for further analysis.

### 5.2.4 High-Speed Camera

A high-speed camera was used to study arc behaviour during the pre-flashover stage and to measure arc length during its propagation period along the insulator. This camera is capable to take the photos at the speed of up to 12000 frames per second, however in this study the recording speed was set to 1000 images per second. The reason was the technically inevitable trade off between the number of recorded frames per second and the recordable time period due to the limited capacity of the memory. That is, the higher number of taken frames the shorter recording time period was possible. The shortest recording time period in which at least one observation of arc length was possible was 3 seconds allowing us to take 1000 frames per second.

The most important technical feature of this camera is its embedded synchronizing data acquisition module which made it possible to measure instantaneous arc length corresponding to the leakage current and residual voltage at any moment of the arc propagation period. This feature of the high speed camera will be explained in detail later in this text where the test procedure for determining the V-I characteristic of the residual voltage is described.

### **5.3 Test procedures**

#### **5.3.1 Test procedure for determining the arc constants and re-ignition parameters**

In order to determine the arc constants ( $A_p$ ,  $n_p$ ) and re-ignition parameters ( $K_p$ ,  $b_p$ ), Plexiglas cylindrical samples were used. The cross section of this kind of sample, as well as the test setup, is depicted in figure 5.2 in a schematic representation. The pollution layer was first formed onto the cylindrical sample using the brushing method. In this method the solution of the required salt amount in combination with the appropriate amount of Kaolin and de-ionized water was prepared as stated in the IEC 60507 standard [57]. As the surface area of the cylindrical sample was known for the given dimension given in figure 5.2; the desired salt deposit density (SDD) was applied onto each sample to be tested. The solution was then distributed uniformly onto the sample surface by means of a brush.

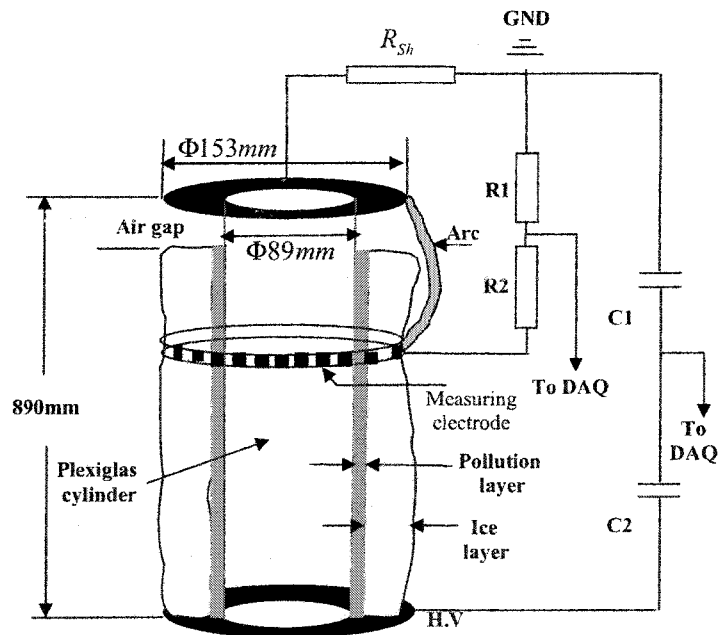
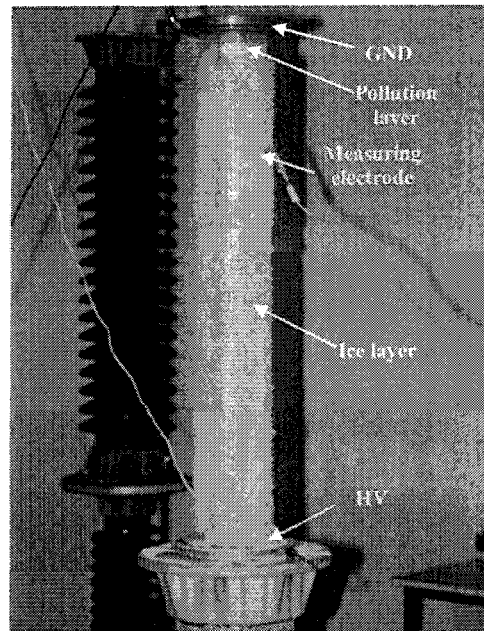


Figure 5.2 Cylindrical sample

In order to accumulate a uniform ice thickness, the cylindrical glass tube was installed vertically in front of the spray system of the climate room and rotated at a speed of 1 rpm. The temperature of the climate room was maintained at  $-12^{\circ}\text{C}$  during ice accretion. The conductivity of freezing water was also adjusted by adding sodium chloride to the de-ionized water. Sodium chloride is an important contaminant in both seacoast and urban (road salting) exposure of high voltage equipment. After having the insulator accumulated by means of the spray system of the climate room, the sample was ready to perform the required tests for investigating the arc characteristics under contamination and icing. Figure 5.3 shows the cylindrical sample used in this study after performing the ice accumulation process.

In order to determine the arc constants and re-ignition parameters, a series of tests was carried out on the cylindrical ice samples. The method used by Farzaneh, Zhang and Chen as described in chapter 3 was followed in this study [27], where, based on several

measurements of arc voltage, leakage current and arc length, the E-I characteristics for different arc lengths were determined. The position of the measuring electrode was readjusted to a given point corresponding to the arc length of 8.5, 10.5 and 12.5 cm for the ice samples having an arcing distance of 89 cm.



**Figure 5.3,** Laboratory sample used for investigating arc characteristic

Once the test voltage was applied to the sample, the arc voltage and leakage current waveform were then simultaneously recorded by means of the data acquisition system (DAQ) during the time period of arc propagation until the flashover happened. Figure 5.4 shows the photo taken from arc propagation on the cylindrical sample using a high speed camera at the moment the arc passes the measuring electrode.

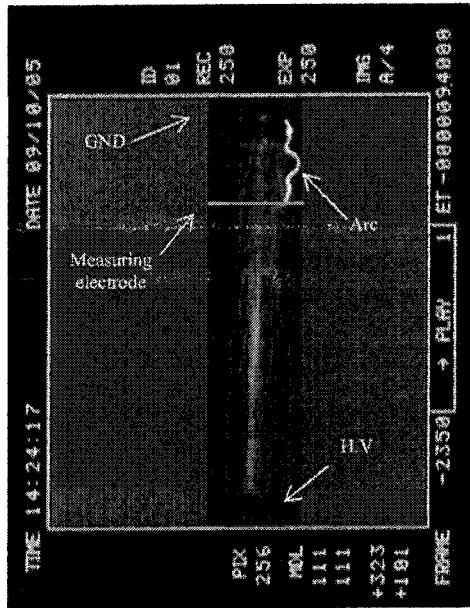


Figure 5.4, Arc propagation along the cylindrical model.

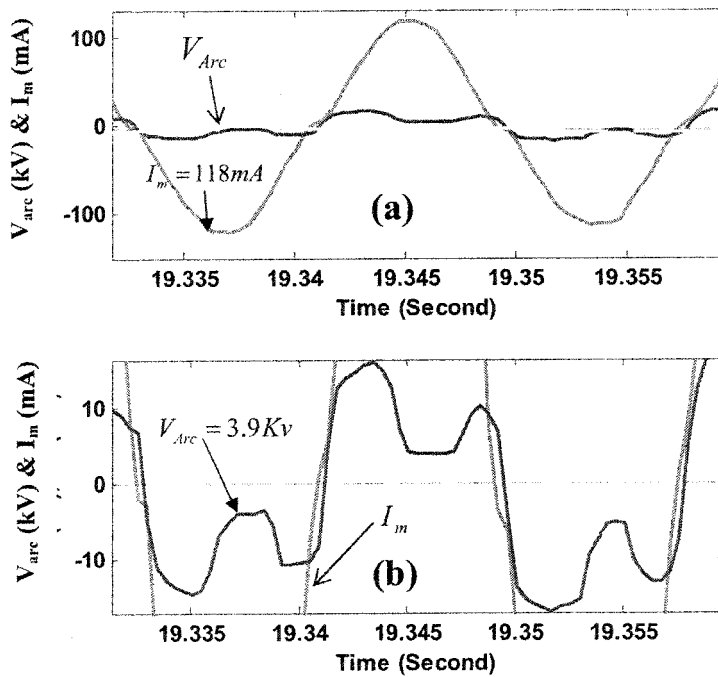


Figure 5.5 Arc voltage and leakage current waveform at the moment when the arc passes the measuring electrode.

By analyzing the arc voltage and leakage current waveforms and localizing the points corresponding to the moments when the arc passes the measuring electrode, a data set in the form of  $(V_{Arc_i}, I_{m_i}, i=1,2,3,..)$  was set up for different arc lengths, enabling us to determine arc constants for each arc length. Figure 5.5 (a and b) depicts a typical arc voltage and leakage current waveform at the moment the arc passes the measuring electrode and how the  $(V_{Arc_i}, I_{m_i})$  is measured. In order to have more precision in the measurement, the magnified size of figure 5.5 (a) is given in figure 5.5 (b). As noted from figure 5.5, the measured values corresponding to this moment for  $(V_{Arc_i}, I_{m_i})$  are (3.9 KV, 118 mA).

As described previously in chapter 4 of this dissertation, the joint effect of pollution and icing accompanied by environmental conditions is the main factor influencing the arc characteristics. In order to better reflect the effect of these parameters on arc characteristics, the experiments were performed under conditions characterized by a wide range of parameter variations as described in Table 5.2. The wide variation ranges of parameters (as summarized in table 5.2,) provided a relatively wide range of leakage current variation and corresponding arc voltage waveforms to be recorded and then analyzed.

**Table 5.2** The range of parameters characterizing test conditions

parameter	Range #1	Range #2	Range #3
$\theta$ (°C)	-5.6_-3.3	-3.3_-2.4	-2.4_0.1
SDD(mg/cm <sup>2</sup> )	0.015-0.05	0.05-0.1	0.1-0.25
$\delta$ (mm)	1.5-2.8	2.8-4.3	4.3-5.1
$\sigma$ ( $\mu$ S/cm)	3-12	12-23	23-30

The following section provides the results obtained for arc constants and re-ignition parameters in this study.

#### 5.3.1.1 Arc constants $A_p$ and $n_p$

The arc constants obtained for different arc lengths are shown in figures 5-6 through 5-8 depicting the  $E/I_m$  curves obtained from laboratory experiments. The mathematical relation between  $E$  and  $I_m$  was obtained by applying the regression method to the data shown in each figure. The horizontal axis in these figures is the leakage current  $I_m$  (A) which is primarily controlled by the level of applied voltage and also the parameters summarized in Table 5.2, and the vertical axis is the electric field intensity across the arc.

By examining the arc constants obtained for different arc lengths, it can be easily concluded that the value of the constant  $A$  decreases with an increase in arc length. This characteristic of arc constants has already been concluded by other researchers [27,28,29,30,11]. The tendency to decrease in value of the constant  $A$  is more significant for shorter arc lengths than that of longer arcs, suggesting that as  $x$  increases further the constant  $A$  will approach a certain value. The arc constant  $n$  does not show a remarkable change with respect to arc length.

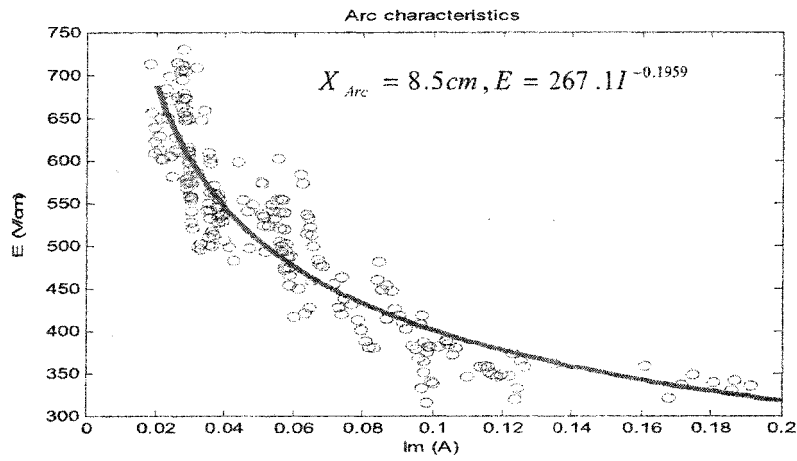


Figure 5.6  $E/I_m$  curve obtained for arc length:  $X=8.5$  cm

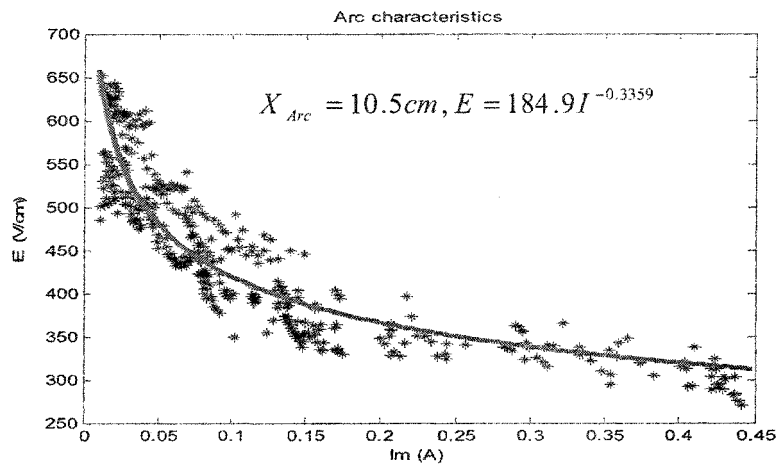
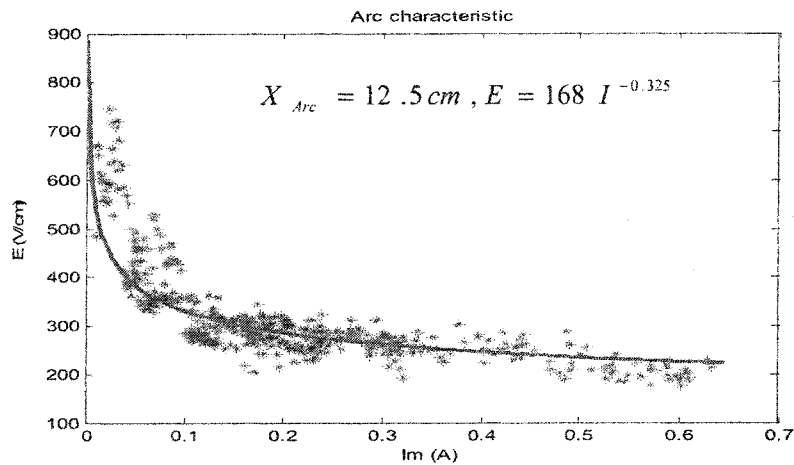


Figure 5.7  $E/I_m$  curve obtained for arc length  $X=10.5$  cm



**Figure 5.8**  $E / I_m$  curve obtained for arc length:  $X=12.5$  cm

The variation of arc constants ( $A$  and  $n$ ) in terms of arc length has been already concluded in [30], where the arc behaviour was studied on clean surfaces covered with ice. The authors have related this variation to the fact that the electrode voltage drop was neglected in calculating the arc voltage gradient. For the shorter arcs as the voltage across the arc length is in the comparable order to the electrode voltage drop, the values determined for parameter  $A$  and  $n$  are affected by electrode voltage, whereas for the longer arc lengths where the arc voltage is considerably higher than electrode voltage drop, the variation of parameter  $A$  and  $n$  versus arc length  $x$  is negligible and approaching almost constant values. This fact can be deduced by comparing arc characteristics illustrated in figures 5.6 to 5.8.

In static modelling of the flashover phenomenon, the most important length of the arc is its critical length, which substantially influences the calculation of flashover voltage. This critical length is about 60~70% of the total insulator length [27,29]. Therefore, in the modelling of the arc in this study, the arc constants should take the values obtained from the longest arc length. Thus, the arc constants  $A$  of 168 and  $n$  of 0.325 were adopted in the

modeling of flashover on the contaminated insulators covered with ice, so the arc characteristic in this study was determined as [99]:

$$E_{Arc} = 168 \cdot I^{-0.325} \quad (5-1)$$

### 5.3.1.2 Arc re-ignition parameters $K_p$ and $b_p$

As described earlier in chapter 2 where the Claverie re-ignition criterion was explained, the re-ignition criterion implies that when the peak value of the applied voltage is  $V_m$  (V) and the peak value of the leakage current is  $I_m$  (A), the length of the arc can reach  $X$  cm. In order to determine the re-ignition parameters, the same experiments as those explained for determining the arc constants were performed, except the data set was established in the form of  $(V_{m_i}, I_{m_i}, i=1,2,3,\dots)$  instead of  $(V_{Arc_i}, I_{m_i})$ .

It should be mentioned that the previous arc re-ignition parameters were determined based on the gradient of the applied voltage measured in V/m in this study. The reason for doing so, was to keep the unit conformity with the formula of residual voltage  $V_{Res}$  where the arc length is measured in (m) which will be explained in upcoming section of this chapter. The critical points collected for determining the arc re-ignition parameters are shown in figure 5.9, where the gradient of applied voltage is measured in V/cm and the current in (A).

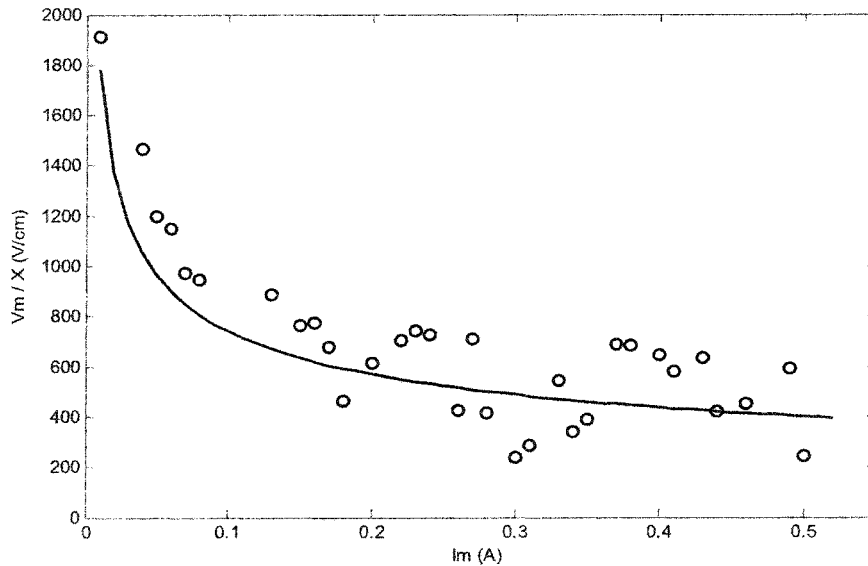


**Figure 5.9** The measured results for the re-ignition condition

By applying the regression method on this data, the mathematical expression for the arc re-ignition condition was found as:

$$\frac{V_m}{x} = \frac{308.4}{I^{0.3811}} \quad (5-2)$$

The arc re-ignition parameters (K and b) for clean surfaces covered with ice were reported as (1118 and 0.5277) in reference [29], and later these parameters have been reported as (1258.6 and 0.53) by the same authors in reference [11]. It would be worthwhile to make a quantitative comparison between the arc re-ignition parameters determined in this study and those reported in references [29] and [11]. According to the values of K and b given in [22], the required applied voltage gradient to re-ignite an extinguished arc current of 0.1 (A) is 3.7668 (kV/cm), i.e. 3766.8 (V/cm) or 376.68 (kV/m); and the voltage gradient due to the K

and  $b$  reported in [11] is 4.2647 (kV/cm), i.e. 4264.7 (V/m) or 426.47 (kV/m). The arc re-ignition parameters ( $K_p$  and  $b_p$ ) as given by equation (5-2) are (308.4 and 0.3811), where the voltage gradient was measured in V/cm. The previous parameters were determined as (1884 and 1.682) where the voltage gradient was calculated in V/m. The required voltage gradient due to the re-ignition parameters of ( $K_p=308.4$  and  $b_p=0.3811$ ) and ( $K_p=1884$  and  $b_p=1.682$ ) are 74.07143 (kV/m) and 90.590 (kV/m) which are considerably lower than the values given by [29] and [11]. The reason for this remarkable decrease in voltage gradient could be the presence of pre-contamination on the insulator surface which facilitates the arc re-ignition immediately after current zero condition.

The comparison between the result of this study and the previous works will be continued in section 5.5 of this chapter where the results of the application of the model to the industrial insulators will be discussed.

### 5.3.2 Test procedure for determining the residual voltage $V_{Res}$

As explained in chapter 4, a new approach based on identification methods was used for determining the residual voltage of the un-bridged part of the insulator in this study. This method relies on our observations acquired from a set of input-output data of the system under several test conditions. In order to fulfil our goal, providing the conditions of the insulator's exposure to the contamination and icing in field conditions was a key point for this step of the study. Obviously, the best way to reflect the field conditions was to collect a large enough number of pre-contaminated insulators from the field and then have them iced in the climate room. Unfortunately, owing to the lack of access to this kind of insulator, artificial pollution was formed on the insulator's surface. The solid layer method as described

in IEC 60507 standards was followed to form the pollution layer on the insulator's surface in this study [57].

The contaminated insulator was then placed in the climate room to be iced. The facilities of the climate room as depicted in figure 5.1 made it possible to perform the required experiments on a five-unit IEEE standard insulator string. In order to take into account the effect of the electrical field on ice formation, a constant service voltage was applied to the insulator in the course of ice accumulation. The ice type formed onto the insulator's surface, as well as the ambient conditions maintained over the ice accumulation period, was exactly the same as summarized in Table 5.1.

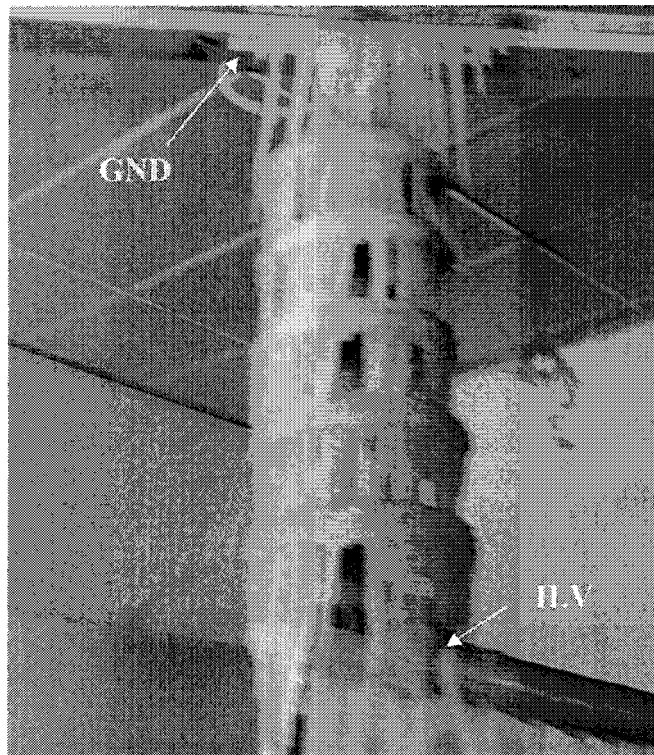


**Figure 5.10** Five-unit IEEE standard insulator string used for determination of  $V_{Res}$

After completing the icing process, the insulator under test looked as shown in figure 5.10.

A series of tests was carried out on this type of insulator and all observations and records obtained from the experiments were then analyzed for determining the parameters of the parametric function to be validated by these experiments.

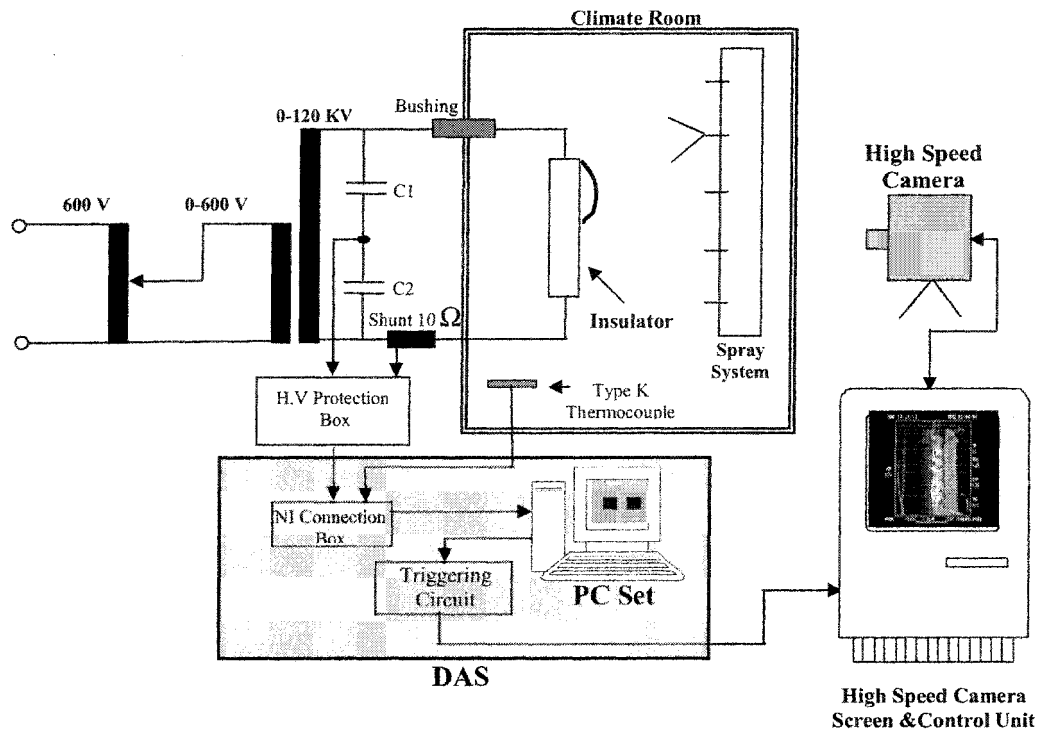


Figure 5.11 Laboratory setup used for determining  $V_{Res}$

Once the insulator was iced, the climate room temperature was allowed to rise from -12 to  $\pm 0.5$  ( $^{\circ}C$ ), which is the moment the insulator is the most susceptible to the initiation of electrical discharge and the formation of stable arcs. At this temperature, the amplitude of the leakage current was above 40 mA where stable and propagating arcs were observed along the

insulator's surface. The laboratory test setup used to carry out the experiments is shown in figure 5.11.

The facilities of data acquisition systems (DAS), as well as those of the high speed camera as shown in figure 5.11, made it possible to synchronize these two recording devices. This feature of the high speed camera played a key role in this part of the study as it was necessary to measure the corresponding arc length at any moment when the leakage current and  $V_{Res}$  were recorded. The electronic circuit depicted as Triggering circuit in figure 5.11 enabled us to trigger the high speed camera via the command signals produced by DAS, so synchronized observation of the arc length was fulfilled.

As explained in chapter 4 where the identification method used in this study was presented in detail, the main goal of this part of the study was to establish the train and test datasets in the form of  $(U_i, y_i)$  to be used in LSE or ANFIS identification methods.

The input and output vectors  $U_i$  and  $y_i$  are  $[SDD_i, \sigma_i, I_i, X_i]$  and  $V_{app} - V_{arci}$ , respectively and  $i=1, \dots, 90$ , of which 60 of this dataset were used for training purposes and the remaining 30 were kept for validating the mathematical model of V-I. The range of input variables is summarized in Table 5.3. It should be mentioned that the ice thickness ( $\delta$ ) made on the insulator's surface was 2 (cm) for all test samples used in experiments.

**Table 5.3** Input variables of train and test dataset

<b>Parameter</b>	<b>Variation Range</b>
<b>SDD (<math>mg / cm^2</math>)</b>	<b>0.013 – 0.238</b>
<b><math>\sigma</math> (<math>\mu S</math>)</b>	<b>10 - 80</b>
<b><math>I</math> (A)</b>	<b>0.02 – 0.25</b>
<b><math>x</math> (mm)</b>	<b>400 - <math>\approx</math>L ( 870 )</b>

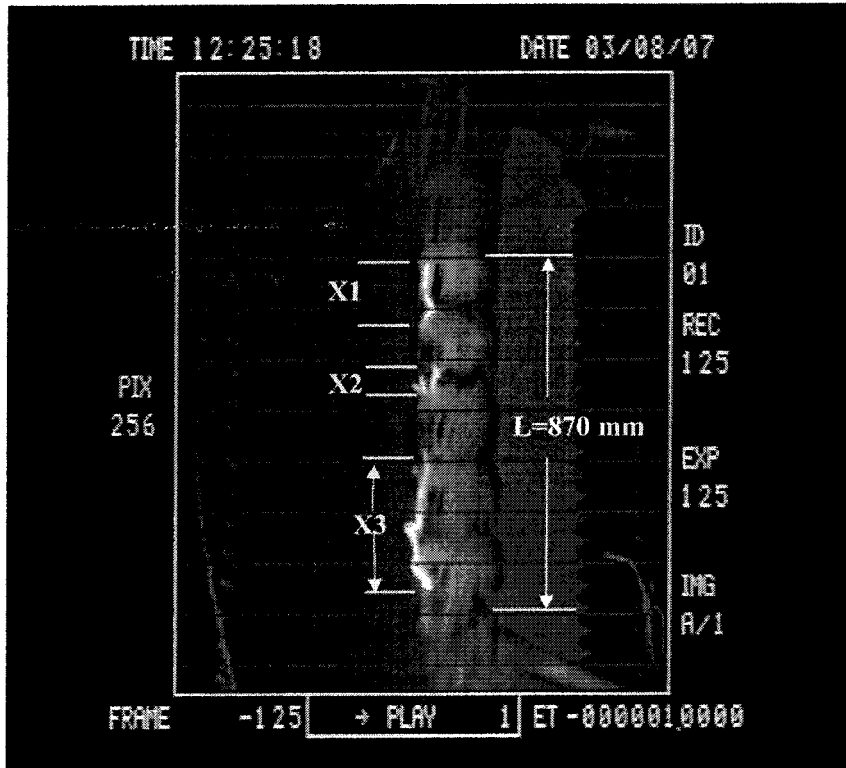


**Figure 5.12** Arc length observation using high speed camera.

Figure 5.12 is a magnified version of the image appearing on the high speed camera screen shown in figure 5.11. As can be noted, a multi arcs condition was shown in this figure; in such cases the arc length recorded in the data set was the sum of all partial arcs, or  $X_r = X_1 + X_2 + X_3$ .

### 5.3.2.1 Determination of V-I characteristic of residual voltage using LSE method

The LSE identification method was applied to the dataset as described above to determine the relevant parameters to the mathematical model as proposed by equation (4-8)

in chapter 4. By rearranging (4-8) as a linear relation of the parameter vector of  $P = [p_1, p_1, p_3]$ , this relation then reads as follow:

$$p_1 \cdot f_1(SDD) + p_2 \cdot f_2(\sigma) + p_3 \cdot f_3(I) = (L - x) \frac{I}{V_{Res}(I)} \quad (5-3)$$

Equation (5-3) describes a linear relation between the parameters to be identified. It has been previously stated that the choice of the appropriate input functions  $f_i$  depends on our knowledge about the nature of the phenomenon, as well as the results obtained after applying the test dataset. This fact was explained in chapter 4 where the structure identification was discussed.

At first attempt, a set of identity functions for  $f_i$  were adopted to be checked in equation (5-3). But the results obtained after applying the test data to the mathematical model were not satisfactory, i.e. the output of the model did not fit enough with the output of the test data.

The criterion for adopting the proper forms for  $f_i$  functions was heavily relying on the results of previous studies aimed at analyzing the mixed effect of pollution and icing on electrical performance of high voltage insulators. As it was previously discussed in section (3.3), the effect of a pollution layer on ice film conductivity during the melting period, as well as on the maximum flashover voltage, was investigated by Shu, Sun, Zhang and Gu in China [100]. It was concluded that the maximum withstand voltage decreases with an increase in the pollution level up to an SDD of  $0.09 \text{ mg} / \text{cm}^2$  and remains constant for higher levels. This

suggests a saturated function in the form of  $(1 - e^{-\frac{SDD}{b_1}})$  for the variable SDD. The parameter  $b_1$  was then determined by trial and error procedure using training and checking (validating) data sets as described earlier in this section. Moreover, it is stated in [22] that the variations

of the maximum withstand stress of a short string of IEEE standard insulators covered with wet-grown ice versus  $\sigma$  was given by a function of exponentiation form. Therefore, the function adopted for the variable  $\sigma$  was in the form of  $\sigma^{b_2}$ , where the parameter  $b_2$  was determined in the similar way as described above.

After trying several candidates chosen based on the foregoing review of previous studies, the satisfactory results were obtained when the functions  $f_i$  were chosen as:

$$\begin{cases} f_1(SDD) = (1 - e^{\frac{-SDD}{0.053}}) \\ f_2(\sigma) = \sigma^{1.27} \\ f_3(I) = I \end{cases} \quad (5-4)$$

The parameter set, based on the  $f_i$ s given by (5-4), was then determined as:

$$p = K.[0.317, 8.503 \times 10^{-5}, 0.1462] \quad (5-5)$$

Where  $K = 10^{-6}$ . Hence, the form of the V-I function determined for residual voltage reads as:

$$V_{Res}(I) = \frac{(L-x)I \times 10^6}{0.317(1 - e^{\frac{-SDD}{0.053}}) + 8.503 \times 10^{-5} \sigma^{1.27} + 0.1462 I} \quad (V) \quad (5-6)$$

Where  $I$ ,  $SDD$ ,  $\sigma$  and  $x$  are given in A,  $mg/cm^2$ ,  $\mu S$  and m, respectively.

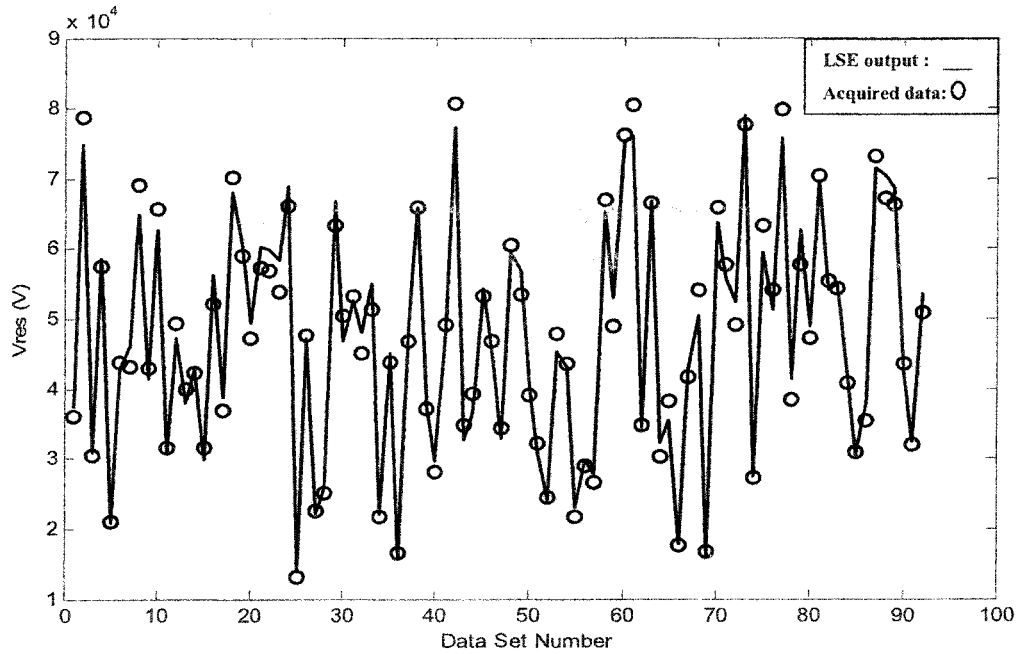


Figure 5.13 Estimated and recorded residual voltage ( $V_{Res}$ )

Figure 5.13 illustrates how  $\hat{V}_{Res}(y_i)$  given by (5-6) fits the recorded voltage ( $y_i$ ) using data acquisition system shown in figure 5.11. The solid line in this figure shows the LSE model output ( $\hat{y}_i$ ) and the circles represent the recorded data ( $y_i$ ). The complete data set comprising the whole recorded data in the form of  $[U_i y_i]$  (i.e.  $[SDD_i \sigma_i X_i I_i y_i]$ , where  $i=1, \dots, 91$ ) is tabulated in Appendix A. It should be mentioned that a new insulator setup was prepared as shown in figure 5.12 corresponding to each value for  $(SDD_i, \sigma_i)$  pairs and one or more readings were recorded for  $X_i$  and  $I_i$  depending on the quality of the images captured from the screen of high speed camera.

In order to better clarify the behaviour of  $V_{Res}$  versus the variation of the leakage current, the V-I characteristic of  $V_{Res}$  under two different conditions is illustrated in figure 5.14 (a and b).

For the purpose of better illustrating the effect of leakage current on residual voltage, the values of  $V_{Res}$  for higher level of leakage currents (above 250 (mA)) have been calculated by extrapolating the equation (5-6) over leakage current, otherwise the power source 120 kV (maximum), 240 kVA used in high voltage laboratory is not capable to cause a current flow of higher than 250 (mA).

As may be noticed from figure 5.14 (a), the linear curve denoted as (1) corresponds to  $P_3=0$  in equation (5-6) leading to a linear relation between  $V_{Res}$  and I, and the non-linear one denoted as (2) was obtained for  $P_3=0.1462$ . The same graphs are shown in a shorter current range of 0 to 0.35 (A) in figure 5.14 (b), where the departure point of the linear and non-linear curves is given with more precision.

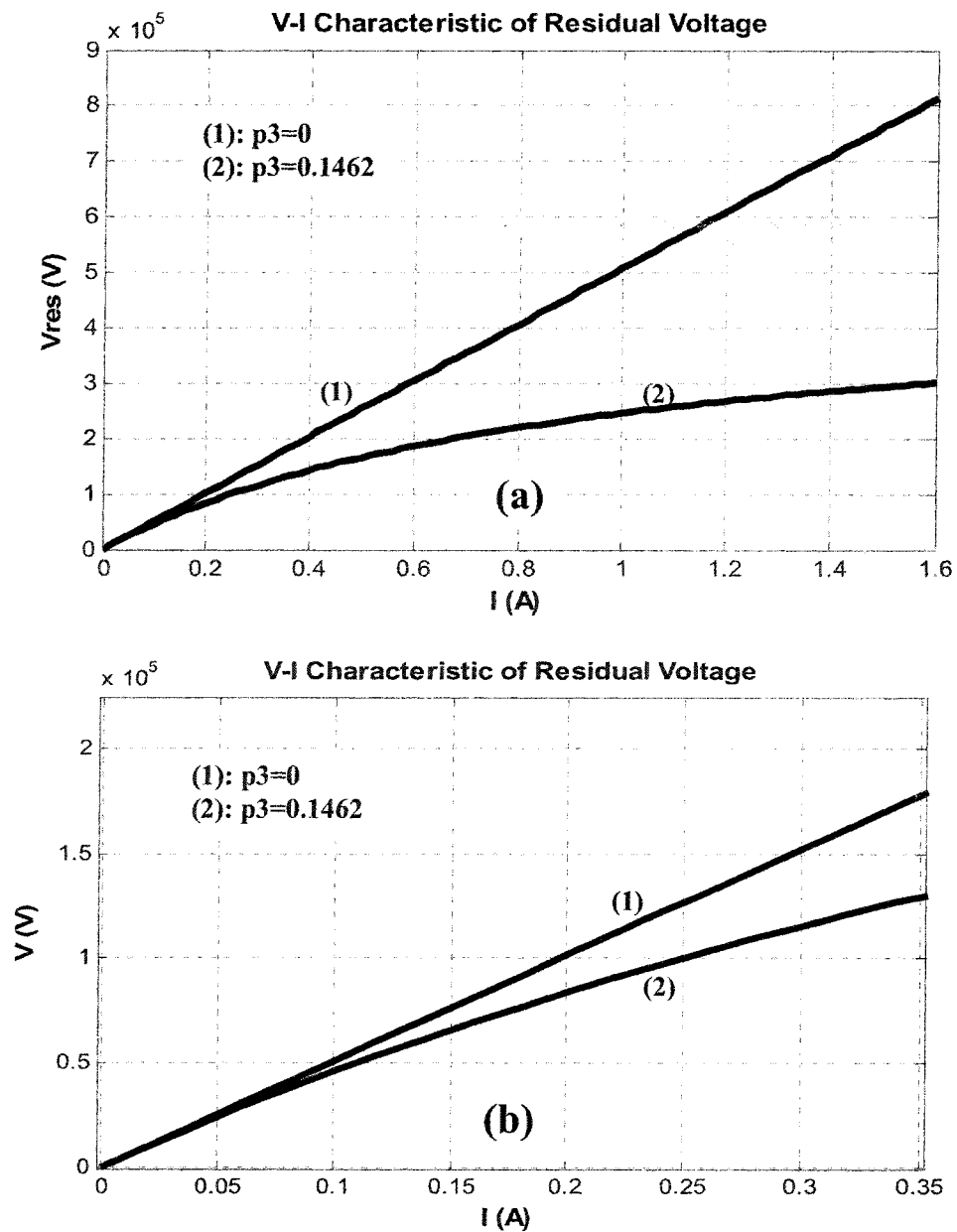


Figure 5.14 V-I characteristic of residual part of insulator.  $x=0.65L$

By examining figure 5.14 (b), it is quite obvious that there is no remarkable difference between (1) and (2) in the current range of 0 to 0.05 (A) (50 mA). In this current range, the current zero corresponds to the physical condition where there are no local discharges along

the insulator's surface. Hence, almost all portions of the applied voltage appear along air gaps and the conductive part of the insulator withstands almost zero percent of the applied voltage [112, 59]. As the leakage current tends to increase up to 0.05 A (50 mA), the residual voltage according to the both linear and non-linear curves increases almost linearly with respect to the leakage current. This range of leakage current illustrates the physical condition when the partial discharges along the insulator's surface were initiated across air gaps but the arc current level is not high enough to initiate the local melting effects at the arc foot. As the leakage current reaches around 0.07 A (70 mA), the effects of local melting and other physical factors (described previously in chapter 4, section 4.2.1) become tangible, leading to a remarkable decrease in residual resistance. Therefore, a greater increase in the leakage current causes a greater difference between curve 1 and 2. In other words, for levels of leakage current higher than 50 (mA), the V-I characteristic demonstrates a non-linear behaviour for this electrical element.

#### 5.3.2.2 Determination of V-I characteristic of residual voltage using ANFIS

As explained in chapter 4, the identification model uses both fuzzy logic and an artificial neural network in its structure. For this reason, it is capable to identify the systems which are not identifiable using classical identification models, even LSE.

MATLAB software has its own toolbox containing a variety of membership functions and rule bases for ANSFIS applications. Once the ANFIS toolbox named "anfisedit" is run in MATLAB environment, the GUI (Graphic User Interface) illustrating the ANFIS editor window as shown in figure 5.15 This window includes four distinct areas to support all

required actions in order to implement Fuzzy Inference System (FIS) in network framework.

The GUI lets user perform the following tasks:

1. The first box from left below the plot area performs load, plot, and clear the data actions. The data (comprising a set of column vectors which the last column should be always the output vector) can be loaded from a file or MATLAB workspace. Similarly an already data can be cleared pressing clear button in this area.

2. The second box generates or loads the FIS (Fuzzy Inference System) model structure. Before starting the FIS training, the user should specify an initial FIS model structure. There are two options to specify the model structure, it can be loaded from a previously saved Sugeno-type FIS structure from a file or directly from the MATLAB workspace.

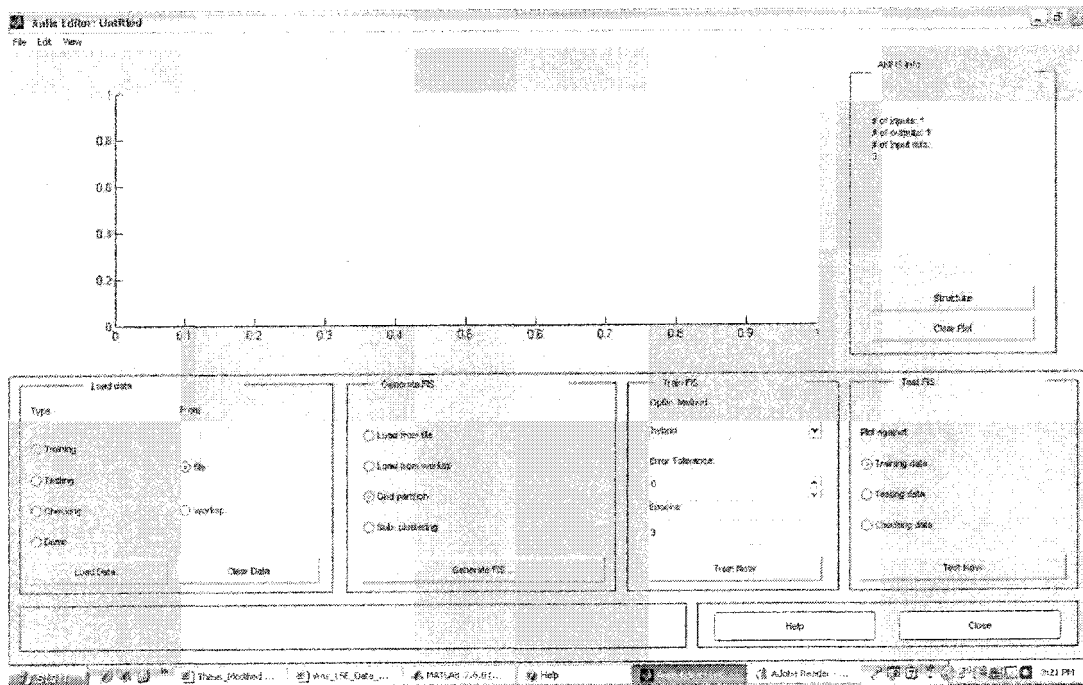


Figure 5.15 MATLAB graphic user interface (GUI) for ANFIS

3. Once the training data was loaded, the FIS can be trained using optimization methods. The initial FIS model can be generated by choosing one of the following partitioning techniques: Grid partitioning which Generates a single-output Sugeno-type FIS by using grid partitioning on the data, and Sub. Clustering which generates an initial model for ANFIS training by first applying subtractive clustering on the data [98]. The second method i.e. ANFIS training method was used in this study. Once the partitioning and training methods were specified, the architecture of the network used in this study appeared as shown in figure 5.16, where the input variables are denoted as SDD,  $\sigma$ , I and L-x .

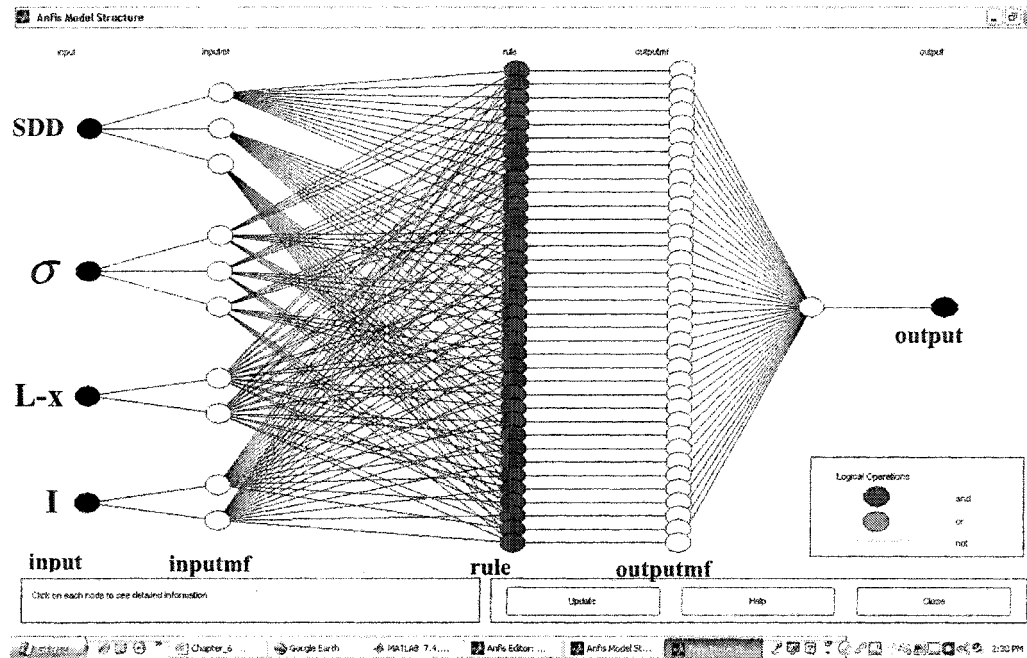


Figure 5.16 ANFIS structure

The membership functions used for the input variables are in Gaussian form providing a sufficient degree of precision. Figure 5.17 shows the membership functions for input variable SDD of the Gaussian type covering the complete variation range of this

variable. The other three membership functions have the same forms as those used for SDD shown in figure 5.17. It may be noted from figure 5.16 that the different numbers of membership functions were used in first layer for input variables. Normally the number of membership functions used for an input variable depends on how the variable influences the overall output of the network. Generally, the more precise input data recording, the more membership functions is required, however there has to be a trade off between precision and the complexity of the architecture of ANFIS. Hence, it is reasonable to reduce the total number of membership functions as low as possible. As it was previously cited from reference [100] and [22] the variable SDD and  $\sigma$  has non-linear effects on  $V_{tes}$  whereas the effect of I and X is relatively linear. Therefore the data recording precision has to be higher for SDD and  $\sigma$  requiring three membership functions, whereas two membership functions was enough for each of variables I and L-X.

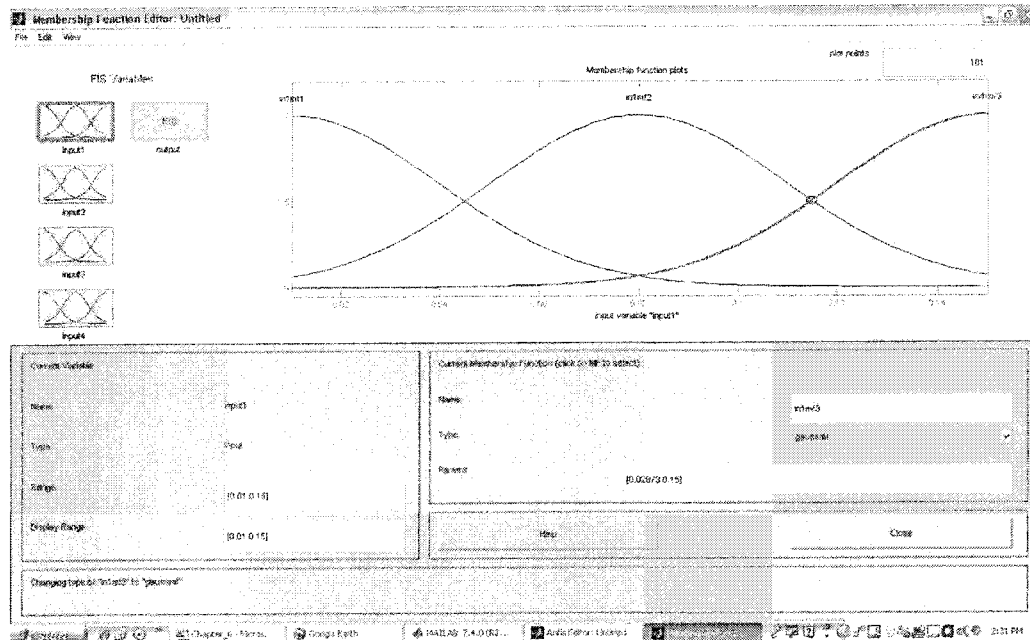


Figure 5.17 Membership functions used for input variable SDD

4. After loading the training data and generating the initial FIS structure, we can proceed with training the FIS. In the third box shown in figure 5.15 there are two options specifying the optimization methods for training the FIS as “Hybrid” or “Back propagation”. The hybrid learning method was used for training the FIS as it provides a very rapid learning process and prevents any possibility of being trapped into relative minimum error holes that it sometimes happens to the single back propagation learning method [98].

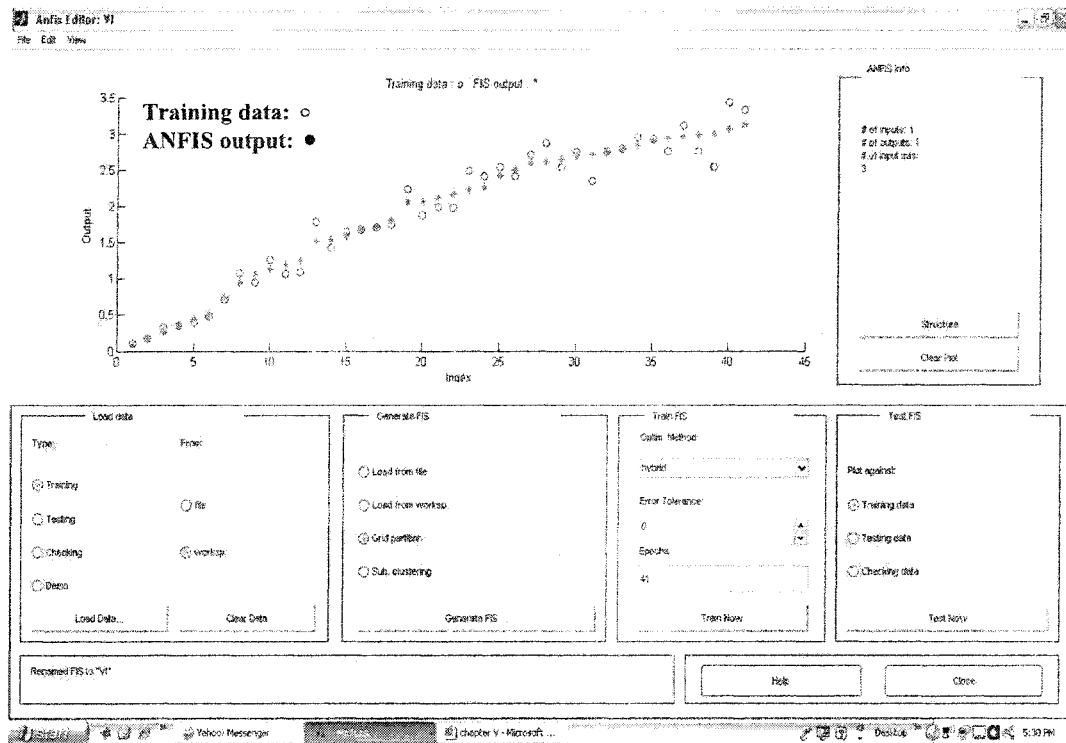


Figure 5.18 ANFIS training

Figure 5.18 shows the ANFIS network output after performing the learning process. In this figure, the circles and solid dots represent the training and ANFIS output, respectively.

In order to make a comparison between  $V_{Res}$  calculated using LSE and the ANFIS method, the output of equation (5-6) and that of ANFIS were plotted against the leakage current as shown in figure 5.19. It may be noted from this figure that ANSIF was more sensitive on training data than LSE, as its curve swings around the LSE curve. This fact may be considered an advantageous point for ANFIS over LSE; however, the mathematical formula introduced by LSE was easier to manipulate in the static model developed in this study.

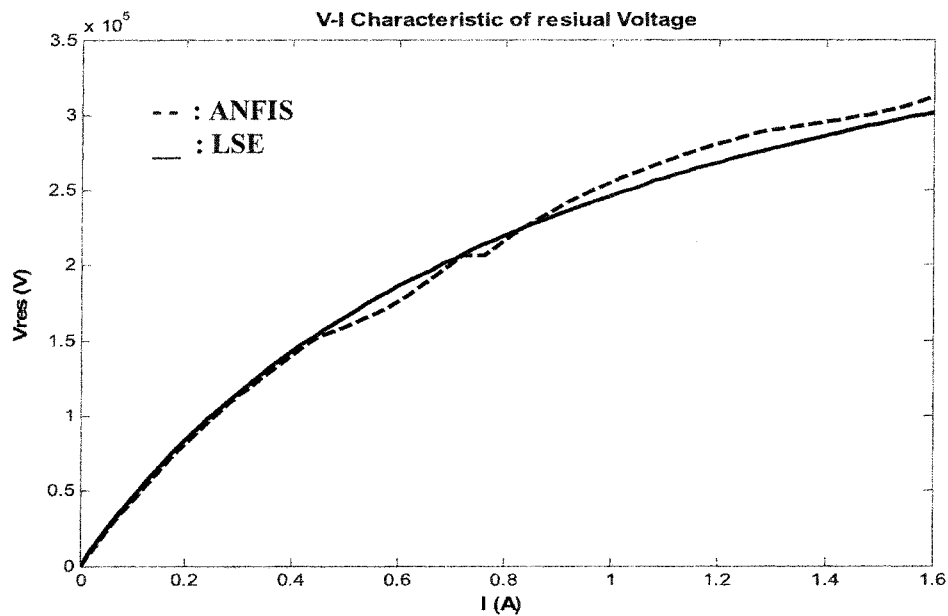


Figure 5.19 Comparison between calculated  $V_{Res}$  using LSE and ANFIS

#### 5.4 Dynamic or differential resistance of contaminated insulator covered with ice

##### 5.4.1 Calculated resistance using LSE

Once the V-I characteristic of the residual voltage was known, it was straight forward to calculate the dynamic resistance of the residual part of the insulator. The dynamic resistance of a non-linear electrical element (device) is given as:

$$R_{dif} = \left. \frac{dV}{dI} \right|_{I=I_0} \quad (5-7)$$

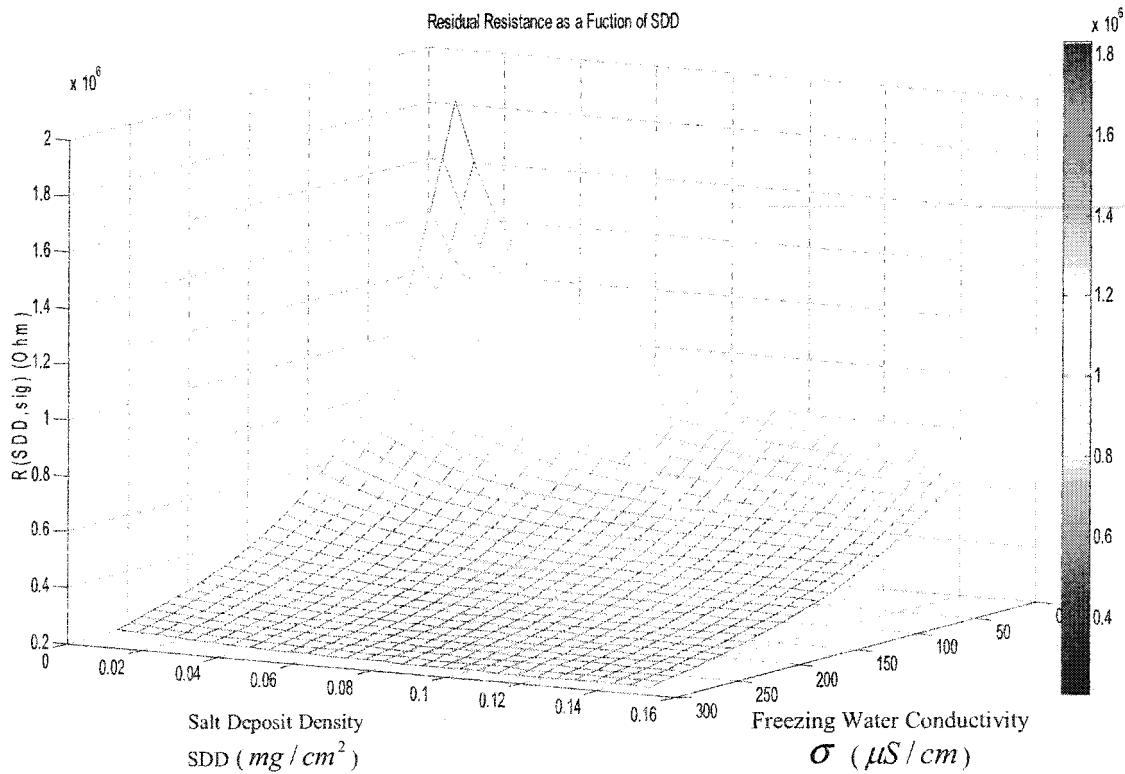
Where R is the resistance and I and V are the current and voltage across the element.

By applying (5-7) to (5-6), the residual resistance of the insulator reads as:

$$R_{din}(SDD, \sigma, I, x) = \frac{L-x}{0.317(1-e^{\frac{-SDD}{0.053}}) + 8.503 \times 10^{-5} \sigma^{1.27} + 0.2924I + \frac{0.0201}{0.317(1-e^{\frac{-SDD}{0.053}}) + 8.503 \times 10^{-5} \sigma^{1.27}}} I^2 \quad (M\Omega) \quad (5-8)$$

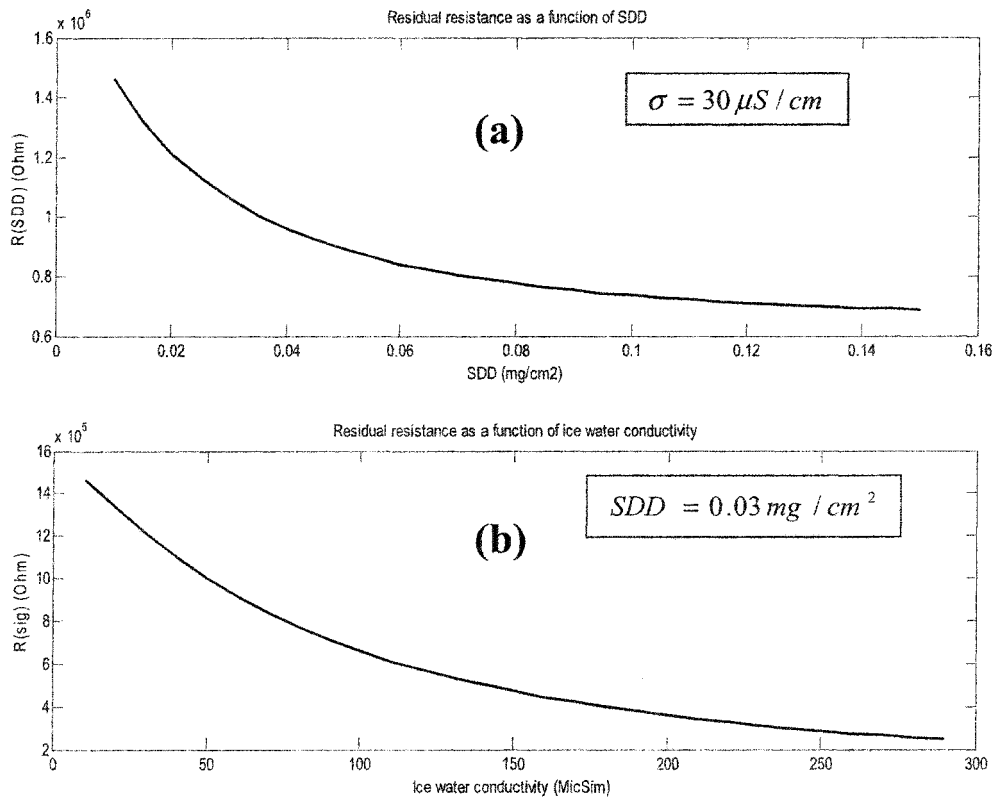
Where SDD is given in  $mg/cm^2$ ,  $\sigma$  in  $\mu S/cm$ , L and x in m and I in A.

Figure 5.20 illustrates a three dimensional graph describing the residual resistance given by equation (5-8). The vertical axis is the magnitude of  $R(SDD, \sigma)$  versus SDD and  $\sigma$  along the horizontal axis.



**Figure 5.20** Dynamic resistance as a function of ESDD and  $\sigma$ .  $I=0.15$  (A) and  $x=0.65L$ .

In order to have a quantitative idea about the sensitivity of the residual resistance on the variation of ESDD and  $\sigma$ , the individual effects of SDD and  $\sigma$  on the overall dynamic resistance are shown in figure 5.21. Figure 5.21 (a) shows the variation of  $R(x)$  with respect to SDD while  $\sigma$  is kept constant at  $30 \mu S/cm$  whereas figure 5.21 (b) describes the effect of  $\sigma$  on  $R(x)$  when SDD is  $0.03 mg/cm^2$ .



**Figure 5.21** Comparison of individual effect of SDD and  $\sigma$  on dynamic residual resistance.

a)  $R(x)$  versus SDD,  $\sigma = 30 \mu S / cm$ ,  $I=0.15$  (A) and  $x=0.65L$

b)  $R(x)$  versus  $\sigma$ ,  $SDD = 0.03 mg / cm^2$ ,  $I=0.15$  (A) and  $x=0.65L$

By comparing these two graphs an immediate result may be concluded concerning the sensitivity of  $R(x)$  to  $\sigma$  and SDD. As can be noted, the residual resistance is more sensitive on  $\sigma$  than SDD. The reason could be explained by considering the different conductive paths with different cross areas provided by pollution and ice. As is known, the pollution is deposited onto the insulator's surface, whereas the ice film appears at the outmost layer of the ice accumulation, the average diameter of which is greater than that of the insulator, creating a greater conductive cross area. Another reason in justification of this phenomenon

may be given based on the effect of the evaporation of the ice film during arc propagation, providing a conductive media in the vicinity of the ice film.

#### 5.4.1.1 Quantitative comparison between dynamic and residual resistance

A comparison between dynamic resistance calculated in this study and the residual resistance calculated by Farzaneh *et al* [28,29] using R. Wilkins formula [116] is provided in this section. Although the concepts of calculating the dynamic and residual resistances are different in nature, as are their applications, however it would be worthwhile, at this step, to make a quantitative comparison between these two resistances to examine their sensitivities to the variation of the leakage current.

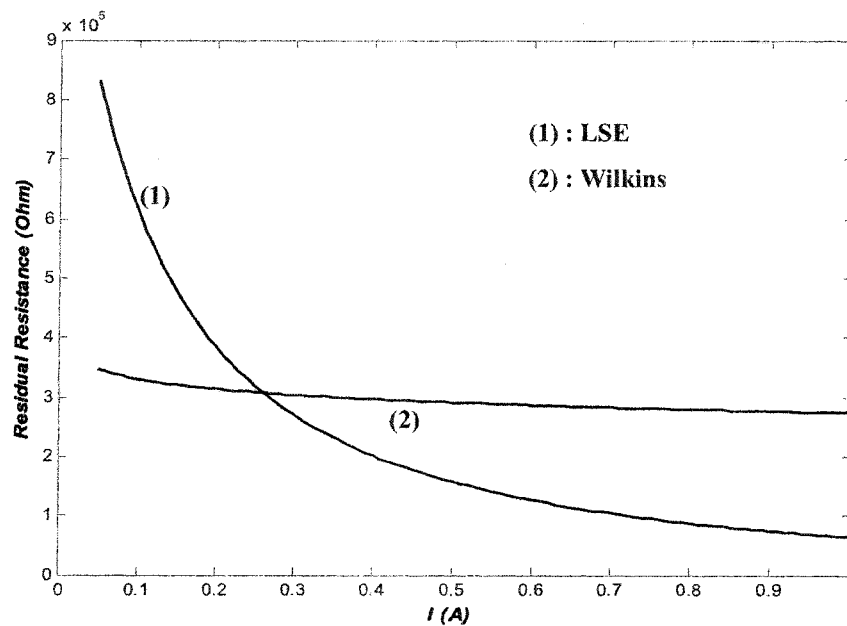


**Figure 5.22** Comparison between calculated resistance using LSE and the formula of R. Wilkins [116]

In these calculations, the freezing water conductivity ( $\sigma$ ), the salt deposit density (SDD) and the ice thickness ( $\epsilon$ ) were  $60 (\mu S / cm)$ ,  $0 (mg / cm^2)$  and  $2 (cm)$ , respectively.

The dimensions of the equivalent surface of the ice were  $W=46.2$  and  $L=80.9$  (cm), as reported in reference [29].

The calculated resistances based on the above mentioned geometrical and physical characteristics are illustrated in figure 5.22, where graph number (1) and (2) denote the resistance calculated using LSE and the formula due to R. Wilkins. The variation of dynamic and residual resistance versus leakage current over the range of 0.05 to 1 (A) is shown in this figure. It can be noticed that the dynamic resistance calculated using LSE demonstrates a higher sensitivity over the leakage current than that of the formula of R. Wilkins. For the leakage current level of 0.05 (A), graph (1) provides a resistance about three times that given by (2). The reason for such a considerable difference may be deduced by examining the ice geometry shown in figure 5.10. It is easy to note that the effective circumference of the ice cylinder is smaller than that of a uniform ice cylinder considered in calculating the width of the equivalent surface. As can be seen, the ice cylinder circumference is made by several individual icicle columns connecting two adjacent insulator units. Such a geometry provides a remarkably smaller circumference than that of a uniform ice cylinder, i.e.,  $W < 46.2$  cm. As the leakage current increases up to orders of 0.2 (A), graph (1) decreases very rapidly from  $850\text{ K}\Omega$  to almost half of its initial level, i.e.  $400\text{ K}\Omega$  ; whereas graph (2) demonstrates a relatively lower sensitivity to leakage current variation, yielding a small change from  $350\text{ K}\Omega$  to  $300\text{ K}\Omega$  . In this current range, due to the local melting effects caused by single or multiple arcs along the ice layer, the thickness of the conductive ice layer gets bulked out so that the ice layer provides volume conductivity with a tangible cross area, instead of surface conductivity. Hence, the effective conductive layer can no longer be considered as surface conductivity. This effect was not reflected by the formula developed by R. Wilkins, since it

was originally developed for calculating the resistance of a uniform and very thin pollution layer, where a constant surface conductivity was considered over a wide range of current variation.

For the leakage current levels above this range, the melting effect causes a greater increase in the thickness of the conductive ice layer, leading to a further decrease in resistance as demonstrated in figure 5.22.

As explained in chapter 4, where the method used for determining the V-I characteristic of the residual voltage was illustrated, since the method uses the observations of input-output of the system under identification, it is able to account for several physical phenomena influencing the behaviour of the system. Thus the above mentioned results were already expected from the mathematical model developed for residual resistance in this study.

#### 5.4.2 Calculation of dynamic or differential resistance using ANFIS

The training dataset used in ANFIS for determining the dynamic resistance was somewhat different from those used for determination of residual voltage. In this case the input vector was the same as the one used for determining the  $V_{Res}$ , but the output vector was the first derivative of the residual voltage with respect to the leakage current, so the train dataset in the form of  $(U_i, (\frac{dV}{dI})_i)$  was used in this case. In order to establish a data set in the form as described above, two approaches were followed as will be explained below:

##### 5.4.2.1 First approach:

The first approach uses the instantaneous Voltage and Current waveforms as shown in Figures 5.23 through 5.25. As illustrated in figure 5.23, by analyzing several waveforms

and calculating the  $(\frac{dV}{dI})_i$ , ( $i=1, \dots, 112$ ) shown in figures 5.24 and 5.25, the required dataset was completed and then used as training data for the ANFIS network. It should be mentioned that the same learning procedure was followed in this case as was explained for determining  $V_{Res}$  in the preceding section.

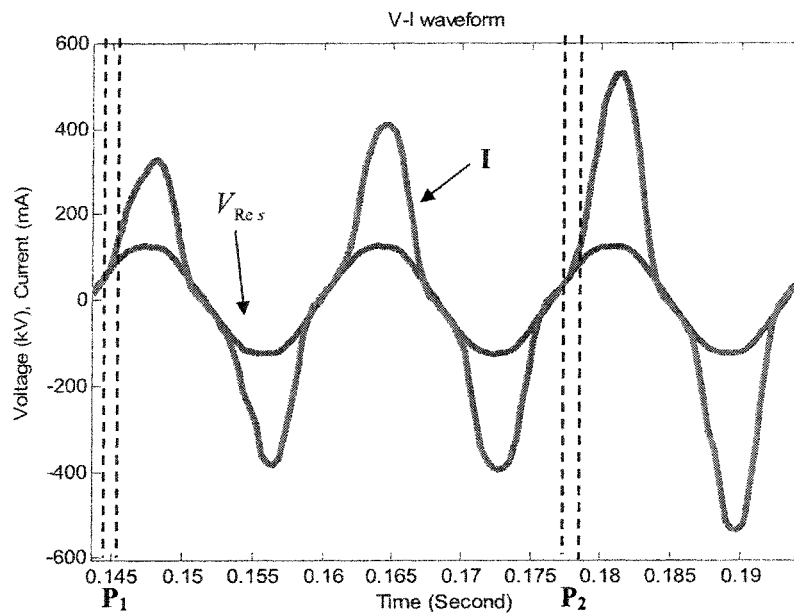


Figure 5.23 A sample waveform used for establishing  $(U_i, (\frac{dV}{dI})_i)$  data set.

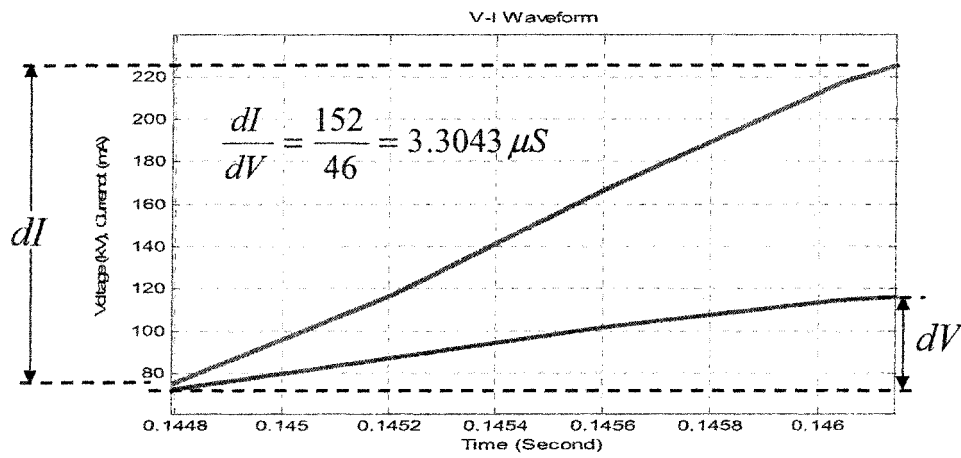


Figure 5.24 Magnified waveform corresponding to the time interval  $P_1$  shown in figure 5.21

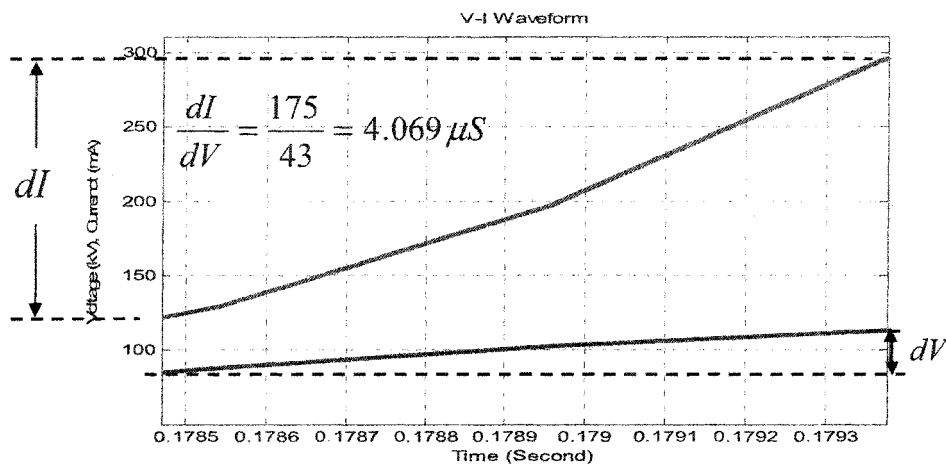
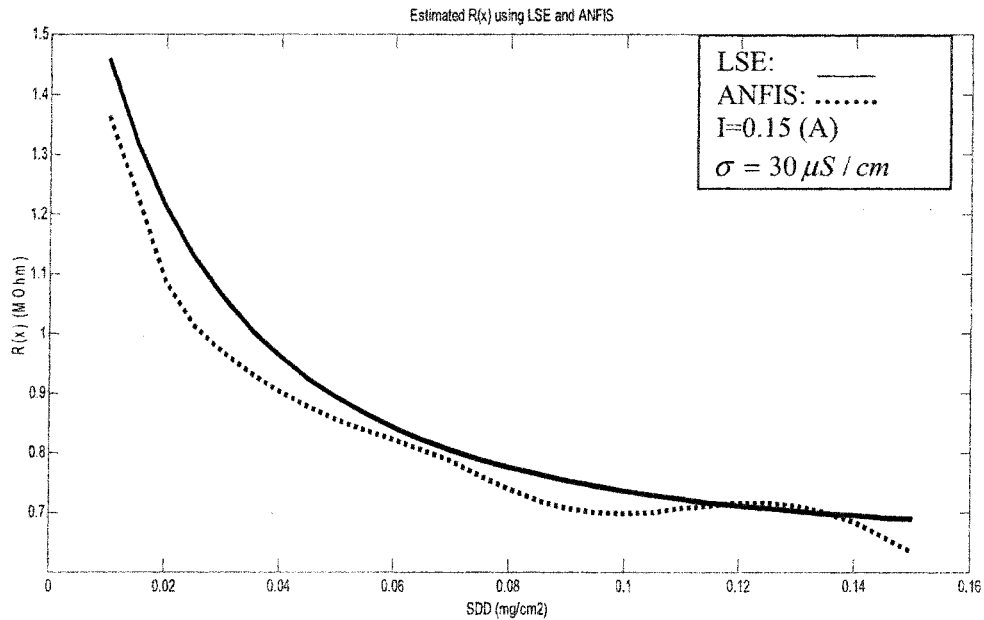


Figure 5.25 Magnified waveform corresponding to the time interval  $P_2$  shown in figure 5.21

The variation of resistance versus SDD is illustrated in figure 5.26, where the solid and dotted curves represent the estimated resistance using LSE and ANFIS, respectively.



**Figure 5.26** Estimated resistance using LSE and ANFIS. (First method)

Figure 5.26 illustrates an acceptable concordance between the results obtained from both ANFIS and LSE methods, but the output of ANFIS is noisier than LSE. Despite the agreement attained between ANFIS and LSE this approach is susceptible to yield erroneous results if the data collected in the form of  $(U_i, (\frac{dV}{dI})_i)$  would be in vicinity of peak and current zero points of instantaneous waveforms. The second approach as described below was capable to cope with the situation as mentioned above.

#### 5.4.2.2 Second approach:

The second approach uses rms values of the voltage and current instead of instantaneous waveforms to calculate the resistance. This method uses the ANFIS network trained for calculating  $V_{Res}$  where the Rms values of voltage and current were used. Figure 5.19 is presented here again in order to illustrate how the resistance was calculated. This

figure illustrates a numerical method to calculate the first order derivative of voltage versus current using the V-I characteristic of residual voltage.

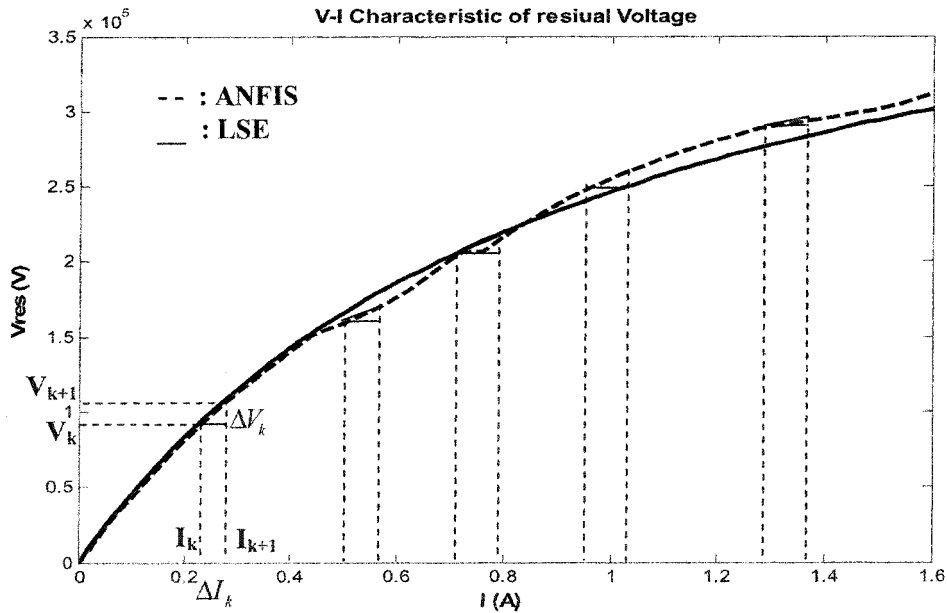
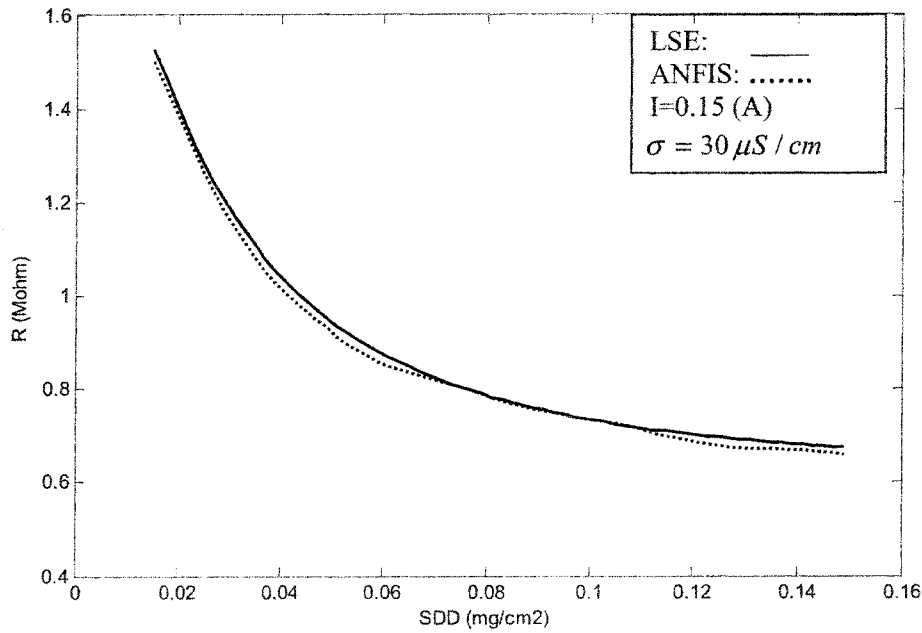


Figure 5.27 V-I characteristic of  $V_{Res}$  used for calculating the resistance

For the purpose of performing numerical derivative the horizontal axis of figure 5.27 was subdivided into the small parts denoted as  $\Delta I_k$  and the corresponding variation in voltage was determined using V-I curve provided by ANFIS. The number of subdivisions shown in figure 5.27 was 78 providing a good precision for performing numerical derivative. According to the equation (5-7) the numerical derivative can be expressed as below:

$$R_k = \left| \frac{\Delta V_k}{\Delta I_k} \right| = \left| \frac{V_k - V_{k-1}}{I_k - I_{k-1}} \right|_{I=I_k \& (SDD, \sigma, x) = Const} \quad (k=2, \dots, 78) \quad (5-9)$$

Where,  $R_k$  is the resistance and  $(\Delta I_k, \Delta V_k)$  are the changes in current and voltage in  $K$ th subdivision. The resistance thus calculated using ANFIS and LSE is shown in figure 5.28.



**Figure 5.28** Estimated resistance using ANFIS and LSE. (Second method)

It may be noted from figure 5.28 that the curve illustrating the resistance determined by ANFIS in this method demonstrates less fluctuations than that of calculated in first approach and the results obtained from LSE and ANFIS show lower differences over full range of current.

### 5.5 Validation tests

A set of experiments has been carried out on the five-unit of the IEEE standard insulator string in the high voltage laboratory of CIGELE. The test standard adopted by Farzaneh *et al* for determining minimum flashover voltage of ice covered insulators was followed [18,19]. Figure 5.10 shows the insulator strings used in the validation tests. Several

tests were carried out and recorded using LABVIEW software. Figures 5.29 and 5.30 describe samples of the recorded tests results with withstand and flashover, respectively.

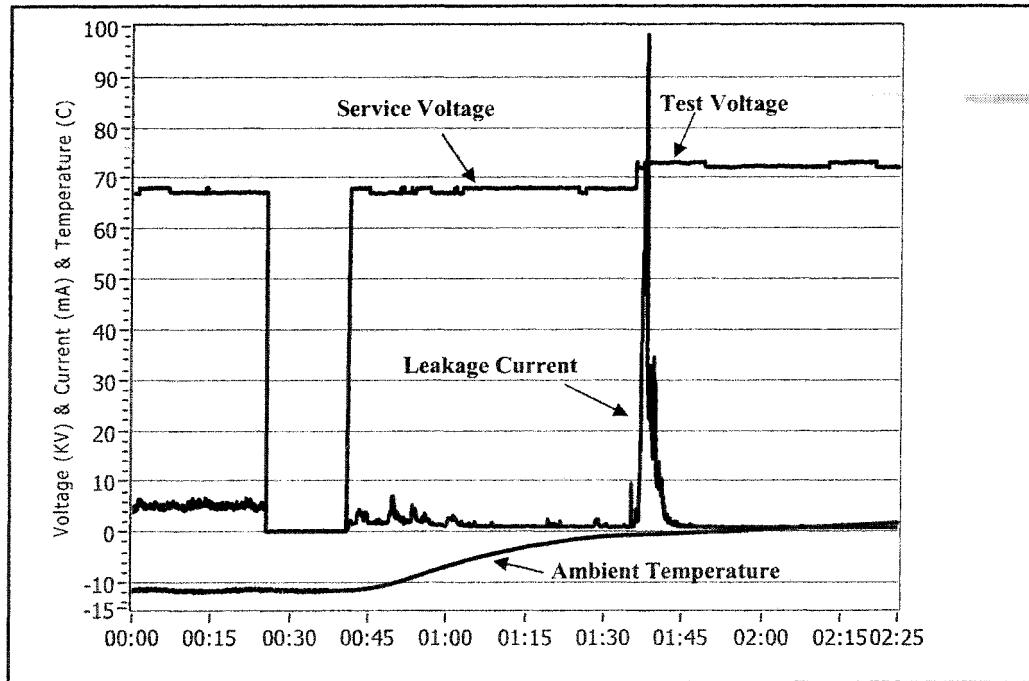
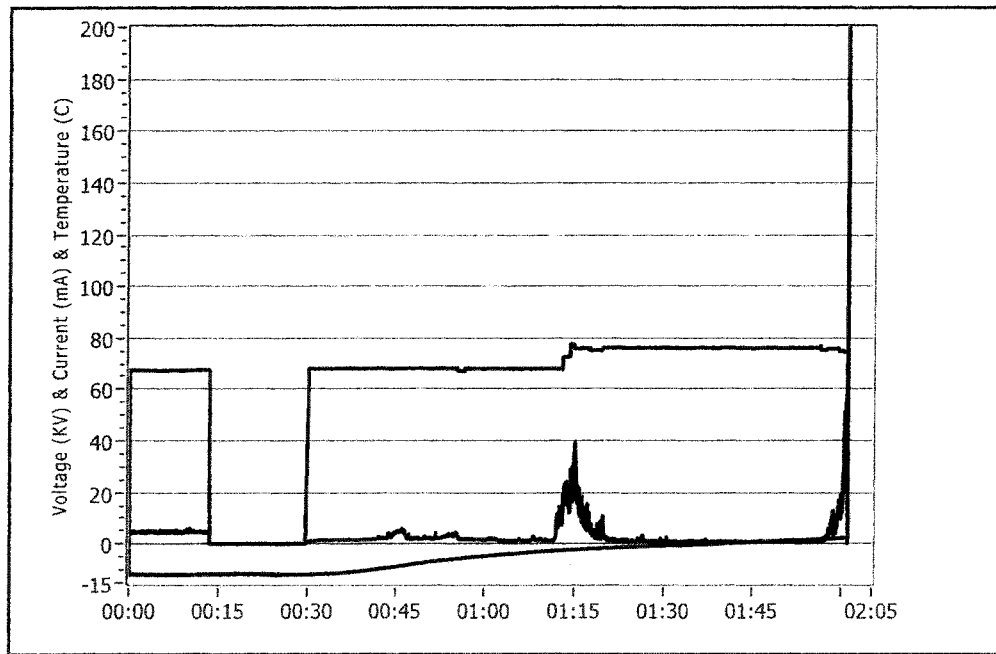


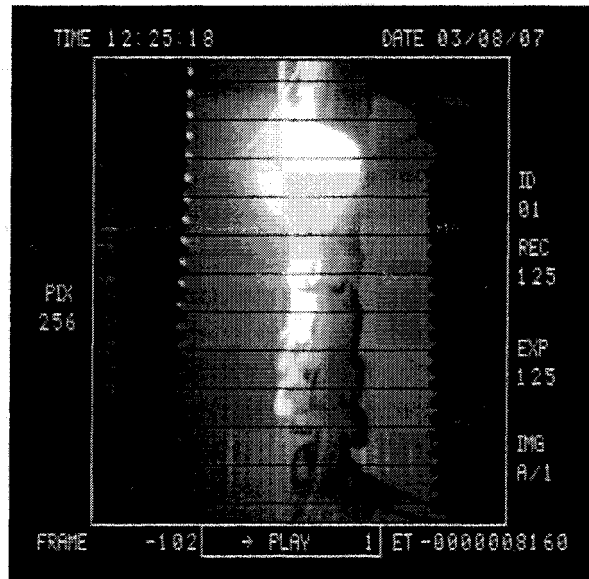
Figure 5.29 Validation test resulted in withstand

Figure 5.25 illustrates the sequence performed in conformity with the standard due Farzaneh *et al.* The ice accumulation process was first performed at a temperature of  $-12^{\circ}\text{C}$  under service voltage. After completing the ice accumulation, the service voltage was removed and the hardening phase was carried out in order to have a dry ice accumulation on the insulator's surface. Following the completion of the hardening phase, the climate chamber was allowed to warm up until the ambient temperature reached around  $0^{\circ}\text{C}$ , which is the temperature at which ice film formation takes place on the ice surface. At this moment the expected test voltage was applied.



**Figure 5.30** Validation test resulted in flashover

Moreover, a Type K thermocouple installed inside the climate room made it possible to record the temperature variation inside the climate room. The physical appearance of the arc at the moment flashover takes place is shown in figure 5.31. At this moment, the flashover had just happened and the arc is being extinguished due to the breaker cut off.



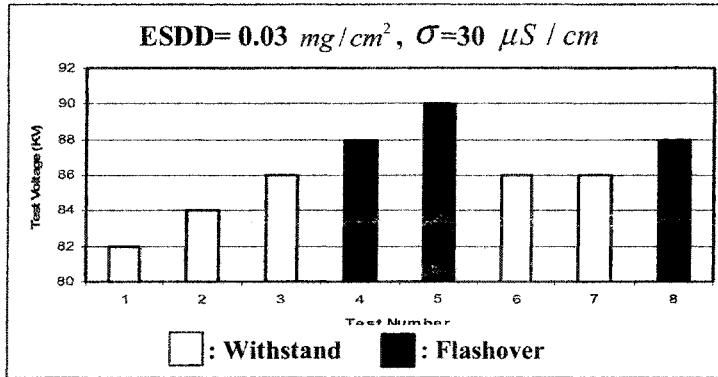
**Figure 5.31** Five-unit IEEE standard insulator string used for validation test and the moment just after flashover.

Owing to the variety of the possible test conditions for different values of SDD and  $\sigma$ , and considering the available facilities in the high voltage laboratory in CIGELE deemed to meet the relatively heavy and coincident demands of all members of GIGELE group for using these facilities, the validation tests carried out in this study were limited to investigating the effect of SDD on flashover voltage while the freezing water conductivity and ice thickness ( $\mathcal{E}$ ) were maintained at  $30 (\mu S/cm)$  and  $2 (cm)$ , respectively.

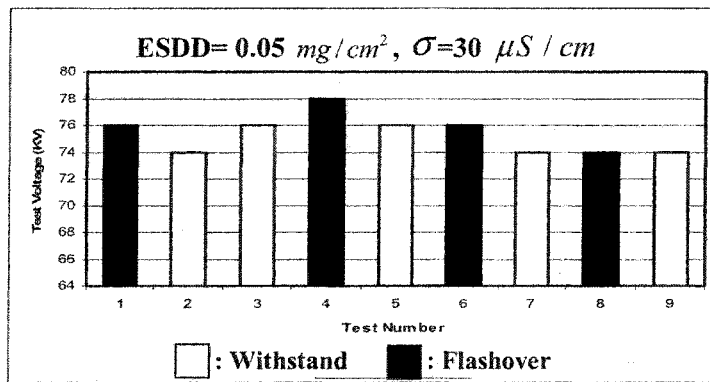
The minimum flashover voltage for each test condition was determined under test conditions as described in Table 5.4

**Table 5.4** Validation test conditions

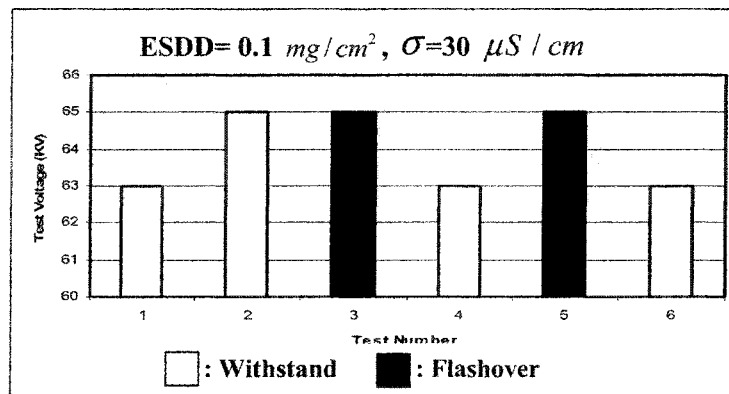
SDD ( $mg/cm^2$ )	$\sigma$ ( $\mu S/cm$ )	$\delta$ (cm)	$V_{MF}$ (kV)
0.03	30	2	88
0.05	30	2	74
0.1	30	2	65



$$V_{MF} = 88 \text{ (KV)}$$



$$V_{MF} = 74 \text{ (KV)}$$



$$V_{MF} = 65 \text{ (KV)}$$

Figure 5.32 Flashover test results on five-unit IEEE standard insulator string

Figure 5.32 summarizes the flashover test results obtained on the five-unit IEEE standard insulator string for three applied SSD levels of 0.03, 0.05 and  $0.1 \text{ mg/cm}^2$ .

## 5.6 Application of the model to the industrial insulators and discussions

In an attempt to validate the model developed in this study, the model was applied to the five units of the IEEE standard insulator. The results of the calculated flashover voltage were then compared with those obtained from the validation tests, as described in section 5.4 of chapter 5. Substituting the physical values of the parameters characterizing the model, the mathematical representation of the model developed in this study reads as follows:

$$\left\{ \begin{array}{l} V_m = 168.x.I_m^{-0.325} + V_{Res}(SDD, \sigma, x, I_m) \quad (5-10) \\ \frac{V_m}{x} = \frac{308.4}{I_m^{0.3811}} \quad (5-11) \\ V_{Res} = \frac{(L-x)I \times 10^4}{0.317(1 - e^{\frac{-SDD}{0.053}}) + 8.503 \times 10^{-5} \sigma^{1.27} + 0.1462I} \quad (5-12) \\ V_{Res} = F_{Res}(SDD, \sigma, x, I_m) \times 10^{-2} \quad (5-13) \end{array} \right.$$

The set of equations as given above was then solved for calculating the flashover voltage of the five units of the IEEE standard insulator under test conditions summarized in Table 5.4. It should be mentioned that the arc length in above mentioned equations is measured in (cm), so in order to account to this change, the arc length in  $V_{Res}$  in equation (5-12) is given in (cm) and the coefficient appearing in numerator is  $10^4$  instead of  $10^6$ . The similar modification was also made to equation (5-13) as the coefficient of  $10^{-2}$  appears in front of  $F_{Res}$  function.

By replacing  $V_{Res}$  and  $I_m$  from equations (5-12) and (5-11) into equation (5-10) the resulting relationship between  $V_m$  and the arc length  $x$  reads as:

$$V_m = 168 x \left( \frac{308.4x}{V_m} \right)^{\frac{-0.325}{0.3811}} + \frac{(L-x) \left( \frac{308.4x}{V_m} \right)^{\frac{1}{0.3811}} \times 10^4}{0.317 (1 - e^{\frac{-SDD}{0.053}}) + 8.503 \times 10^{-5} \sigma^{1.27} + 0.1462 \left( \frac{308.4x}{V_m} \right)^{\frac{1}{0.3811}}} \quad (5-14)$$

It was previously stated in section 3.5.1.2 that the  $V_m$  reaches its maximum value when equation (5-14) is numerically solved for  $x$  varying in the range of  $[0 L]$ . This maximum value for  $V_m$  takes place at an arc length denoted as critical arc distance  $x_c$  and the corresponding voltage as the critical voltage  $V_c$ . The calculated maximum flashover voltage was then converted to rms values. The numerical solutions of equation (5-14) for three levels of  $SDD=[0.03 \ 0.05 \ 0.1]$  ( $\text{mg}/\text{cm}^2$ ) and  $\sigma=30(\mu\text{S})$  are given in figures 5.33 through 5.35, respectively. The MATLAB codes developed for numerical solution of (5-14) are given in Appendix B.

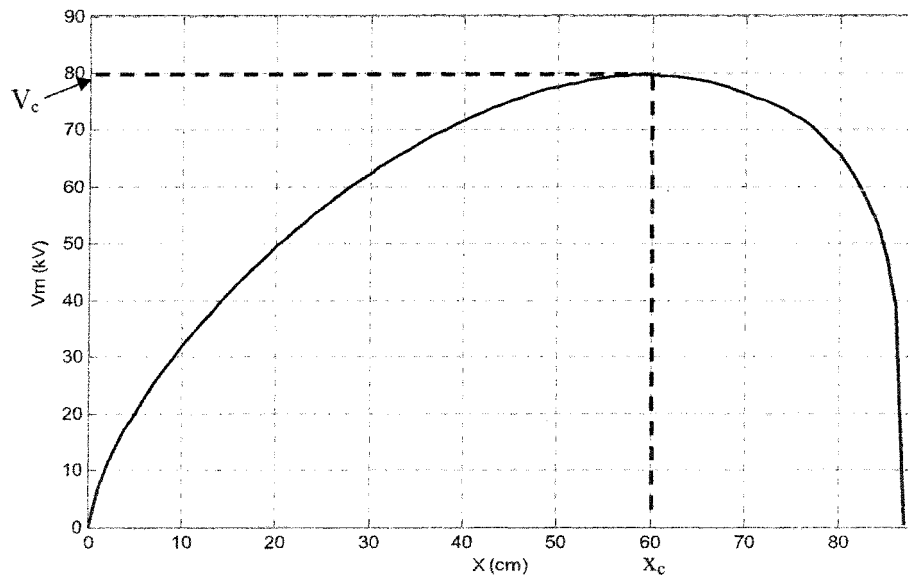


Figure 5.33  $V_m$  versus  $x$ . SDD=0.03 ( $\text{mg}/\text{cm}^2$ ) and  $\sigma = 30(\mu\text{S})$

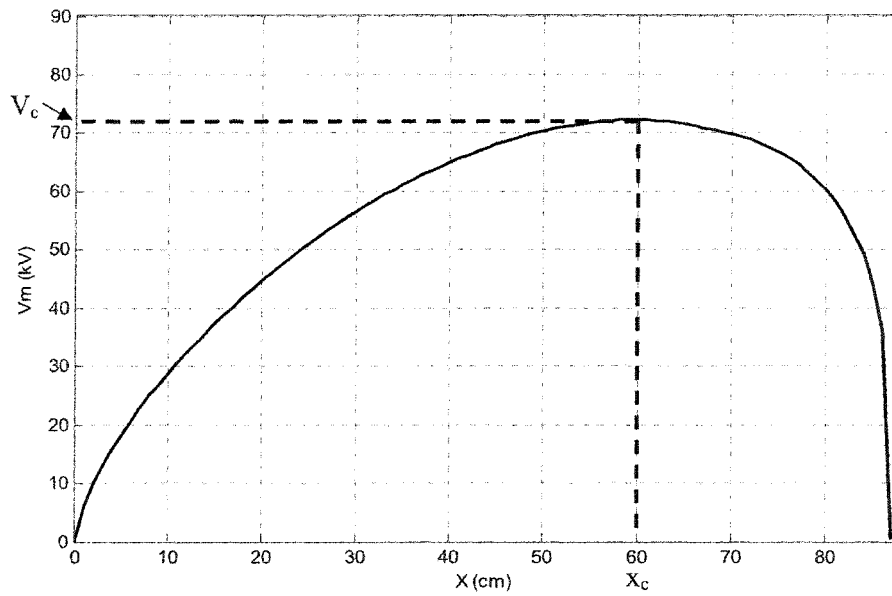
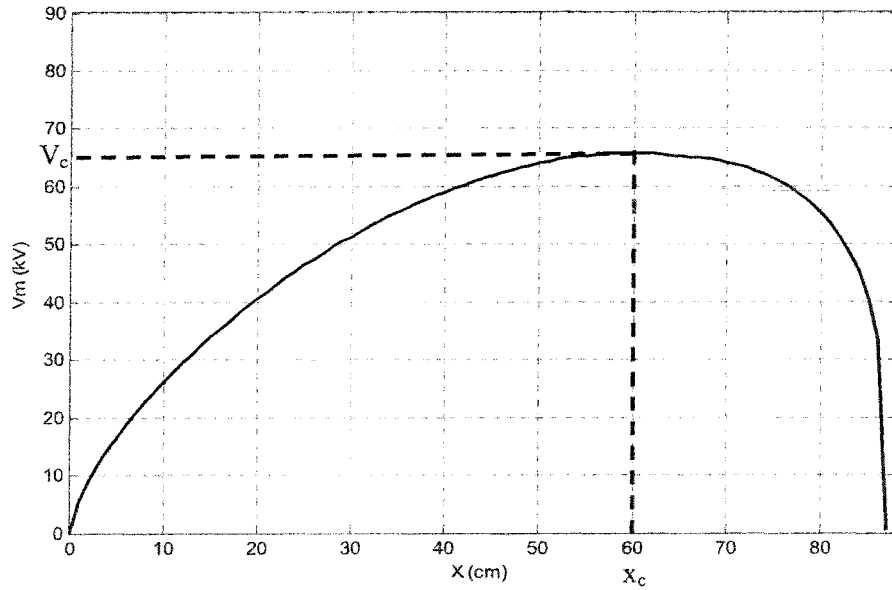


Figure 5.34  $V_m$  versus  $x$ . SDD=0.05 ( $\text{mg}/\text{cm}^2$ ) and  $\sigma = 30(\mu\text{S})$



**Figure 5.35**  $V_m$  versus  $x$ . SDD=0.1 (mg/cm<sup>2</sup>) and  $\sigma = 30(\mu S)$

It is obvious from the figures 5.33 to 5.35 that the critical voltage for all degree of SDD takes place at a critical arc distance  $x_c$  that is independent of SDD, or in other word  $V_{Res}$  which is a function of SDD and  $\sigma$ . The same result has been already concluded for DC flashover where maximizing the mathematical relationship between applied voltage  $U$  over arc distance  $x$  resulted in the critical arc length as [95]:

$$x_c = \frac{L}{1+n} \quad (5-15)$$

Where,  $L$  is the insulator length and  $n$  is arc constant. For arc constant determined as  $n=0.325$  in this study, the equation (5-15) yields a critical arc length of 75.47% of insulator length  $L$ , however, the critical arc distance and corresponding critical voltage over full range of variation of  $x$  takes place at  $x_c=60$  (cm) or 68.97% of insulator length.

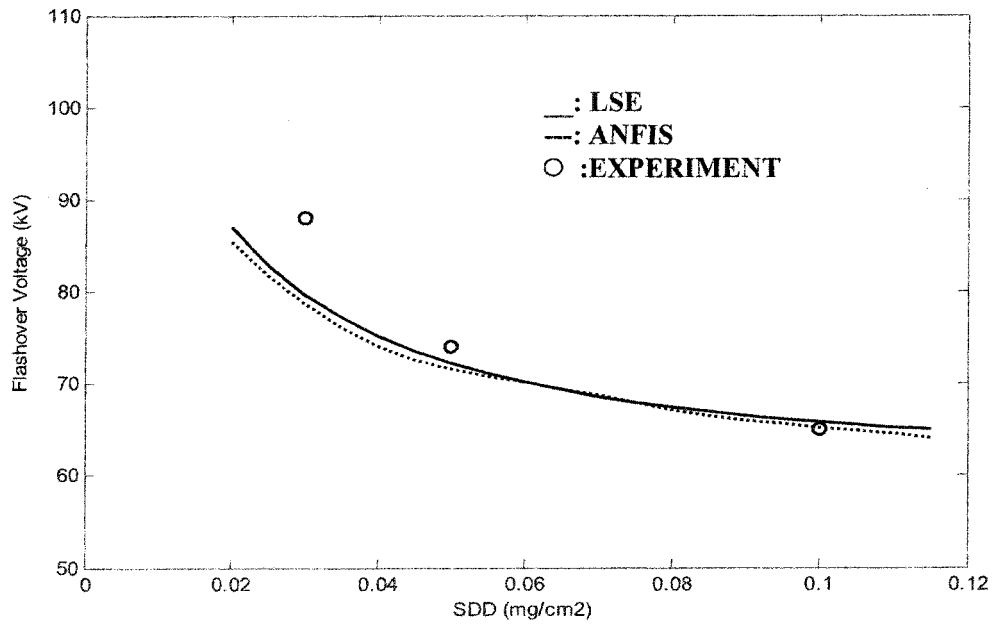


**Figure 5.36** Calculated and experimental results for flashover voltage of 5 units of IEEE standard insulators

The results obtained from both LSE and ANFIS methods were then compared with the experimental results as shown in figure 5.36, where the experimental results are denoted by circles and those of LSE and ANFIS are plotted in heavy and dashed lines, respectively.

#### 5.6.1 Discussion of the results

By examining the calculated and experimental results, it may be deduced that a small increase in SDD over low levels on flashover voltage is very considerable as the flashover voltage decreases rapidly versus increase in SDD. The fall in flashover voltage for a small increase in SDD over its lower level of  $\Delta SDD = 0.05 - 0.03 = 0.02$  (mg/cm<sup>2</sup>) is  $\Delta V_{MF} = 88 - 74 = 14$  (kV) for lower degree of SDD, whereas a relatively higher increase in SDD of  $\Delta SDD = 0.1 - 0.05 = 0.05$  (mg/cm<sup>2</sup>) over its higher levels causes a slightly lower drop in

flashover voltage as  $\Delta V_{MF} = 74 - 65 = 9$  (kV). The same result has been also concluded by Shu, Sun, Zhang and Gu in China [100]. The physical process causing this situation may be explained by analyzing the interaction of pollution and ice. At the earlier stages of the arc propagation the melted ice moisturizes the pollution layer thereby increases the mobility of a portion of this layer in contact surfaces. The wet pollutants thus become capable to penetrate inside ice layer and reach the outer surface of ice. This situation causes a rapid increase in the density of ionized particles on ice surface leading to a considerable decrease in flashover voltage. However, the portion of the pollution layer capable of reaching to the ice surface or being absorbed by ice layer is limited, i.e. the ice layer is capable to conduct rapidly a little part of pollutants from its inner layers to its surface. This process depends on the physical structure of the ice. In addition, the process of migration the pollutants from inner layer to the ice surface is a function of time which could be discussed in the diffusion context where the mechanism of the propagation of a flux comprised of pollutants inside a media of ice layer is deemed to be analyzed. The time constant of this process could be much higher than the time needed for a whole arc propagation process resulted in a final flashover, thus the effect of further increase in SDD can not be completely appeared on ice surface and tends to a saturated level.

Comparison of the calculated and experimental results reveals that the model thus developed in this study could successfully account for the main variables causing the physical situation as mentioned above. The residual voltage as developed in this study incorporates a proper form of non-linear functions reflecting the effect of interactions of ice and pollution over time period of arc propagation.

The other effect of the presence of pollution on ice covered insulators is the drastic decrease in the required voltage level to re-ignite the extinguished arc. In section 5.2.1.2 the arc re-ignition parameters  $K_p$  and  $b_p$  were compared with those reported in references [29] and [108]. It was concluded that the re-ignition voltage given by  $K_p$  and  $b_p$  is considerably (about 4 times) less than the voltage levels calculated from references [29] and [11].

The variation of flashover voltage and the corresponding critical current versus SDD is also shown in figure 5.37, where the solid and dashed line is the flashover voltage (kV) and critical current (mA), respectively.

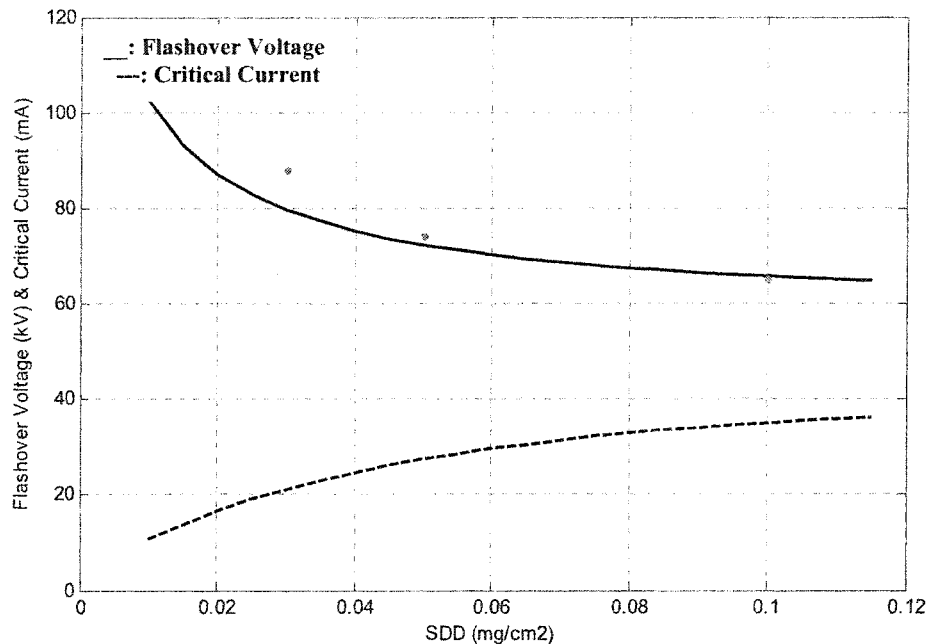


Figure 5.37 Flashover voltage & Critical current versus SDD

The critical current for a SDD level of  $0.05 \text{ mg/cm}^2$  is about 29 (mA) and corresponding flashover voltage is 72.5 (kV) as given by the critical current graph in figure 5.37. It would be worthwhile to analyze one of the recorded waveforms to make a comparison between the calculated and the experimental values for critical currents. Figure 5.38 illustrates the last moments (41 Seconds) of the flashover test carried out with an applied pollution level of  $0.05 \text{ mg/cm}^2$ . It may be noted that over this time period the arc current increases from 20 (mA) up to about 59 (mA) in a fluctuating manner and finally the flashover happens at the moment when the current tends to increase vertically. By recalling the arc re-ignition parameters given by equation (5-2), the re-ignition voltage for an arc current of 59 (mA) with the length of about 60 (cm) reads as 61.257 (kV) which is well below the calculated voltage of 47.68 (kV Peak) or 33.715 ( $\text{kV}_{\text{rms}}$ ) shown in figure 5.37.

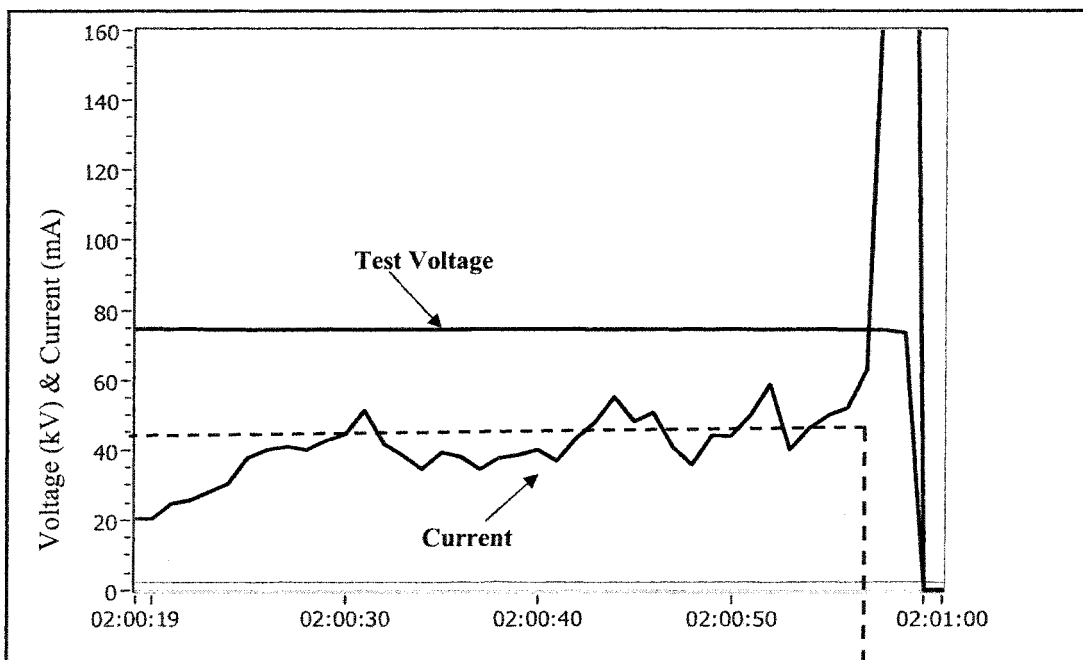
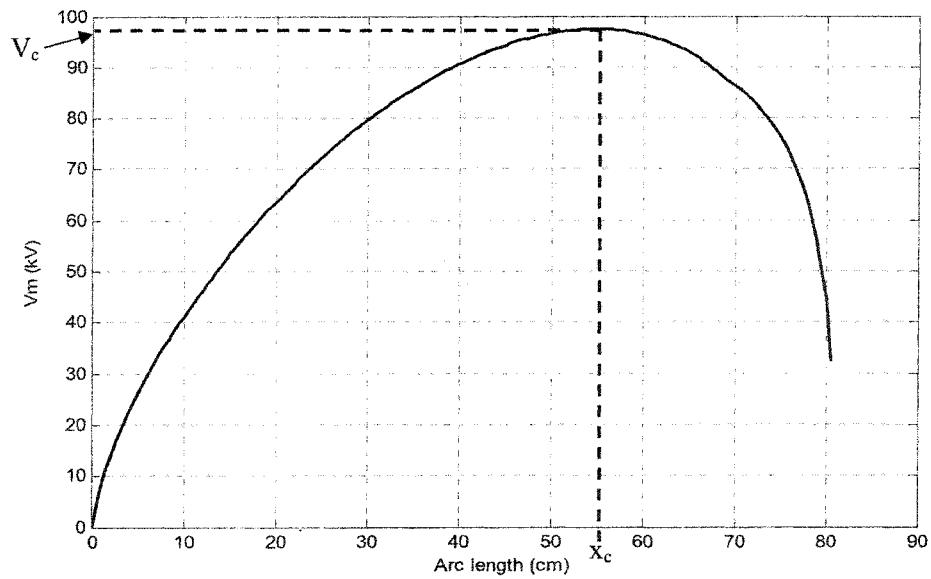


Figure 5.38 Recorded Voltage and Current waveforms during last minute of flashover test  
Elapsed Time (hh:mm:ss)

### 5.6.1.1 Flashover voltage prediction for lower levels of SDD and $\sigma$

Since the test conditions and the type of insulators used for carrying out the experiments are the same, a comparison can be made between the calculated flashover voltages of present model with those obtained from the model as presented in [29]. The flashover voltage was calculated for very low levels of SDD and  $\sigma$  for the insulator length used in model presented in [29].



**Figure 5.39** Calculated flashover voltage for SDD=0.01 ( $\text{mg}/\text{cm}^2$ ),  $\sigma = 10(\mu\text{S})$  and L=809 (mm)

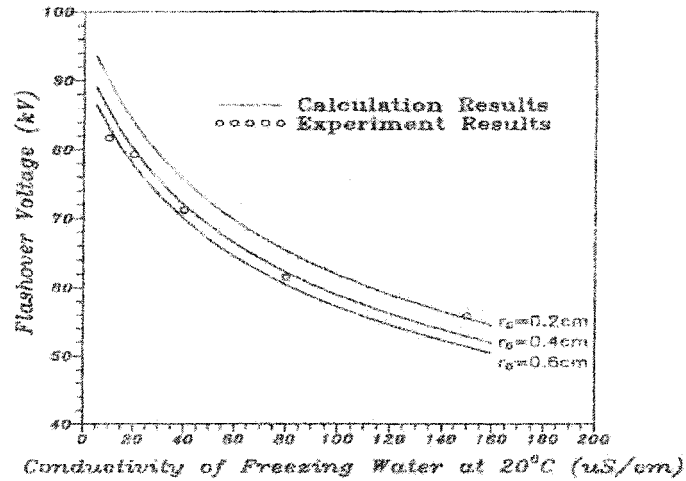


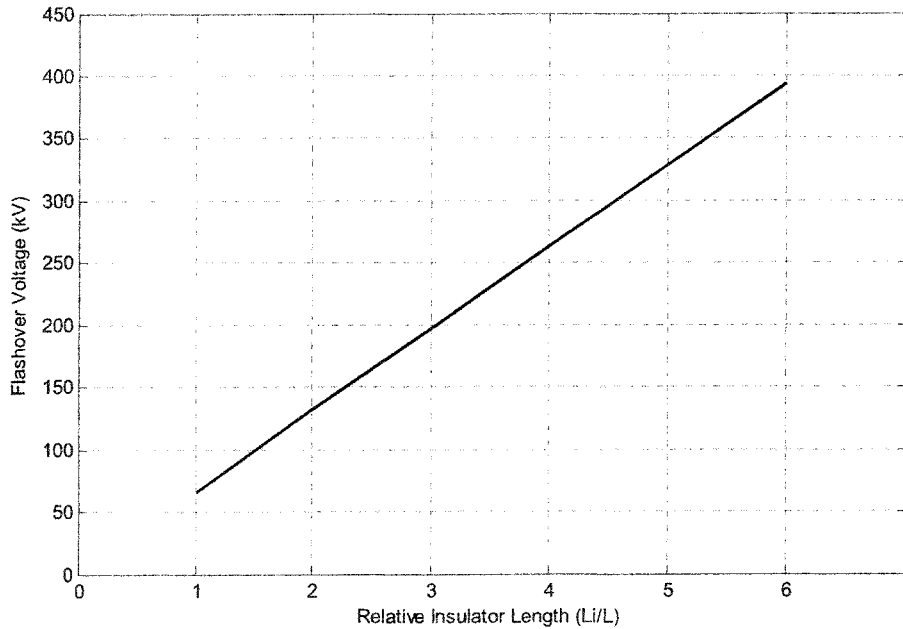
Figure 5.40 Flashover voltage versus freezing water conductivity [29]

Figure 5.39 shows the variation of  $V_m$  with respect to arc distance for the insulator length of 809 (mm),  $SDD=0.01$  ( $\text{mg}/\text{cm}^2$ ) and  $\sigma = 10(\mu\text{S})$ . It may be noted from figure 5.39 the flashover voltage is 97.5 (kV) and takes place at arc length of 55 (cm) or (550 mm). According to the figure 5.40 the flashover voltage calculated by the model presented in reference [29] is about 92(kV) which is in good agreement with 97.5 (kV). Despite the relatively good agreement concluded for this value of SDD, the difference between the results of two models become discouraging when  $SDD=0$  ( $\text{mg}/\text{cm}^2$ ), i.e. for purely ice covered insulators, the calculated flashover voltage of this model for  $\sigma = 10(\mu\text{S})$  is 268 (kV). The lack of enough training data mainly focused on a wide range of variation of freezing water conductivity could be the origin of this disagreement. This has, thus, limited the capability of this model solely for analyzing the mixed effect of pollution and ice on electrical performance of high voltage insulators. The applicability of this model, however,

could be improved by performing a set of experiments covering a wide range of variations of various factors influencing the electrical performance of high voltage insulators.

#### 5.6.1.2 The effect of arcing distance on flashover voltage

The flashovers voltages of longer insulators were calculated using this model. It is shown in figure 5.41 that the flashover voltage varies linearly with respect to the insulator lengths of  $L=870$  (mm) up to length of  $6L=5220$  (mm) or 5.22 (m). The results should be compared with the tests performed on longer Pin-Cap insulators used in EHV and transmission lines.



**Figure 5.41** Calculated flashover voltage versus relative insulator length.  $L=870$  (mm),  $SDD=0.1$  ( $\text{mg}/\text{cm}^2$ ) and  $\sigma = 30(\mu\text{S})$

The foregoing discussion reveals that the model thus presented in this study could successfully account for the effect of the major variables influencing the electrical performance of high voltage insulators. Unfortunately, due to the limited number of validation tests, the validity of the model was not proved under various physical conditions such as the different insulator length, the effect of variation of freezing water conductivity and ice thickness. These studies could be considered as a part of any future works aimed at developing the present model.

## 5.7 Conclusion

The results and discussions given through various parts of this chapter were indeed a quantitative representation of the static flashover model developed in this study as its theoretical basis was explained in chapter 4. The main results obtained from several experiments carried out in this study may be reviewed in brief as follows:

- Using the cylindrical laboratory test samples the arc E-I characteristic was investigated under conditions of contamination accompanied by icing. The arc constants and re-ignition parameters were determined as given by equations (5-1) and (5-2), respectively.
- Based on LSE and ANFIS identification methods, a new method was developed for determining the V-I characteristic of the residual voltage of real insulators. The formula represents the residual voltage  $V_{Rc_s}$  as a function of the major parameters

---

influencing the V-I characteristic of contaminated insulators covered with ice. The formula was given by (5-6).

- A mathematical formula given by (5-8) was extracted for residual resistance from the V-I characteristic of the insulator.
- The sensitivity of dynamic or differential resistance to pollution and freezing water conductivity was analyzed. It was concluded that the resistance is more sensitive to variation of freezing water conductivity ( $\sigma$ ) than that of effective salt deposit density (SDD) in the range of [0.01 0.1] ( $\text{mg}/\text{cm}^2$ ).
- The results of the calculated dynamic or differential resistance based on based on LSE and those given by the formula due R. Wilkins were compared. It was concluded that the residual resistance obtained from (5-8) is more sensitive to leakage current variation than that given by the formula of R. Wilkins.
- The differential resistance was also determined using the ANFIS network and the comparison between the outputs of LSE and ANFIS confirmed good agreement between the results obtained from the two methods.
- A series of validation tests was carried out to determine the minimum flashover voltage of the five-unit IEEE standard insulator string for three SDD levels of 0.03, 0.05 and  $0.1(\text{mg}/\text{cm}^2)$ . The calculated minimum flashover voltage based on LSE

---

and ANFIS are in good agreement with experimental data obtained from flashover tests carried out in this study as illustrated in section 5.4 of this chapter.

- The calculated critical currents have also been compared with recorded voltage-current waveforms. The results confirmed the appropriate arc re-ignition parameters were determined in this study.

## CHAPTER VI

### CONCLUSIONS AND RECOMMENDATIONS

#### 6.1 Concluding remarks

The power outages caused by flashover of high voltage insulators is one of those major and inevitable phenomenon frequently happening in power networks leading to a considerable deterioration in power system reliability. To the best of our knowledge about the history of investigations carried out on understanding the deteriorating effects of natural contaminants on electrical performance of high voltage insulators, the joint effects of pollution and icing had been still left an untouched issue until now. The present study was carried out within the framework of CIGELE/INGIVRE at UQAC with the aim of modeling the flashover of contaminated insulators covered with ice. The results of the observations, measurements and the number of experiments carried out for identifying the physical nature of the phenomenon and the relevant factors paved the way toward establishing the theoretical basis of present model. The intelligent identification methods was used in this study, the arc constants and re-ignition parameters, the V-I characteristic of residual voltage and the residual resistance were determined. Based on the results obtained from this study, the following conclusions may be drawn.

- Static AC modeling of flashover based on Obenaus discharge model was proposed for contaminated insulators covered with ice.

- Using the cylindrical laboratory test samples the arc characteristics was investigated under condition of contamination and icing. The mathematical relation between electrical stress (E) and the arc current (I) was determined as:

$$E_{Arc} = 168I^{-0.325}$$

Where, the arc voltage gradient is given in (V/cm) and current in (A).

The mathematical representation of arc re-ignition criterion was also determined as:

$$V_m \geq \frac{308.4X}{I^{0.2811}}$$

Where, the applied voltage is given in (V Peak), the current in (A Peak) and X in (cm).

- The electrical field inside a two dimensional geometry composed of the materials with different electrical properties in presence of arc was calculation. The results revealed a highly non-linear distribution of electrical field between high and low voltage electrodes in presence of electric arc.
- The presence of very high electrical field accompanied by considerably high temperature of arc at the contact point can easily mobilize the different pollutants, thereby paving the way toward the change in physical properties of equivalent conductive layer during arc discharge.
- The effect of local melting phenomenon initiating the interaction of different pollutants during arc propagation on the surface of real insulator was discussed. It

was concluded that the equivalent surface criterion for calculating the residual resistance is not applicable to the complex geometry of combinational pollution on the real insulator surface.

- A new approach based on identification methods for determining the voltage of residual part of contaminated insulators covered with ice is proposed in this study. The method is applicable to either contaminated insulator under filed condition or artificially contaminated in the laboratory.
- The application of LSE identification method made it possible to derive a mathematical representation of residual voltage as a function of major variables influencing the V-I characteristic of residual voltage. The residual voltage of five-units of IEEE standard insulator string was then determined as:

$$V_{Res}(I) = \frac{(L-x)I \times 10^6}{0.317(1 - e^{\frac{-SDD}{0.053}}) + 8.503 \times 10^{-5} \sigma^{1.27} + 0.1416I} \quad (V)$$

Where, V is given in (V), I in (A), (L-x) in (m), SDD in (mg/cm<sup>2</sup>) and  $\sigma$  in ( $\mu S$ ).

- The V-I characteristic of residual part of insulator was also determined using Adaptive Network-Based Fuzzy Inference System (ANFIS). It was concluded that the V-I characteristic obtained using ANFIS was more sensitive to the training dataset than that of LSE, providing more precise representation of residual voltage.

- The differential or dynamic resistance of real contaminated insulator covered with ice was determined using both LSE and ANFIS. A mathematical formula representing the residual resistance of five-units of IEEE standard insulator string was extracted as:

$$R(SDD, \sigma, I, x) = \frac{L-x}{0.317(1-e^{\frac{-SDD}{0.053}}) + 8.503 \times 10^{-5} \sigma^{1.27} + 0.2924I + \frac{0.0201}{0.317(1-e^{\frac{-SDD}{0.053}}) + 8.503 \times 10^{-5} \sigma^{1.27}}} I^2 \quad (M\Omega)$$

Where, V is given in (V), I in (A), (L-x) in (m), SDD in (mg/cm<sup>2</sup>) and  $\sigma$  in ( $\mu S$ ).

- The sensitivity of dynamic or differential resistance to the pollution and freezing water conductivity was analyzed. It was concluded that the resistance is more sensitive to variation of freezing water conductivity ( $\sigma$ ) than that of effective salt deposit density (ESDD) in the range of [0.01 0.1] (mg/cm<sup>2</sup>).
- The results of calculated dynamic or differential resistance obtained based on LSE and that of given by the formula due R. Wilkins were compared. It was concluded that the differential resistance is more sensitive to leakage current variation than that of given by the formula due R. Wilkins. Hence, it could better reflect the variation of ice layer conductivity over the leakage current range of 0.02 to 1 (mA), where the physical condition of ice changes from a very thin conductive surface to bulky volume conductivity.

- 
- According to the calculated results obtained for flashover voltage using equation (5-14), it was concluded that the critical arc length ( $x_c$ ) always happens at 68.97% of insulator length. This means that the  $x_c$  is independent of Salt Deposit Density (SDD) and Freezing Water Conductivity ( $\sigma$ ). In other word, the critical arc length  $x_c$  is dependent on arc constants  $A_p$  and  $n_p$ , and it is not dependent on V-I characteristics of residual part of insulator  $V_{Res}$ .
  - A series of validation tests were carried out to determine the minimum flashover voltage of five-units of IEEE standard insulator string for three SDD levels of 0.03, 0.05 and  $0.1(mg/cm^2)$ . The calculated results obtained using LSE and ANFIS were compared with those obtained from experiments. The maximum error due LSE and ANFIS was 6.8% and 3.4%, respectively, confirming the good agreements attained from both methods used this study.
  - Good agreement was also concluded between calculated critical current and the data observed from voltage-current waveforms recorded over flashover tests. This fact confirmed the appropriate arc re-ignition parameters adopted in this study.

## 6.2 Recommendations for future works

The main goal of this study was to take the tentative steps towards establishing an inclusive model capable of incorporating the higher number of variables influencing the flashover of contaminated insulators covered with ice. The originality of this work may be easily deduced by comparing this model with the previous models from the viewpoints of the way of mathematical representation of static AC model, as well as the methods used for determining the residual voltage and resistance. Although the results obtained from the model were in good agreement with those of experiments, the model proposed in this study is still in its infancy, so it may be modified or completed by future studies carried out in this domain. The results obtained in this study may be served to the future works based on this model or be compared with the results of alternative methods as proposed below:

- The primary recommendation may be the complementary studies pursuing the re-adjustment of the mathematical models derived in this study, thereby making the model applicable to the variety of naturally or artificially contaminated insulator types and lengths.
- By means of an appropriate test setup, it is possible to perform the online LSE parameter tuning process referred to as “recursive inline tuning”. This setup might utilize the online image processing module making it possible to perform simultaneous arc length measurement over the test period. More specifically, the input of image processing module will be the instantaneous images received from high speed camera and its output will be the arc length measured using image

---

processing methods. In so doing, the data acquisition system (DAS) will perform the online parameter tuning process, so the process of measuring the arc length, which the most time consuming step of parameter identification process, would be cut away.

- With the aim of extracting the mathematical arc model, it is also proposed to perform the identification methods utilized in this study using the test setup as illustrated above incorporating an additional camera of the infrared type. The proposed arc model determined as a function of the major parameters influencing the arc states such as arc length, arc current and arc column radius may be used for estimating the variation of arc temperature over the time period of its propagation.
- An alternative method is also proposed, based on finite element method, for determining the residual resistance as illustrated in of chapter 4 (section 4.2.13) of this dissertation. It is possible to solve Laplace and Heat diffusion equations simultaneously inside the complex geometry of real contaminated insulator covered with ice using Finite element software. The calculated electric field ( $E$ ) and the temperature dependent volume conductivity ( $\sigma(\theta)$ ) can be then served to the equation (4-3), as given in chapter 4, for calculating the resistance between high and low voltage electrodes. The results obtained from the method mentioned above may be then compared with the residual resistance calculated in this study.

## REFERENCES

- [1] Al-Baghdadi A., "The Mechanism of Flashover on Polluted Insulators," Thesis of Ph.D., University of Manchester, USA, pp. 67, 1970.
- [2] Alston L. L. & Zoeledziowski S., "Growth of discharges on polluted insulation," Proc. IEE, Vol. 110, No. 7, pp. 1260-1266, July 1963.
- [3] Andersson, Dag: "Current instability and chopping with arcs in series". IEEE Proceedings, Vol. 132, Pt. C, No. 4, July 1985
- [4] Anjana S. & Lakshminarasimha C. S., "Computation of Flashover Voltages of Polluted Insulators Using Dynamic Arc Model," Proc. of 6th Int. Sym. on High Voltage Eng., New Orleans, USA, Paper No. 30.09, 1989.
- [5] Boehme H. & Obenaus F., "Pollution Flashover Tests on Insulators in the Laboratory and in Systems and the Model Concept of Creepage Path Flashover," CIGRE, No. 407, 1966.
- [6] Boyer A. E. & Meale J. R., "Insulation Flashover under Icing Conditions on the Ontario-Hydro 500 kV Transmission Line System," Proc. Of CEA Spring Meeting, Montreal, Canada, March 1988.
- [7] Browne T. E., "Discussion of "The Electric ARC as a Circuit Element", J. Electrochem. Soc., Volume 102, Issue 12, pp. 693-693 (1955)
- [8] Cassie A. M., "Arc Rupture and Circuit Severity: A New Theory," CIGRE Report, No. 102, Paris, France, 1939.
- [9] Charneski M. D., Gaibrois G. L. & Whitney B. F., "Flashover Tests on Artificially Iced Insulators," IEEE Transactions on Power Apparatus & Systems, Vol. PAS-101, No. 8, pp. 2429-2433, 1982.
- [10] Chaurasia D. C., "Scintillation Modelling for Insulator Strings Under Polluted Conditions," High Voltage Eng. Sym., IEE Conf. Pub., No. 467, August 1999.
- [11] Chen X., "Modeling of Electrical Arc on Ice Surfaces," Thesis of Ph.D in Engineering, UQAC-École Polytechnique de Montréal, 1999.
- [12] Chen Junhong, "Direct-Current Corona Enhanced Chemical Reactions", Ph.D. Thesis, University of Minnesota, USA. August 2002.
- [13] Chisholm W. A. et al., "The Cold-Fog Test", Proc. of IEEE Trans PWRD Vol. 11 pp. 1874-1880, 1996

- [14] Claverie P., "Predetermination of the Behavior of Polluted Insulators," IEEE Transactions on Power Apparatus and Systems, Vol. PAS-90, pp. 1902-1908, 1971.
- [15] Claverie P. & Porcheron Y., "How to Choose Insulators for Polluted Areas," IEEE Trans, on Power Apparatus and Systems, Vol. PAS-92, No. 3, pp. 1121-1131, 1973.
- [16] Dhabbi-Megriche N. & Béréal A., "Flashover Dynamic Model of Polluted Insulators under ac Voltage," IEEE Trans, on Dielect. and Elec. Insul., Vol. 7 No. 2, pp. 283-9, 2000.
- [17] Farag A. S. & Cheng T. C., "Interfacial Breakdown on Contaminated Electrolytic Surfaces," IEEE Elec. Ins. Conf., 1997.
- [18] Farzaneh M. & Drapeau J. F., "AC Flashover Performance of Insulators Covered with Artificial Ice," IEEE Trans, on Power Delivery, Vol. 10, No 2, pp. 1038-1051, April 1995.
- [19] Farzaneh M., Kiernicki J., Chaarani R., Drapeau J. F. & Martin R., "Influence of Wet-grown Ice on the AC Flashover Performance of Ice Covered Insulators," Proc. of 9th Int. Symp. on High Voltage Eng., Austria, Paper No. 3176, pp. 1-4, 1995.
- [20] Farzaneh M., Kiernicki J. & Dallaire M. A., "AC and DC Flashover Performance of Ice-covered Insulators during a De-Icing Period," Proc. of 5th Int. Workshop on the Atmospheric Icing of Structures, Tokyo, Japan, Paper No. B-48, pp. 1-4, 1990.
- [21] Farzaneh M., Kiernicki J. & Drapeau J. F., "Ice accretion on energized line insulators," Int. Offshore and Polar Eng. Conf, Vol. 2, No. 3, Montreal, pp. 228-233, 1992. 187188
- [22] Farzaneh M. & Kiernicki J., "Flashover Performance of ice-covered Insulators," Canadian Journal of Elec. and Computer Eng., Vol. 22, No. 3, pp. 95-109, July 1997.
- [23] Farzaneh M. & Kiernicki J., "Flashover Performance of IEEE Standard Insulators under Ice Conditions," IEEE Trans, on Power Delivery, Vol. 12, No. 4, pp. 1602-1613, October 1997.
- [24] Farzaneh M. & Kiernicki J., "Flashover Problems Caused by Ice Buildup on Insulators," IEEE Trans, on Elec. Ins., Vol. EI-11, No. 2, pp. 5- 17, 1995.
- [25] Farzaneh M. & Zhang J., "Behavior of DC Arc Discharge on Ice Surfaces," Proc. of Int. Workshop on the Atmospheric Icing of Structures, Iceland, pp. 193-197, 1998.
- [26] Farzaneh M., Zhang J., Chaarani R. & Fikke S. M., "Critical Conditions of AC arc propagation on Ice surfaces," Conf. Record of the 2000 IEEE, Int. Symp. On Electrical Insulation, Anaheim, CA, USA, pp.211- 215, April 2000.

- [27] Farzaneh M., Zhang J. & Chen X., "A laboratory study of leakage current and surface conductivity of ice samples," Proc. Conf. on Elec. Ins. and dielec. Phenomena, Arlington, USA, Article 9456-1, pp. 631-638, 8A-1, Oct. 1994.
- [28] Farzaneh M., Zhang J. & Chen X., "DC characteristics of Local Arc on Ice Surface," Atmospheric Research, Vol. 46, pp.49-56, 1998.
- [29] Farzaneh M., Zhang J. & Chen X., "Modeling of the AC Arc Discharge on Ice Surfaces," IEEE Trans, on Power Delivery, Vol. 12, No. 1, pp.325-338, 1997.
- [30] Farzaneh M. & Zhang J., "Modeling of DC Arc Discharge on Ice Surfaces," IEE Proc. Generation, Transmission and Distribution, Vol. 147, No. 2, pp. 81-86, 2000.
- [31] Farzaneh-dehkordi J., "Experimental Study and Mathematical Modeling of Flashover of EHV Insulators Covered with Ice," Master Thesis in Engineering, UQAC, 2004.
- [32] Farzaneh M. et al., "Selection of Station Insulators with Respect to Ice or Snow - Part I: Technical Context and Environmental Exposure," A Position Paper prepared by the IEEE TF on icing performance of station insulators, IEEE Transactions on Power Delivery, réf. TPWRD- 186187 00110-2004.
- [33] Farzaneh M. et al., "Selection of Station Insulators with Respect to Ice or Snow - Part II: Methods of Selection and Options for Mitigation," A Position Paper prepared by the IEEE TF on icing performance of station insulators, IEEE Transactions on Power Delivery, réf. TPWRD- 00111-2004.
- [34] Farzaneh M., "Ice Accretions on High-Voltage Conductors and Insulators and related phenomena", Phil. Trans, of the Royal Society, Vol. 358, No. 1776, pp. 297-3005, November 2000.
- [35] Farzaneh M., Fofana I., Tavakoli C. & Chen X. "Dynamic Modeling of DC Arc Discharge on Ice Surfaces," IEEE Trans, on Diel. and Elec. Ins., Vol. 10, No. 3, pp. 463-474, 2003.
- [36] Farzaneh M., "Effect of Ice Thickness and Voltage Polarity on the Flashover Voltage on Ice Covered High Voltage Insulators," Proc. of 7th Int. Symp. on High Voltage Eng., Dresden, Germany, Vol. 4, Paper No. 43.10, pp.203-206, 1991.
- [37] M. Farzaneh, I. Fofana, C. Tavakoli and A. Bérroual, "A Mathematical Model of Arc Development on Ice Surfaces under DC Voltage", IASTED Int. Conf. on Power and Energy Systems, paper 337-070, Rhodes, Greece, July 3-6th 2001.

- [38] Farzaneh M. & W.A. Chisholm, *Insulators for icing and polluted environments*, IEEE Press series on Power Engineering, IEEE/John Wiley, New York, ISBN 9780470282342, 700 p. (à paraître en juillet 2009)
- [39] Farzaneh M., Chairman and Principal Author and Members, "Insulator Icing Test Methods and Procedure", A position paper prepared by the IEEE task force on insulator icing test methods, *IEEE Transactions on Power Delivery*, Vol. 18, October 2003.
- [40] FARZANEH M., C. VOLAT & C. TAVAKOLI, « Étude de la tension de tenue des isolateurs de postes en présence de glace atmosphérique en vue d'un choix approprié de type et configuration d'isolateurs de postes à 735 kV. Volume 5: Étude comparative des performances électriques de colonnes isolantes précontaminées ». Report submitted to Hydro-Québec TransÉnergie, Direction expertise et support technique de transport, Vol. 5, March 2006, 37 p.
- [41] Fikke S. M., Hanssen J. E. & Rolfseng L, "Long Range Transported Pollution and Conductivity on Atmospheric Ice on Insulators," *IEEE Trans, on Power Delivery*, Vol. 8, No. 3, pp. 13411-1321, July 1993.
- [42] Forest J. S., "The Performance of High Voltage Insulators in Polluted Atmospheres," *Proc. of IEEE Winter Meeting*, New York, 1969
- [43] Francis V. J., "Fundamentals of Discharge Tube Circuits". Methuen, London, 1948.
- [44] Fujimura T., Naito K., Hasegawa Y., Kawaguchi T.K. (1979), "Performance of Insulators Covered with Snow or Ice", *IEEE Transactions on Power App. & Syst.* Vol.PAS-98. pp. 1621-1631.
- [45] Goia L. M. & Balan G., "Romanian Experience Regarding Operational Behavior of HV OIs," *Proc. 7th Int. Workshop of atmospheric Icing of Structures*, Chicoutimi, pp. 216-221, 1996.
- [46] Gopal S. & Rao Y. N., "On the Flashover Mechanism of Polluted Insulators," *ISPPISD, HT, Madras*, 1983.
- [47] Gopal H. G., Kumar U. & Nagbhusan G. R., "Parametric Analysis of Various Scintillation Models Used in Pollution Flashover Studies Using PSPICE," *Proc. Of the National Seminar on EHV Transmission Line Insulation held at REC Calicut*, 12-13 Dec. 1995.
- [48] Ghosh P. S. & Chatterjee N., "Arc Propagation over Electrolytic Surfaces under Power Frequency Voltage," *IEEE Trans, on Dielec. and Elec. Ins.*, Vol. 3, No. 4, pp. 529-536, 1996.

- [49] Hampton B. F., "Flashover Mechanism of Polluted Insulation", Proc. IEE, Vol. 11, No. 5, pp. 985-990, 1964.
- [50] Hara M. & Phan C. L, "Leakage Current and Flashover Performance of Iced Insulators," IEEE Trans, on PAS, Vol. PAS-98, No. 3, pp. 849- 859, 1979.
- [51] Hara M. & Phan C. L, "A Study of the Leakage Current of H.V. Insulators under glaze and rime," Can. Elec. Eng., J., Vol. 3, pp. 15-22, 1978.
- [52] Holtzhausen J. P., "Application of a Re-ignition Pollution Flashover Model to Cap and Pin Insulator Strings," Proc. Of the IASTED Int. Conf, POWER AND ENERGY SYSTEMS, Rhodes, Greece, July 2001
- [53] Hoyaux M.F. "Arc Physics", Volume 8, Applied Physics and Engineering, International Series, Springer-Verlag, Berlin Heidelberg New York, 1968.
- [54] Hesketh S., "General Criterion for the Prediction of Pollution Flashover," Proc. of IEE, Vol. 114, No. 4, pp. 531-532, 1967.
- [55] Hydro-Québec Committee of Experts, "January 1998 ice storm," Report for Hydro-Québec, 1998.
- [56] IEC 60815: Selection and dimensioning of high-voltage insulators intended for use in polluted conditions. Part 3: Polymer insulators for A.C. systems, Edition 1.0, Oct. 2008.
- [57] IEC 60507 Artificial Pollution Tests on High-Voltage Insulators to be used on A.C. Systems, Publication Date: Apr 1, 1991.
- [58] Ishii M. & Ohashi H., "Polarity effect in DC withstand voltages of contaminated surfaces," IEEE Trans, on Elec. Insul., Vol. 23, No. 6, 1988.
- [59] Jaiswal, Vinay Kumar, "Finite element modeling of electric field distributions around a resistive glazed post station insulator covered with ice =Modélisation par éléments finis de la distribution du champ électrique autour d'un isolateur de poste avec une couche semi-conductrice recouvert de glace". Thèse de doctorat (Université du Québec à Chicoutimi, 2005.
- [60] Jolly D. C, Cheng T. C. & Otten D. M., "Dynamic Theory of Discharge Growth over Contaminated Insulator Surfaces," IEEE PES WinterPower Meeting, New York, USA, Paper, No. C74 068-3, 1974.
- [61] Jolly D. C., "Contamination flashover, Part 1: Theoretical Aspects", IEEE Trans. PAS-91, 1972

- [62] Kawai M., "AC Flashover Tests at Project UHV on ice-covered Insulators," IEEE Transactions on Power Apparatus & Systems, Vol. PAS-89, No. 8, pp. 1800-1805, Dec. 1970.
- [63] King Ronald W. P. (1963). Fundamental Electromagnetic Theory. New York: Dover, pp. 139.
- [64] Kuffel E. & Abdullah M., High Voltage Engineering, Pergamon Press, 1970.
- [65] Kuffel, E. and Zaengl W.S. (1984). High-Voltage Engineering Fundamentals, Pergamon Press.
- [66] Kuroiwa D., "Icing and Snow Accretion," Monograph Series of Research, Institute of Applied Electricity, Japan, pp. 1-30, 1958.
- [67] Khalifa M. M. & Morris R. M., "Performance of Line Insulators under Rime Ice," IEEE Trans, on Power Application and Systems, Vol. PAS- 86, pp. 692-698, 1967.
- [68] Kopplin, H.: "Mathematische Modelle des Schaltlichtbogens". ETZ Archiv Bd. 2 (1980) H. 7
- [69] Keith R. Carver, John D. Kraus, "Electromagnetics" , McGraw-Hill electrical and electronic engineering series, 1973, ISBN 0-07-035396-4
- [70] Lambeth P.J., "Effect of Pollution on High-Voltage Outdoor Insulators", Proc. IEE Reviews, Vol. 118, NO.9R, September 1971, p. 1107-1130.
- [71] Larcombe P. J., Kunda W., Poots G. & Elliott J. W., "Accretion and shedding of ice on cables incorporating frees streamline theory and the joule effect," Proc. 3rd Int. Workshop of atmospheric Icing of Structures, Vancouver, pp. 389-395, 1991.
- [72] Lowke J. J., Zollweg R. J. & Liebermann R. W., "Theoretical description of arcs in mercury and argon," J. Phys. D: Appl. Phys., Vol. 46, No. 2, 1975.
- [73] Li Y., Farzaneh M. & Zhang J., "Effects of Voltage Type and Polarity on Flashover Performances at Low Atmospheric Pressure on an Ice Surface," Proc. of 8th Int. Offshore and Polar Eng. Conf, Montreal, Canada, pp. 543-546, 1998.
- [74] Li Y., "Étude de l'influence de l'altitude sur les caractéristiques de l'arc électrique à la surface de glace polluée," Thesis of Ph.D. in Engineering, UQAC, 2002.
- [75] Matsuda H., Komuro H. & Takasu K., "Withstand Voltage Characteristics of Insulator String Covered with Snow and Ice," IEEE Trans, on Power Delivery, Vol. 6, No. 3, pp. 1243-1250, July 1991.

- [76] Melo O. T., Tam Y. T. & Farzaneh M., "Freezing Rain and Fog Events in Southern Ontario: Properties and Effect on EHV Transmission Systems," Proc. of 4th Int. Workshop on Atmospheric Icing of Structures, Paris, France, pp. 70-75, 1988.
- [77] Meier A. & Niggli W. M., "The Influence of Snow and Ice Deposits on Supertension Transmission Line Insulator Strings with Special Reference to High Altitude Operation," IEEE Conference Publ.44, London, England, pp. 386-395, Sept. 1968.
- [78] Mayr O., "Beitrag zur Théorie der Statischen und der Dynamischen Lichtbogens," Archiv fur Elektrotechnik, Vol. 37, pp. 588-608, 1943.
- [79] Mekhaldi A., Namane D., Bouazabia S. & Bérroual A., "Flashover of Discontinuous Pollution Layer on HV Insulators," IEEE Trans. On Dielect. and Elec. Ins., Vol. 6, No. 6, 1999.
- [80] Maikopar A. S., "The Open Small Current Arc," Elektrichestvo, No. 2, pp. 22-25, 1965.
- [81] Maeker H., - "Uber die Charakterististiken Zylindrischer Bogen", Zeitschrift fur Physik, Vol. 157, 1959, p. 1-29.
- [82] Nasser E., "Contamination Flashover of Outdoor Insulation," ETZ-A, Vol. 93, No. 6, pp. 321-325, 1972.
- [83] Obenaus F., "Fremdschichtuberschlag und Kriechweglange," Deutsche Elektrotechnik, Vol. 4, pp. 135-136, 1958.
- [84] Obenaus F., "Die Uberschlagspannung verschmutzter Isolatoren," ETZ, 56, 369, 1935.
- [85] Obenaus F. " Contamination flashover and creepage path length", ETZ 12, 1958, pages 135 - 136.
- [86] Peek F.W. (1929). Dielectric Phenomena in High Voltage Engineering. McGraw-Hill. ISBN 0-9726596-6-8. <http://www.ee.vill.edu/ion/p183.html>.
- [87] Phan C. L. & Matsuo H., "Minimum Flashover Voltage of Iced Insulators," IEEE Trans, on Electrical Insulation, Vol. EI-18-6, pp. 605- 618, 1983
- [88] Ravelomanantsoa N., M. Farzaneh & W.A. Chisholm, « Laboratory investigation of the hv insulator contamination process under winter conditions », Proceedings of the International Conference on High Voltage Engineering and Application (ICHVE), Chongqing, China, November 2008, pp. 116-119
- [89] Rahal A. M. & Huraux C., "Flashover Mechanism of High Voltage Insulators," IEEE Trans, on Power Apparatus and Sys., Vol. PAS-98, No. 6 pp. 222 2231, 1979.

- [90] Raether M., *Electron Avalanches and Breakdown in Gases*. Butterworths, 1964.
- [91] Raizer Yu. P., *Gas Discharge Physics*. Springer, 1991.
- [92] Reece A. B. J. and T. W. Preston, "Finite Element Methods in Electrical Power Engineering", A. B. J. Reece and T. W. Preston. Oxford Science Publications, 2000.
- [93] Renner P.E, HILL H.L. and RATZ O. (1971 June). Effects of Icing on DC Insulation Strength. *IEEE Trans. on Power Am. & Svst.*, Vol. PAS-90, 1201 -1206.
- [94] Rizk F. A. M. & Nguyen D. H., "Digital Simulation of Source-Insulator Interaction in HVDC Pollution Tests," *IEEE Trans. On Pow. Del.*, Vol. 3, No. 1, 1988.
- [95] Rizk F. A. M., "Mathematical Models for Pollution Flashover," *Electra*, Vol. 78, pp. 71-103, 1981.
- [96] Rizk, F.A.-M.: "Interruption of small inductive currents with air-blast circuit-breakers". Thesis, Chalmers Institute of Technology, Gothenburg 1963
- [97] Rizk F. A. M. – " Analysis of Dielectric Recovery with Reference to Dry Zone Arc on Polluted Insulators", *IEEE Conf. Paper*, No. 71 C 134 PWR, Winter Power Meeting, New York, Janvier/Fevrier 1971
- [98] Roger J.-S. Jang, Chuen-Tsai Sun and Eiji Mizutani, " Introduction to Neuro-Fuzzy and soft computing". Chapters 2,4,5,7,8 1997, Prentice-Hall Inc.
- [99] Sabri Y., M. Farzaneh, J. Zhang, "Arc characteristic of Polluted Insulators covered With Ice". *CEIDP 2006 Annual Report Conference of Electrical Insulation and Dielectric Phenomena*. Pp. 437-440
- [100] Shu L. C. Sun, J. Zhang and L. Gu, "AC Flashover Performance of Iced and Polluted Insulators for High Altitude Regions", *Proceedings of 7th I.S.H.*, Vol. 4, pp. 303-306, August 1991.
- [101] Sundararajan R. & Gorur R. S., "Dynamic Arc Modeling of Pollution Flashover of Insulators under DC Voltage," *IEEE Trans, on Elec. Insul.*, Vol. 28, No. 2, 1993.
- [102] Singh R. R. P. & Sinha J. N., "Simulation Studies on Pollution Performance of Insulators," *Journal of the Institution of the Engineers part I, EL 4*, Vol. 75, pp. 26-34, 1994. 194195
- [103] Swift D. A., "Flashover of Polluted Insulators: Electric Field in the Arc," *6th Int. Sym. of High Voltage Eng.*, New Orleans, Paper No. 30.10, Sep 1989.

- [104] Swanson B. W., Rodit R. M. & Browne T. E, Jr. *Electrotech*, Z , 93, pp. 375, 1972.
- [105] Schneider H. M., "Artificial Ice Tests on Transmission Line Insulators-A Progress Report," *Proceedings of IEEE/PES Summer Meeting, San Francisco, USA*, Paper No. A75-491-1, pp. 347-353, 1975.
- [106] Sugawara N. et al., "Insulation Resistance of Transmission Line Insulators Depending on the Accretion of Ice," *Proc. of 5th Int. Workshop on Atmospheric Icing of Structures*, Tokyo, Japan, Paper No. B4-9, pp. 1-6, 1990
- [107] Su F. & Jia Y., "Icing on Insulator String of HV Transmission Lines and Its Harmfulness," *Proc. of 3rd Int. Offshore and Polar Eng. Conf*, Singapore, pp.655-658, 1993.
- [108] Tavakkoli Ch., "Dynamic modeling of AC arc development on ice surfaces". Thesis of Ph.D. in Engineering, University of Quebec in Chicoutimi, UQAC. November 2004.
- [109] Topalis F., Leontides N. & Stathopoulos I. A., "Investigation of the dielectric behavior of non-uniformly polluted insulators," *Proc. of Int. Conf. on Gas Discharges and their Applications*, Vol. 2, pp. 564-567, Swansea, September 1992
- [110] Van der Sluis, L.; Rutgers, W.R.; Koreman, C.G.A. "A physical arc model for the simulation of current zero behavior of high-voltage circuit breakers", *IEEE Transactions on Power Delivery*, Volume 7, Issue 2, Apr 1992 Page(s):1016 – 1022
- [111] Verma M. P., "Insulation Performance of DC Apparatus-housing under Pollution," *ETZ-Archive*, Vol. 5, No. 9, 1983.
- [112] Volât C, "Calcul de la distribution du potentiel du champ électrique le long des surfaces de glace recouvrant les isolateurs haute-tension et dans les intervalles d'air entre celles-ci," Thesis of Ph.D. in Engineering, UQAC, 2002. 195196
- [113] Vuckvic Z. and Z. Zdravkovic, "Effect of Polluted Snow and Ice Accretions on High-Voltage Transmission Line Insulators", *5th International Workshop on Atmospheric Icing of Structures*, Tokyo, October 1990.
- [114] Watanabe Y., "Flashover Tests of Insulators Covered with Ice or Snow," *IEEE Trans.*, Vol. PAS-97, No. 5, pp. 1788-1794, 1978.
- [115] Wareing J. B. & Bracey R. H., "Failure mechanisms in wood poles under severe conductor ice loading," In *Proc. 8th Int. Workshop of atmospheric Icing of Structures*, Reykjavik, pp. 35-41, June 1998.

- 
- [116] Wilkins R., "Flashover Voltage of High Voltage Insulators with Uniform Surface Pollution Films," Proc. IEE, Vol. 116, No. 3, pp. 457-465, 1969.
- [117] Woodson H. H. & McElroy A. J., "Insulators with Contaminated Surfaces Part II: Modeling of Discharge mechanisms," IEEE Trans., Vol. PAS-89, No. 8, pp. 1858-1867, 1970.
- [118] Zhicheng G. & Renyu Z., "Calculation of dc and ac Flashover Voltage of polluted Insulators," IEEE Trans. On Electrical Insulation, Vol. 25, No. 4, August 1990.
- [119] Zhang J., Guerrero T. & Farzaneh M., "Experimental Study on the Flashover Performance of Ice-covered Insulators under Impulse Voltage Ice," IEEE Conference on Electrical Insulation and Dielectric Phenomena, 2004 Annual Report, Boulder, Colorado, USA, pp. 635- 638, October 2004.196197
- [120] Zhang J. & Farzaneh M., "Propagation of DC Arc on Ice Surfaces," Proc. of 8th Int. Offshore and Polar Eng. Conf, Montreal, Canada, pp. 547-550, 1998.

## Appendix A

Training data set used for determining  $V_{Res}$ .

**Table.1**

SDD ( $mg/cm^2$ )	$\sigma$ ( $\mu S$ )	X (m)	I (A)	$V_{Res}$ (kV)
0.0992	11.0000	0.627	0.042	36.11
0.1611	29.0000	0.629	0.132	78.71
0.2331	63.0000	0.630	0.043	30.48
0.0557	66.0000	0.677	0.071	57.41
0.0865	28.0000	0.639	0.024	21.13
0.1566	56.0000	0.417	0.030	43.84
0.0573	61.0000	0.625	0.044	43.03
0.2173	68.0000	0.619	0.089	69.05
0.0883	41.0000	0.494	0.03	42.86
0.0630	77.0000	0.655	0.073	65.70
0.1398	11.0000	0.504	0.025	31.61
0.2027	52.0000	0.597	0.057	49.40
0.1663	52.0000	0.680	0.065	40.00
0.0498	42.0000	0.658	0.042	42.35
0.2216	35.0000	0.684	0.052	31.63
0.1736	15.0000	0.411	0.038	52.13
0.0446	60.0000	0.485	0.020	36.97
0.1036	70.0000	0.530	0.060	70.06
0.1285	57.0000	0.515	0.053	58.90
0.0898	65.0000	0.673	0.072	47.13
0.1497	46.0000	0.449	0.045	57.35
0.1935	77.0000	0.429	0.045	56.75
0.0316	78.0000	0.496	0.026	53.88
0.0411	67.0000	0.474	0.034	66.04
0.1402	79.0000	0.692	0.025	13.14
0.0929	30.0000	0.656	0.061	47.64
0.0795	25.0000	0.656	0.026	22.46
0.1334	32.0000	0.643	0.035	25.11

0.1284	55.0000	0.627	0.087	63.24
0.0907	58.0000	0.661	0.063	50.47
0.1216	13.0000	0.655	0.073	53.15
0.2283	26.0000	0.454	0.037	45.13
0.0702	25.0000	0.526	0.039	51.32
0.1622	23.0000	0.602	0.026	21.72
0.2002	42.0000	0.597	0.054	43.76
0.1840	51.0000	0.694	0.029	16.59
0.0997	68.0000	0.441	0.033	46.74
0.1225	33.0000	0.645	0.089	65.80
0.1185	16.0000	0.688	0.061	37.23
0.1066	17.0000	0.461	0.020	28.03
0.1409	50.0000	0.657	0.071	49.11
0.0618	35.0000	0.645	0.082	80.60
0.0618	35.0000	0.669	0.038	34.83
0.1795	74.0000	0.432	0.028	39.23
0.2159	47.0000	0.667	0.090	53.13
0.1698	69.0000	0.618	0.059	46.75
0.1315	56.0000	0.618	0.041	34.38
0.2134	40.0000	0.544	0.060	60.56
0.1379	37.0000	0.678	0.093	53.40
0.2079	30.0000	0.681	0.071	39.03
0.1084	10.0000	0.569	0.029	32.10
0.1425	57.0000	0.675	0.039	24.57
0.1875	73.0000	0.594	0.055	47.77
0.0758	22.0000	0.554	0.034	43.66
0.1975	29.0000	0.681	0.039	21.58
0.1530	29.0000	0.433	0.021	29.02
0.1982	16.0000	0.640	0.038	26.71
0.1619	34.0000	0.455	0.049	66.93
0.1768	11.0000	0.611	0.065	48.94
0.0916	14.0000	0.680	0.111	76.26
0.0456	22.0000	0.401	0.031	80.35
0.1260	75.0000	0.651	0.049	34.74

0.0576	15.0000	0.570	0.049	66.53
0.0982	38.0000	0.689	0.050	30.22
0.1602	25.0000	0.649	0.052	38.18
0.1726	20.0000	0.687	0.030	17.64
0.2334	19.0000	0.689	0.077	41.62
0.2279	53.0000	0.458	0.041	54.10
0.2203	18.0000	0.666	0.025	16.78
0.1237	48.0000	0.407	0.042	65.84
0.1517	25.0000	0.645	0.078	57.68
0.1829	48.0000	0.605	0.065	49.21
0.0678	50.0000	0.422	0.043	77.70
0.0710	20.0000	0.598	0.024	27.34
0.1071	51.0000	0.619	0.071	63.34
0.1692	51.0000	0.594	0.061	54.10
0.2247	39.0000	0.569	0.084	79.81
0.0907	58.0000	0.563	0.038	38.32
0.1560	75.0000	0.614	0.081	57.70
0.0170	29.0000	0.673	0.024	47.31
0.1891	22.0000	0.506	0.061	70.27
0.0740	57.0000	0.401	0.030	55.27
0.1515	13.0000	0.668	0.085	54.33
0.1557	43.0000	0.546	0.040	40.75
0.2334	19.0000	0.452	0.023	30.98
0.1008	25.0000	0.498	0.028	35.37
0.1497	52.0000	0.411	0.049	73.12
0.0240	36.0000	0.602	0.034	67.11
0.1559	19.0000	0.496	0.057	66.30
0.1497	52.0000	0.673	0.069	43.58
0.1861	21.0000	0.691	0.058	32.02
0.1982	77.0000	0.673	0.094	50.78

## Appendix B

MATLAB codes for calculating the flashover voltage:

```
-----  
clc  
clear all  
close all  
L=87;  
A=168;  
n=.325;  
K=308.4;  
b=.3811;  
x=[0:.5:L];  
SDD=[0.01:.005:.115];  
sig=30;  
vv=[];  
ii=[];  
v=[];  
v_iter=[];  
v(:,1)=0;  
for ss=1:length(SDD)  
    for l=1:length(x)  
        p=.317*(1-exp(-SDD(ss)/.053))+8.503e-5*sig^1.27;  
        vv(ss,l,1)=1;  
        for j=2:500  
            vv(ss,l,j)=A*x(l)*(K*x(l)/vv(ss,l,j-1))^(n/b)+(L-x(l))*1e4*(K*x(l)/vv(ss,l,j-1))^(1/b)/(p+0.1462*(K*x(l)/vv(ss,l,j-1))^(1/b));  
            v_iter(ss,j)=vv(ss,l,j);  
        end;  
        v(ss,l)=(vv(ss,l,j)+vv(ss,l,j-1))/2;  
        [mm nn]=max(v(ss,:));  
        vf(ss)=max(v(ss,:));  
        icr(ss)=(K*x(nn)/vf(ss))^(1/b);  
    end;  
end;  
testx=[.03 .05 .1];  
testv=[88 74 65];  
plot(x,v(9,:)/(1000*sqrt(2)));  
%plot(SDD,vf/(1000*sqrt(2)),testx,testv,'.',SDD,icr*1e3)  
grid;  
%axis([0 .12 0 120])  
-----
```